

**GROUNDWATER FLOW AND CONTAMINANT
TRANSPORT MODELING
NIAGARA FALLS STORAGE SITE
LEWISTON, NEW YORK**

Prepared for



Contract Number DACW49-00-D-0001

**U.S. Army Corps of Engineers
Buffalo District
1776 Niagara Street
Buffalo, New York 14207**

December 2007

**GROUNDWATER FLOW AND CONTAMINANT
TRANSPORT MODELING
NIAGARA FALLS STORAGE SITE
LEWISTON, NEW YORK**

Prepared for



Contract Number DACW49-00-D-0001

U.S. Army Corps of Engineers
Buffalo District
1776 Niagara Street
Buffalo, New York 14207

Prepared by

HGL
Northway 10 Executive Park
313 Ushers Road
Ballston Lake, New York 12019

December 2007

This page was intentionally left blank.

TABLE OF CONTENTS

Page

EXECUTIVE SUMMARY	ES-1
1.0 INTRODUCTION.....	1-1
1.1 LOCATION	1-2
1.2 BACKGROUND.....	1-2
1.3 OBJECTIVE.....	1-3
1.4 REPORT STRUCTURE.....	1-3
2.0 CONCEPTUAL MODEL.....	2-1
2.1 PHYSIOGRAPHY	2-1
2.1.1 Climate	2-1
2.1.2 Topography	2-1
2.1.3 Drainage.....	2-2
2.2 GEOLOGY	2-3
2.2.1 Regional Geology.....	2-3
2.2.2 Local Geology.....	2-4
2.2.2.1 Depositional Origin.....	2-4
2.2.2.2 Three-Dimensional Geologic Structure.....	2-6
2.2.2.3 Lithologic Descriptions	2-6
2.2.2.3.1 Fill.....	2-6
2.2.2.3.2 Upper Clay Till	2-7
2.2.2.3.3 Glacio-Lacustrine Clay Unit	2-7
2.2.2.3.4 Middle Silt Till Unit.....	2-8
2.2.2.3.5 Alluvial Sand and Gravel Unit.....	2-8
2.2.2.3.6 Basal Red Till	2-8
2.2.2.3.7 Queenston Formation	2-9
2.3 HYDRAULIC PROPERTIES	2-9
2.3.1 Upper Clay Till Unit	2-10
2.3.2 Glacio-Lacustrine Clay Unit	2-11
2.3.3 Middle Silt Till Unit.....	2-11
2.3.4 Alluvial Sand and Gravel Unit.....	2-11
2.3.5 Basal Red Till Unit	2-12
2.3.6 Queenston Formation	2-12
2.4 HYDROSTRATIGRAPHIC UNITS	2-12
2.4.1 Upper Water Bearing Zone	2-13
2.4.2 Upper Aquitard	2-15
2.4.3 Lower Water Bearing Zone	2-15
2.5 WATER-LEVEL DATA	2-16
2.5.1 Upper Water Bearing Zone	2-16
2.5.2 Lower Water Bearing Zone	2-20
2.6 WATER BUDGET.....	2-21
2.7 SUMMARY OF HYDROGEOLOGIC CONCEPTUAL MODEL.....	2-22
3.0 GROUNDWATER FLOW MODEL.....	3-1
3.1 METHODOLOGY	3-1

TABLE OF CONTENTS (continued)

	Page
3.2	PREVIOUS MODELING STUDIES..... 3-1
3.3	MODEL CONSTRUCTION..... 3-3
3.3.1	Code Selection 3-3
3.3.2	Model Discretization 3-4
3.3.3	Boundary Conditions 3-6
3.3.3.1	External Boundaries 3-6
3.3.3.2	Precipitation Recharge 3-7
3.3.3.3	Surface Water 3-7
3.3.4	Hydraulic Conductivity Zonation 3-8
3.4	GROUNDWATER FLOW MODEL CALIBRATION..... 3-9
3.4.1	Model Calibration Methodology 3-9
3.4.2	Calibration Targets 3-11
3.4.3	Calibration Results 3-12
3.4.3.1	Calibrated Hydraulic Parameters 3-12
3.4.3.2	Model Calibration Results 3-13
3.4.4	Particle Tracking Analysis 3-15
4.0	SOLUTE TRANSPORT MODEL..... 4-1
4.1	INTRODUCTION..... 4-1
4.1.1	Origin of Primary Contaminant Sources 4-1
4.1.2	IWCS Design and Operation..... 4-2
4.1.3	Additional Sources of Contamination..... 4-3
4.1.4	Transport Modeling Objectives..... 4-3
4.2	TRANSPORT MODELING APPROACH 4-4
4.2.1	Source Term Modeling 4-4
4.2.2	Solute Transport in the Saturated Zone 4-6
4.3	SOURCE TERM MODEL DEVELOPMENT 4-8
4.3.1	Unsaturated Zone Model Parameters 4-8
4.3.1.1	Approach 4-8
4.3.1.2	Unsaturated Zone Model Parameters 4-8
4.3.1.2.1	Precipitation 4-8
4.3.1.2.2	Solar Radiation, Temperature and Evapotranspiration..... 4-10
4.3.1.2.3	Waste Zone Geometry 4-10
4.3.1.2.4	Hydraulic Parameters..... 4-11
4.3.1.3	HELP Model Results 4-13
4.3.2	Source Leaching Model..... 4-14
4.3.2.1	Constituents of Concern 4-14
4.3.2.2	Model Discretization 4-16
4.3.2.3	Source Term 4-16
4.3.2.4	Transport Parameters..... 4-17
4.3.2.5	Source Leaching Model Results 4-17
4.4	REGIONAL SOLUTE TRANSPORT MODEL DEVELOPMENT 4-18
4.4.1	Three-Dimensional Transport Modeling Approach 4-18
4.4.2	Boundary and Initial Conditions..... 4-19
4.4.2.1	IWCS-Derived Contamination 4-19

TABLE OF CONTENTS (continued)

	Page
4.4.2.2 Contamination in Soil	4-20
4.4.2.3 Plume Maps.....	4-20
4.4.3 Transport Parameters	4-21
4.4.3.1 Effective Porosity	4-21
4.4.3.2 Dispersivity	4-21
4.4.3.3 Adsorption	4-22
4.4.3.4 Degradation/Decay	4-24
4.4.3.4.1 Radioactive Decay.....	4-24
4.4.3.4.2 Biodegradation	4-25
4.4.3.5 Solubility	4-26
4.5 PREDICTIVE SOLUTE TRANSPORT SIMULATIONS.....	4-26
4.5.1 Baseline Conditions.....	4-29
4.5.2 Worst-Case Scenario, Failure Events	4-32
4.5.2.1 Breach of IWCS Cap	4-33
4.5.2.2 Earthquake Scenario.....	4-34
4.5.2.3 Inadvertent Penetration of IWCS Cap	4-36
4.6 UNCERTAINTY ANALYSIS	4-37
4.6.1 Parameter Sensitivity.....	4-37
4.6.2 IWCS Water Level Sensitivity.....	4-40
5.0 RESULTS AND CONCLUSIONS	5-1
5.1 LONG-TERM EFFECTIVENESS OF IWCS INFERRED FROM MODELING RESULTS.....	5-1
5.2 SUMMARY OF CONSTITUENTS PREDICTED TO EXCEED SCREENING LEVELS.....	5-3
6.0 REFERENCES.....	6-1

LIST OF TABLES

Table 2.1	Monthly Average Temperatures in Lewiston, New York
Table 2.2	Monthly Precipitation in Lewiston, New York
Table 2.3	Summary Statistics Describing the Thickness of Each Lithologic Unit Encountered Within the Area of Interest
Table 2.4	Summary of Hydraulic Conductivity Statistics Calculated from Observed Data
Table 2.5	Comparison of Hydraulic Conductivity Values Used in Previous Modeling Studies to Field-Measured Data
Table 2.6	Summary of Vertical Hydraulic Gradients Between the Upper Clay Till Unit and the Alluvial Sand and Gravel Unit
Table 2.7	Summary of Vertical Hydraulic Gradients Between the Alluvial Sand and Gravel Unit and the Queenston Formation
Table 2.8	Summary of Major Water Budget Components From Historical Site Investigations and Regional Studies
Table 3.1	Summary of Lake Ontario Water Levels
Table 3.2	Model Calibration Data Set
Table 3.3	Summary of Calibrated Values of Hydraulic Conductivity
Table 4.1	Summary of Residues Stored in the IWCS
Table 4.2	Summary of Contaminants of Potential Concern for Simulation
Table 4.3	Model Source Term Components for Each Constituent
Table 4.4	HELP Modeling of Water Flux Through IWCS, Summary of Soil and Design Data
Table 4.5	Contaminant Residue Physical Properties and Calculations of Dissolved Concentrations
Table 4.6	1D Transport Modeling of Mass Flux Through IWCS, Summary of Model Design and Transport Parameters
Table 4.7	Values of Effective Porosity Assigned to the NFSS 3D Transport Model
Table 4.8	Baseline Case Predicted Maximum Constituent Concentrations and Initial Screening Level Exceedances, Model Layers 1 to 4
Table 4.9	Comparison of Baseline and Worst Case Scenario Results for Initial Screening Level Exceedances On-Site Due to IWCS Sources
Table 4.10	A Comparison Between Baseline Case and Sensitivity Analysis Results for U238
Table 4.11	Screening Level Exceedance in 1,000 years, by Model Source Term, Model Layer 1 – Upper Clay Till Unit

LIST OF FIGURES

Figure 1.1	Site Location Map
Figure 2.1	Topographic Map of North Eastern Niagara County, New York
Figure 2.2	Topographic Contours for NFSS and Adjacent Sites
Figure 2.3	Regional Surface Water Features
Figure 2.4	Local Surface Water Features
Figure 2.5	Surficial Geology of Niagara County, New York
Figure 2.6	Bedrock Geology of Niagara County, New York
Figure 2.7	Regional Geologic Cross Section
Figure 2.8	Borehole and Well Locations
Figure 2.9	Generalized Geologic Column
Figure 2.10	Profile of Geologic Structure, View to the North
Figure 2.11	Geologic Cross Sections Beneath NFSS and Adjacent Properties
Figure 2.12	3D Perspective View of Geologic Structure
Figure 2.13	Isopach Map of Upper Clay Till Unit
Figure 2.14	Location, Top Elevation and Thickness of Sand Lenses in the Upper Clay Till Unit
Figure 2.15	Top Surface Elevation of Glacio-Lacustrine Clay Unit
Figure 2.16	Isopach Map of Glacio-Lacustrine Clay and Middle Silt Till Units
Figure 2.17	Top Surface Elevation of Alluvial Sand and Gravel Formation
Figure 2.18	Isopach Map of Alluvial Sand and Gravel Unit
Figure 2.19	Isopach Map of Basal Red Till Unit
Figure 2.20	Top Surface Elevation of Queenston Formation
Figure 2.21	Hydraulic Conductivity of Upper Clay Till Unit
Figure 2.22	Hydraulic Conductivity of Glacio-Lacustrine Clay/Middle Silt Till Unit
Figure 2.23	Hydraulic Conductivity of the Alluvial Sand and Gravel Unit
Figure 2.24	Hydraulic Conductivity of the Basal Red Till Unit
Figure 2.25	Hydraulic Conductivity of Upper Queenston Formation
Figure 2.26	Schematic of Conceptual Hydrostratigraphic Units
Figure 2.27	Generalized Potentiometric Surface of the Upper Water-Bearing Zone May 2000
Figure 2.28	Generalized Potentiometric Surface of the Upper Water-Bearing Zone Sept./Oct. 2000
Figure 2.29	Regional Groundwater Flow Patterns
Figure 2.30	Generalized Potentiometric Surface of the Lower Water-Bearing Zone May 2000
Figure 2.31	Generalized Potentiometric Surface of the Lower Water-Bearing Zone October 2000
Figure 3.1	Finite Difference Grid and Model Boundary Conditions for Groundwater Flow
Figure 3.2	Model Cross Sections A-A' and B-B'
Figure 3.3	Location of Lake Ontario Gauging Stations
Figure 3.4	Distribution of Precipitation Recharge in Model Layer 1
Figure 3.5	Hydraulic Conductivity Zonation in Model Layer 1
Figure 3.6	Groundwater Flow Model Calibration Targets – Layer 1 (Average Water Levels)

LIST OF FIGURES (continued)

Figure 3.7	Groundwater Flow Model Calibration Targets – Layer 2 (Average Water Levels)
Figure 3.8	Groundwater Flow Model Calibration Targets – Layer 3 (Average Water Levels)
Figure 3.9	Groundwater Flow Model Calibration Targets – Layer 4 (Average Water Levels)
Figure 3.10	Simulated Hydraulic Head and Residuals, Model Layer 1
Figure 3.11	Simulated Hydraulic Head and Residuals, Model Layer 2
Figure 3.12	Simulated Hydraulic Head and Residuals, Model Layer 3
Figure 3.13	Simulated Hydraulic Head and Residuals, Model Layer 4
Figure 3.14	Simulated Regional Hydraulic Heads – Layer 4
Figure 3.15	Simulated Versus Observed Hydraulic Heads (All Layers)
Figure 3.16	Regional Bedrock Faults, Fractures and Lineament Trends
Figure 3.17	Local Bedrock Fractures, Faults and Lineament Trends
Figure 3.18	Simulated Particle Trace under Calibrated Flow Field Conditions
Figure 3.19	Simulated Particle Trace with Fracture K One (1) Order of Magnitude Greater than QFM
Figure 3.20	Simulated Particle Trace with Fracture K Two (2) Orders of Magnitude Greater than QFM
Figure 4.1	NFSS Exposure Units
Figure 4.2	Plan View of the IWCS
Figure 4.3	East-West Cross-Sectional View of the NFSS IWCS
Figure 4.4	Model Row and Column Numbering Convention

LIST OF APPENDICES

Appendix A	Station Location Summary
Appendix B	Geostatistical Evaluation of Hydrogeologic Heterogeneity
Appendix C	Hydraulic Conductivity Data Summary
Appendix D	Geochemical Analysis Report
Appendix E	Supplementary Transport Model Data Results
	E-1 HELP Model Predictions of Water Flux Through Each Waste Zone
	E-2 1D Model Predictions of Mass Flux Through Each Waste Zone
	E-3 Screen Captures of Plume at Screening Exceedances Times
	E-4 Sensitivity to Lead Distribution Coefficient (Kd)
	E-5 Saturated IWCS Case
Appendix F	Digital Information
	F-1 NFSS Environmental Database
	F-2 Water-Level Hydrographs and Vertical Gradient Calculations
	F-3 3D Model Source Terms
	F-4 Screen Captures
	F-5 3D Transport Simulation Animations

LIST OF ACRONYMS AND ABBREVIATIONS

AEC	Atomic Energy Commission
amsl	above mean sea level
ANL	Argonne National Laboratory
AOI	area of interest
ARAR	Applicable or Relevant and Appropriate Requirements
As	arsenic
ba	Barium
Bechtel	Bechtel National, Inc.
BP	before present
BRA	baseline risk assessment
BTEX	benzene, toluene, ethyl benzene and xylenes
2EHP	bis(2-ethylhexyl)phthalate
°C	degrees Celsius
Cd	cadmium
CERCLA	Comprehensive Environmental Response, Compensation and Liability Act
<i>cis</i> -DCE	<i>cis</i> -1,2-dichloroethene
cm	centimeters
cm/d	centimeters per day
cm/s	centimeters per second
cm/yr	centimeters per year
COC	constituents of concern
COPC	constituent of potential concern
Cs	constituent concentration in soil
C _w	constituent concentration in water
CWM	Chemical Waste Management Chemical Services, LLC
CY	calendar year
DEM	digital elevation model
EPDM	ethylene propylene diene monomer (geo-synthetic barrier liner)
ERDA	Energy Research and Development Administration
EU	exposure unit
°F	degrees Fahrenheit
Fe	Iron
ft	feet
ft/d	feet per day
foc	fraction total organic content
FS	feasibility study
FUSRAP	Formerly Utilized Sites Remedial Action Program
GIS	Geographical Information System
GPR	ground penetrating radar

LIST OF ACRONYMS AND ABBREVIATIONS (continued)

GPM	U.S. gallons per minute
ha	hectare
HELP	Hydrologic Evaluation of Landfill Performance
HGL	HydroGeoLogic, Inc.
in	inches
in/d	inches per day
in/yr	inches per year
IWCS	Interim Waste Containment Structure
K	hydraulic conductivity
K _d	distribution coefficient
km	kilometers
K _{oc}	organic carbon partition coefficient
K _z	vertical hydraulic conductivity
K _x	horizontal hydraulic conductivity
L/kg	liters per kilogram
L/s	liters per second
LOOW	Lake Ontario Ordnance Works
LULC	land use/land cover
μg/L	micrograms per liter
m	meters
MED	Manhattan Engineer District
MC	methylene chloride
mCi/hour	millicuries per hour
MCL	maximum contaminant levels
mg/L	milligrams per liter
mi	miles
MINTEQ	Geochemical Equilibria in Water Model
ML	Modern Landfill, Inc.
Mn	manganese
Mo	molybdenum
mph	miles per hour
NRC	National Research Council
NFSS	Niagara Falls Storage Site
NOAA	National Oceanic and Atmospheric Administration
NY	New York
NYSDEC	New York State Department of Environmental Conservation
1D	one-dimensional

LIST OF ACRONYMS AND ABBREVIATIONS (continued)

Pb	lead
pCi/L	picocuries per liter
ρ_b	bulk density
PCE	perchloroethene
PCG	Preconditioned Conjugate Gradient
PEST	Parameter Estimation Software Tool
PRG	preliminary remediation goal
Ra	radium
RI	remedial investigation
RMS	root mean squared
RSS	residual sum of squares
S	solubility coefficient
Sb	antimony
SAIC	Science Applications International Corporation
SESOIL	Seasonal Soil Compartment Model
2D	two-dimensional
3D	three-dimensional
TCE	trichloroethene
Th	thorium
TNT	trinitrotoluene
TOC	total organic carbon
USACE	U.S. Army Corps of Engineers
USDOE	U.S. Department of Energy
USEPA	U.S. Environmental Protection Agency
USGS	U.S. Geological Survey
UTL	upper tolerance limit
U-235	Uranium - 235
U-238	Uranium - 238
VC	vinyl chloride
Vt	total volume
Vv	volume of voids
α_v	vertical dispersivity

EXECUTIVE SUMMARY

HydroGeoLogic, Inc. (HGL) completed a groundwater modeling investigation to predict the migration of contaminants originating from the Niagara Falls Storage Site (NFSS). This model was used to determine future migration under baseline (current) conditions and for three worst-case hypothetical scenarios. The project was completed in three stages including: 1) conceptual model development; 2) groundwater flow model development and calibration; and 3) solute transport model development and application.

During the first phase of the investigation, HGL developed a hydrogeologic conceptual model for the NFSS and surrounding area. This hydrogeologic conceptual model synthesizes the key process that controls groundwater flow and contaminant migration within the area of interest. It was developed based on historical studies and a reevaluation of data that have been collected at NFSS, Chemical Waste Management Chemical Services, LLC (CWM), and Modern Landfill, Inc. (ML). These data were incorporated into a comprehensive Geographical Information System (GIS)/database management system that facilitated statistical and spatial analyses. Key components of the hydrogeologic conceptual model include:

- Groundwater flow is controlled by three hydrostratigraphic units: Upper Water Bearing Zone, Upper Aquitard, and Lower Water Bearing Zone;
- Unweathered shale bedrock (Queenston Formation) forms the base of the lower groundwater flow system;
- Due to the low permeability associated with the Upper Water Bearing Zone, precipitation recharge is extremely low (< 1 in/yr [2.54 centimeters/year (cm/yr)]);
- Regional groundwater flow is primarily to the northwest toward the Niagara River, although, localized groundwater flow patterns are influenced by creeks and drainage ditches;
- The sediments comprising the Upper Water Bearing Zone are heterogeneous, creating complex localized groundwater flow patterns;
- High permeability sand lenses within the Upper Water Bearing Zone are limited in areal extent and do not act as conduits for preferential groundwater flow and contaminant migration; and
- The spatial distributions of contaminants in groundwater are limited in extent, indicating that groundwater flow velocities are low.

A 3D groundwater flow model was constructed and calibrated using the MODHMS modeling code. The groundwater flow model was developed based on the hydrogeologic conceptual model. This groundwater model was developed to simulate groundwater flow within the NFSS and surrounding area. The model consists of four model layers representing the three hydrostratigraphic units underlying the site. The lowermost hydrostratigraphic unit was divided into two separate model layers representing the Alluvial Sand and Gravel and Upper Queenston Formation. Boundary conditions and hydraulic parameters were assigned in the model based on previous studies, the hydrogeologic conceptual model, and data contained in the NFSS GIS/database management system.

The groundwater flow model was calibrated by adjusting hydraulic conductivity and precipitation recharge rates in order to match water level elevations measured in the field. The completed groundwater flow model provides a good match between observed and simulated water levels. In addition, the parameters assigned in the model are in good agreement with field measurements and previous modeling studies. Consequently, there is an acceptable degree of uncertainty associated with the flow model predictions.

Upon the successful completion of the groundwater flow model, a numerical, 3D solute transport model was developed using MODHMS. The transport model utilizes the same numerical grid as the flow model, and advective transport calculations are based on the groundwater velocities calculated using the groundwater flow model.

A multi-step approach was employed to simulate source releases and unsaturated zone transport within the Interim Waste Containment Structure (IWCS) and elsewhere at the NFSS. This approach utilized separate modeling codes to (1) estimate the water flux through the IWCS; and (2) predict vertical transport of contaminants through the unsaturated zone. Collectively, the modeling tools used were applied to predict long-term, contaminant mass-loading rates to the water table. The predicted mass-loading rates were then assigned as time-varying source terms in the NFSS 3D transport model, which was subsequently applied to simulate the transport of the contaminants within the saturated zone.

Once developed, the transport models were used to predict contaminant migration under baseline (current) and three worst-case scenario conditions. These simulations accounted for the following transport processes:

- Leaching and migration of radiological residues, waste, contaminated soil and other material in the reinforced concrete cellars of former Buildings 411 and 413/414 in the IWCS;
- Leaching and migration of contaminated soil and other contaminated materials of the former R-10 waste pile in the IWCS;
- Vertical transport of contaminants contained in unsaturated soil to the water table;
- 3D migration of contaminant plumes currently observed in groundwater; and
- Future migration of contaminants currently contained in the IWCS or surrounding soils through regional groundwater flow within the saturated zone.

The transport modeling results suggest that, for the baseline scenario, constituent concentrations may exceed screening levels within the NFSS sometime between 1,000 and 10,000 years from the start of the simulations. The model predicts that U-238, U-234, U-235, *cis*-1,2-dichloroethene, and vinyl chloride will exceed their respective screening levels within the NFSS property after 1,000 years. The model also predicts that the U-238 and U-235 will exceed their screening level at the NFSS property boundary after 1,000 years. The model also predicts that several constituents will exceed their screening levels under the three hypothetical worst-case scenarios. However, these scenarios are extreme cases and have very low probabilities of occurring.

**GROUNDWATER FLOW AND CONTAMINANT TRANSPORT
MODELING REPORT
NIAGARA FALLS STORAGE SITE
LEWISTON, NEW YORK**

1.0 INTRODUCTION

In 2000, HydroGeoLogic, Inc. (HGL) was contracted by the United States Army Corps of Engineers (USACE) – Buffalo District to assist with the Data Management, Environmental Modeling, and Risk Communication project at the Niagara Falls Storage Site (NFSS), Lewiston, New York (NY). HGL was tasked with the development of a three-dimensional (3D) groundwater flow and contaminant transport numerical model to simulate dissolved chemical and radiological contaminants present in the multi-layered aquifer system underlying NFSS. The broader modeling effort included the development of a local and regional conceptual model, Geographical Information System (GIS), database management system and development and calibration of a 3D numerical groundwater flow model.

In calendar year (CY) 2002, an initial three-layer model was developed and calibrated (HGL, 2002). An additional model layer was added in CY 2003 to provide increased resolution in the subsurface units identified at NFSS and the resulting four-layer model was recalibrated. The four-layer model provides the basis for subsequent modeling efforts and the analyses described herein.

Building upon earlier efforts, work activities performed in CY 2004 focused on additional testing of the conceptual model and preparations for transport model development. A geostatistical analysis was performed to evaluate the spatial continuity of glacio-fluvial sand lenses in the Upper Clay Till unit. (HGL, 2004a) The objective of this study was to determine whether continuous sand lenses exist beneath the Interim Waste Containment Structure (IWCS), potentially providing pathways for preferential contaminant migration. A literature review and geochemical modeling were also performed in CY 2004 to support the compilation of representative values for key transport model input parameters including constituent specific distribution coefficients and solubility limits (HGL, 2004b).

In CY 2005, a 3D transport model was developed and applied to support the ongoing Remedial Investigation (RI) /Feasibility Study (FS) program and to quantify the risks associated with long-term transport of waste and residues on the NFSS. Multiple simulations were performed to evaluate solute transport under baseline conditions (existing current conditions) and three worst-case scenario, failure events. In the future, this model will also be used to evaluate the performance of remedial alternatives developed as part of the ongoing FS being conducted by Science Applications International Corporation (SAIC) and the USACE.

1.1 LOCATION

The NFSS is located north of Pletcher Road in Lewiston, NY (Figure 1.1). It is approximately 19 miles (mi) (30 kilometers [km]) north of Buffalo, 4 mi (6.4 km) south of Lake Ontario and 3.1 mi (5 km) east of the Niagara River.

The area of interest (AOI) for this study centers on the NFSS, but also includes the adjacent CWM and Modern Landfill, Inc. (ML) properties where detailed studies of lithology, hydrogeology and contaminant pathways have been carried out (Figure 1.1). CWM operates a commercial hazardous waste disposal operation permitted by the New York State Department of Environmental Conservation (NYSDEC), bordering the northern boundary of the NFSS. East, and southeast of the NFSS, ML operates a solid waste disposal facility permitted by the NYSDEC.

1.2 BACKGROUND

NFSS, CWM and ML properties are parcels of the former 7,500-acre (3,035-hectare [ha]) Lake Ontario Ordnance Works (LOOW), established by the War Department in 1942. The original LOOW property has since been apportioned and utilized for a variety of industrial activities including borane fuel plants, jet engine testing facilities, a NIKE missile facility, radiological and chemical waste storage, municipal and hazardous waste landfills and testing of experimental communications equipment.

The present-day NFSS was originally part of the LOOW operations area that supported trinitrotoluene (TNT) production on the present-day CWM property. TNT manufacturing operations were discontinued in 1943 and lands were transferred to the USACE - North Atlantic Division in 1944. Shortly afterwards, a 1,500-acre (610-ha) parcel of the USACE property was acquired by the Manhattan Engineer District (MED) for the storage of pitchblende residues and other low-level radioactive materials derived from atomic research during the Cold-War era.

The MED property was subsequently transferred to the Atomic Energy Commission (AEC) in 1947, the Energy Research and Development Administration (ERDA) in 1975 and finally to the U.S. Department of Energy (USDOE) in 1977. The present day NFSS consists of a 191-acre (77-ha) portion of the former MED property.

In the mid-1980s, the USDOE investigated and remediated high (including K-65 residues) and low (including L-30, F-32 and L-50 residues) activity radioactive residues from properties on and adjacent to the NFSS as part of the Formerly Utilized Sites Remedial Action Program (FUSRAP). Radioactive residues, radium (Ra) contaminated sand, soil and building rubble were consolidated and placed in the 10-acre (4-ha) IWCS on the NFSS between 1981 and 1996. In 1991, 60 drums of radioactively contaminated material from on-site remediation operations were consolidated into the IWCS. It is estimated that the IWCS contains 13,750 cubic yards (10,520 cubic meters) residues, 169,600 cubic yards (129,670 cubic meters) contaminated soils/wastes, 46,610 cubic yards (35,640 cubic meters) contaminated rubble and 142,940 cubic yards (109,280 cubic meters) of miscellaneous contaminated soil for a total

waste volume of 372,900 cubic yards (285,110 cubic meters). Currently, the USACE, Buffalo District manages environmental activities at the NFSS under the FUSRAP.

1.3 OBJECTIVE

The primary objectives of the Data Management, Environmental Modeling, and Risk Communication project at the NFSS include the following:

- Compile all available hydrogeological and contaminant data in an electronic database;
- Develop a conceptual model (understanding) of the groundwater flow conditions at the site, which incorporates the results of a comprehensive review and analysis of all available geologic and hydrogeologic data;
- Construct and calibrate a groundwater flow model that simulates groundwater flow conditions;
- Develop a solute transport model that is capable of predicting the migration of site-related and off-site contaminants of concern;
- Quantify the short- and long-term risks of contaminant transport from the IWCS to the environment;
- Develop visual representations (including animation) that effectively communicate site-specific conditions and potential future risk to the public; and
- To inform stakeholders about the presence or absence of imminent danger of failure of contaminant breakthrough from the IWCS.

1.4 REPORT STRUCTURE

This report presents a comprehensive summary of HGL's environmental modeling efforts dating back to 2000. Content from previous draft reports, including the conceptual model, 3D numerical groundwater flow model (HGL, 2002) and others, are presented herein, with revisions made where necessary, to address USACE comments or to reflect work that was completed after the submittal of the draft documents. This report is organized into four sections:

- Section 1: Introduction
- Section 2: NFSS Conceptual Model, GIS and Database Development
- Section 3: Groundwater Flow Model Development and Application
- Section 4: Solute Transport Model Development and Application

Section 2 summarizes the conceptual hydrogeological model developed for the NFSS with supporting details in tables and figures generated from the NFSS database and GIS. Results from a geostatistical analyses conducted to evaluate the continuity of high permeability sand lenses are also discussed in Section 2.

Section 3 documents the groundwater flow modeling approach and results. The model domain, numerical grid, hydraulic flow properties, model calibration and other model construction details are outlined, and respectively, rationale is presented for each. The baseline, calibrated groundwater flow model, is presented in Section 3, as well as results from

a sensitivity analysis. Particle tracking simulations are also presented in Section 3. The purposes of these simulations were to determine likely groundwater flow and contaminant migration pathways and to determine the impact of hypothetically enlarged and interconnected bedrock fractures on the predicted flow field.

Section 4 outlines the 3D, transport modeling approach and presents simulation results extending to 10,000 years, which allow for the quantification of risk and solute migration for 26 constituents of concern. Rationale for the selection of constituents that were included in the modeling analysis is provided. The methodology used to represent the constituent source terms and initial concentrations in the model is also detailed including: 1) constituents contained within the IWCS, 2) localized constituent plumes identified through groundwater sampling, and 3) constituents that have been found at elevated concentrations in soil. Modeling results are provided in this section for baseline (current) conditions and for three (3) hypothetical worst-case scenario failure events.

This modeling effort supports the Comprehensive Environmental Response, Compensation and Liability Act (CERCLA) investigation being conducted by USACE at NFSS. In accordance with the CERCLA process, USACE conducted a preliminary evaluation of potential Applicable or Relevant and Appropriate Requirements (ARAR) that may provide the statutory and regulatory basis for managing the NFSS wastes (SAIC, 2003b). ARARs under consideration for NFSS include 10 CFR Part 40 Appendix A and 40 CFR Part 192 Subparts A, B, and C. Both potential ARARs require remedial measures to be effective for up to 1,000 years to the extent reasonably achievable and in any case for at least 200 years. For this reason, model simulations were conducted to present results extending to at least 1,000 years. Recognizing the potential for ingrowth of some of the long-lived radioisotopes and in the interest of a conservative simulation approach, results are presented for simulations extending to 10,000 years, which is considerably beyond the regulatory guided simulation timeframe of 1,000 years.

2.0 CONCEPTUAL MODEL

2.1 PHYSIOGRAPHY

2.1.1 Climate

Niagara County is characterized by a humid, continental type of climate. Summers are warm and winters are moderately long and cold.

The close proximity of Lake Ontario moderates the temperatures of the region and reduces high and low temperature extremes in the summer and winter, respectively. In the spring, the cold waters of the Great Lakes serve as a heat sink and in the fall the warmer lake temperatures prolong the growing season.

Temperature and precipitation data for Lewiston, NY, nearby the AOI, are available from the National Oceanic and Atmospheric Administration (NOAA) for the time period from 1935 through 1971 and 1987 through 1994. Based on the Lewiston temperature recordings, and as summarized in Table 2.1, July is the hottest month of the year with a mean temperature of 72.3 degrees Fahrenheit (°F) (22.4 degrees Celsius [°C]) and January is the coldest with a mean temperature of 26.2 °F (-3.2 °C).

Moisture is primarily derived from air masses that originate in the surrounding Great Lakes region, the Atlantic Ocean to the south and the Gulf of Mexico to the southwest. Niagara County typically receives less snowfall than Buffalo and adjacent regions to the south, which are influenced to a greater degree by lake-effect snowfall from Lake Erie.

Precipitation measured in Lewiston, presented in Table 2.2, is somewhat consistent throughout the year with minor deviations from month to month. The average annual total precipitation is 29.7 inches (in) [75.4 centimeters (cm)]. The wettest months include April and May whereas the driest, non-freezing conditions occur in October and November.

2.1.2 Topography

The AOI is situated on the Ontario Plain, a physiographic region that extends from the shore of Lake Ontario to the Niagara escarpment 8 mi (13 km) to the south. The Ontario Plain is characterized by low relief and gentle topography that slopes toward Lake Ontario. The mean elevation of Lake Ontario is 250 feet (ft), above mean sea level (amsl) (76.2 meters [m], amsl), as read from NY Department of Transportation topographic coverage.

Within the Ontario Plain, there are several geomorphic features that differ from the otherwise flat topography (Figure 2.1). One is a sinuous ridge up to 30 ft (9 m) in relief that marks the shoreline of former Lake Iroquois and is now transversed by U.S. Highway 104 (Ridge Road). Another is the Niagara Escarpment, a northward facing bluff that rises as much as 200

ft (61 m), and in some places features an overhanging face of rock. The Niagara Escarpment separates the Huron plain to the south from the Ontario Plain to the North.

Detailed topographic contours for the AOI are shown in Figure 2.2. Numerous drainage channels are illustrated on this figure as linear depressions in the ground surface. Note that these drainage channels form a grid pattern over the landscape. The IWCS on the NFSS property is clearly visible on the topographic map, as are landfills on the ML and CWM sites. Built-up berms containing the waste lagoons on the CWM property are also evident. Elsewhere the landscape is essentially flat lying. The land surface elevations within the NFSS property ranges from 306 ft, amsl (93.3 m, amsl) in a creek ditch near the northern boundary to 348 ft, amsl (106 m, amsl) at the top of the IWCS.

2.1.3 Drainage

The low relief of the landscape lends to poor drainage, swampy and flood-prone regions. Three creeks comprise the major flow channels in the vicinity of the NFSS: Fourmile, Sixmile and Twelvemile Creeks (Figure 2.3). Each of these creeks has several minor tributaries, some of which have intermittent flow and dry stretches, particularly in the upstream reaches. Fourmile and Sixmile Creeks flow northward from the AOI and ultimately empty into Lake Ontario. Twelvemile creek flows in a general northeasterly direction with its headwaters near the southeast ML property boundary. The channels cut by these creeks are typically shallow with more pronounced valley shapes closer to Lake Ontario. Creeks south of the Niagara escarpment drain into the Niagara River.

The NFSS is drained by man-made ditches flowing east-west and north-south (Figure 2.4). These were constructed in the 1940s [Betchel National, Inc. (Bechtel), 1982] to divert all surface water on the LOOW Property into a central, on-site drainage ditch. Sixmile Creek originally flowed across the NFSS and was diverted around the southwest corner of the NFSS property. The original head waters of Sixmile Creek now flow westward via the Southwestern Drainage Ditch and empty into Fourmile Creek. Surface waters southeast of the NFSS originally flowed east to Twelvemile Creek and were diverted to flowing westward to the South-31 Ditch. At present Sixmile and Twelvemile Creeks do not receive runoff directly from the NFSS property.

The current surface water flow configuration on the NFSS property remains altered, with Central Drainage Ditch is the main drainage channel, and naturally flowing creeks diverted around the NFSS. The Central Drainage Ditch originates near the southern NFSS boundary, flows northward dividing the NFSS. The Central Drainage Ditch continues northward beyond the NFSS, flowing beneath Balmer Road, eventually west and emptying into Fourmile Creek (Figure 2.3), before discharging into Lake Ontario. The West Drainage Ditch originates a few hundred yards south of the NFSS and flows northward along the western NFSS boundary. Its flow is intermittent throughout the year, and it is frequently dry during summer months. The West Drainage Ditch converges with the Central Drainage Ditch north of the NFSS property. The major westward flowing channels on the NFSS are the South-31 Drainage Ditch and the South-16 Drainage Ditch. Both of these ditches empty into the Central Drainage Ditch. The

South-16 Drainage Ditch receives surface water runoff and groundwater discharge from the ML site and is prone to high flow levels.

2.2 GEOLOGY

2.2.1 Regional Geology

Unconsolidated materials, ranging in thickness from 10 to 100 ft (3 to 30 m), blanket the Ontario Plain in Niagara County. These overburden materials are primarily of glacial origin deposited during the late Pleistocene Epoch (10,000 to 75,000 years before present [BP]). Till, outwash sand and gravel and lacustrine deposits are commonly encountered in Niagara County, as shown in Figure 2.5. The stratigraphy and interpreted origin of overburden units encountered during geologic investigations within the AOI are discussed in greater detail in Section 2.2.2.

The bedrock underlying overburden deposits beneath the Ontario Plain is shale of the late Ordovician Queenston Formation (approximately 440 million years BP) (Figure 2.6). This unit is on the order of 984 ft (300 m) thick and has a south trending dip of approximately 1 percent (%). The upper contact of the Queenston Formation is typically weathered and has been eroded and scoured by glacial activity. The Queenston Formation extends beneath Lake Ontario, continuing northward while decreasing in thickness. Kindle and Taylor (1914) describe the Queenston shale:

The formation consists characteristically of bright cherry-red shale, marked by perfectly regular lamination and entire absence of cross-bedding, with numerous intercalated beds of green shale one to two inches thick. The upper part of the formation is almost wholly shale, but in the lower part, the shale is interbedded with thin layers of gray or greenish sandstone, one to eight inches thick. The sandstone beds, some of which are ripple marked, are exposed in the outcrops along or near the shore of Lake Ontario.

The shale is friable and breaks down rapidly under atmospheric weathering, forming a talus of small fragments at the base of each outcrop. Where exposed in considerable thickness, it is discolored in zones an inch or so thick along bedding planes and joint cracks. The ultimate product of weathering is a sticky, red clay.

Pre-Cambrian (approximately >600 million years BP) metamorphic rocks underlie the Queenston Formation. South of the AOI, the Queenston Formation is overlain by Silurian-age (approximately 430 million years BP) sedimentary rocks, as is evident from rock outcrops in the face of the Niagara Escarpment, the Niagara River gorge, and exposed roadside cuts. This younger stratigraphic sequence consists of approximately 200 ft (60 m) of less resistant limestone, sandstones and shales capped with an estimated 50 ft (15 m) of resistant dolostones from the Lockport Formation. A north-south schematic cross-section is presented in Figure 2.7 to illustrate the stratigraphy of the bedrock units in relation to overburden deposits on the Ontario Plain between Lake Ontario and the Niagara Escarpment.

2.2.2 Local Geology

2.2.2.1 Depositional Origin

A conceptual understanding of the depositional history and stratigraphy of the AOI was attained by conducting a comprehensive review of available reports, consultant studies, and bore logs. The geologic structure ascertained from these data sources was confirmed and further refined using visualization aids that incorporate information from more than 700 boreholes drilled on the NFSS, CWM and ML properties (Figure 2.8). Acres American Inc. (1981) provides the first thorough description of overburden stratigraphy at the NFSS and is commonly used as a basis for geological descriptions in subsequent reports. The lithologic description herein draws on the explanation from Acres American Inc. (1981) and includes salient details from several other reports, most notably Wehran Engineering Corporation (Wehran) (1977), and Wehran (1979) for the ML site; and Golder Associates, Inc. (Golder) (1985), and Golder (1993), for the CWM site. Well construction details and other pertinent well data were obtained from numerous consultant studies and through contact with the NYDEC, ML, Tetra Tech (formerly Maxim Technologies), Environmental Solutions, Golder and CWM.

The overburden materials encountered within the AOI are glacial in origin, and predominantly consist of either glacio-lacustrine clays, glacial-outwash or till. Till is a genetic term for non-sorted material deposited by ice. Tills may consist of a variety of rocks of varying grain sizes, and often a high proportion is derived from underlying bedrock and other materials scoured by the advancing glacier. Glacial outwash deposits are either of the ice contact stratified drift variety (e.g., kames, eskers, kame deltas) or consist of more uniform outwash fans or plain deposits. Glacio-lacustrine sediments are typically fine-grained and are derived from lakes of glacial melt water. The texture and composition of the sediments vary with position in the lake, sediment supply and velocity of streams entering the lake.

In the ensuing description of the events leading to the deposition of overburden within the AOI, glaciation refers to a period of glacial expansion. Episodes of glaciation are subdivided into Stades – periods of ice advance, and Interstades – warmer substages during which there is temporary recession of the ice. Interglacials, representative of the current age, are periods of glacial withdrawal.

The generalized geologic structure in the vicinity of the AOI is shown in Figure 2.9. Given that glacial advances are marked by the deposition of till, the presence of three distinct till sheets (Basal Red, Middle Silt and Upper Clay) provides evidence for three glacial advances or oscillations across Niagara County. This assertion is supported by the available literature (e.g., Wehran [1979], Golder [1985]).

Prior to glacial advances over the AOI in the late Pleistocene age, the Queenston Formation was exposed at the ground surface. The heavily weathered upper portion of the shale attests to a period of erosion that probably coincided with its exposure during pre-Wisconsin times (Kindle and Taylor, 1914). It is postulated that glaciation further scoured the surface of the

Queenston shale and led to the deposition of the Basal Red Till (as shown in Figure 2.9). The time of deposition of the Basal Red Till is a point of contention in the literature. Wehran (1977) and Kindle and Taylor (1914) correlate the Basal Red Till as pre-Wisconsin (<75,000 years BP) in origin whereas Golder (1985) speculate it to be late Wisconsin (20,000 to 10,000 years BP).

During the Sangamonian interglacial period (100,000 to 75,000 years BP) or at some time thereafter erosion and channel down cutting through the Basal Red Till occurred. Evidence from bore logs and the intermittent spatial distribution of the Basal Red Till affirm this to be correct. It is likely that the lower portion of the Alluvial Sand and Gravel Unit was deposited in the channel valleys during this interglacial period.

At the onset of glaciation in the Wisconsin age (75,000 to 10,000 years BP), water levels increased and shallow proglacial lake deposits led to further accumulation of Alluvial Sand and Gravel Unit deposits throughout the AOI. As the glacial lake transgressed, water levels increased, depositional energies decreased, and the lower portion of the Glacio-Lacustrine Clay Unit was deposited.

The occurrence of the Middle Silt Till Unit provides evidence for a second glacial advance over the AOI. However, the intermittent occurrence of this unit, its typically thin profile and positioning between lithologically similar strata of clay suggest that its deposition is associated with a minor and perhaps local glacial oscillation. Deposition of the Middle Silt Till was probably associated with the Port Huron Stadial (13,000 years BP) glacial advance (Golder, 1985). The scouring action during this glacial advance probably removed a significant portion of the original Glacio-Lacustrine Clay prior to deposition of the Middle Silt Till.

A resumption of the glacial lake environment led to further accumulation of the Glacio-Lacustrine Clay Unit above the Middle Silt Till Unit, where present. It is noted that deposits of a second, distinct till unit within the Glacio-Lacustrine Clay Unit have been identified in some boreholes on the CWM site. It is likely that this till is the product of yet another minor glacial oscillation, similar to that which deposited the Middle Silt Till (Golder, 1985).

The Upper Clay Till Unit overlies the Glacio-Lacustrine Clay Unit (Figure 2.9) and provides evidence of a third glacial advance over the AOI. It is postulated that the advancing glacier associated with this till removed a significant depth of the underlying glacio-lacustrine deposits by abrasion as did the preceding glacial advance. Glacial recession at about 10,000 years BP left the AOI submerged by Lake Iroquois, albeit for an insufficient period of time, to allow notable depositional accumulation to occur.

The landscape has remained unchanged by glacial activity since the Wisconsin age. Much of the surface of the AOI has been graded thereby removing any remnants of glacial direction such as aligned till ridges, which were observed within the AOI in the early 1900s. Unconsolidated fill materials or a thin veneer of alluvium overlie the Upper Clay Till Unit in the AOI.

2.2.2.2 Three-Dimensional Geologic Structure

3D perspectives of the geologic structure under the AOI are depicted in Figures 2.10, 2.11 and 2.12, showing the AOI subsurface as an exploded profile, cross-sectional fence plot and a 3D perspective view. The profile view shown in Figure 2.10 shows that the Middle Silt Till Unit is more prevalent on the northern reaches of the AOI. This suggests that the glacial advance that led to the deposition of the Middle Silt Till may have terminated within the AOI boundaries. The irregular surface of the Queenston Formation is also clearly shown in Figure 2.10. The cross-sections of Figure 2.11 portray the continuity of the Glacio-Lacustrine Clay Unit and its thickness in relation to other overburden deposits. Figure 2.12 provides a 3D rendering of the geologic units underlying the AOI. Localized continuity of sand lenses can be inferred from Figure 2.12.

2.2.2.3 Lithologic Descriptions

A detailed evaluation of the geology underlying the AOI was completed based on information provided in over 700 geologic logs created during historical drilling activities at the NFSS, ML, and CWM properties. The elevations of lithologic units were compiled into a site-specific database developed by HGL for this project. The elevations and depths associated with individual geologic units were either determined or confirmed by HGL prior to entering these data into the database. Due to incomplete or missing records, it was not always possible to determine the land surface elevation for all individual borings; consequently, the elevation of the various geologic units could not be determined for all borings. In addition, some boring logs could not be used to aid with the geologic interpretation of the site, because the coordinates for the boring could not be determined. Prior to entering geologic data into the database, HGL evaluated the quality of the individual well logs. If the depth and/or elevation of the geologic units could not be clearly defined based on an individual boring log, the geologic data associated with the log were not incorporated into the database. A summary of the station locations including boreholes, monitoring wells, piezometers etc. that were used in this project is provided in Appendix A.

A description of the physical nature of each of the overburden units is provided below, proceeding from the uppermost (youngest) unit downwards. Isopach maps and elevation contours are utilized to convey information about the spatial extent and thickness of each unit within the AOI. Table 2.3 presents a statistical summary of the lithologic data contained in the database. The statistical summary provided in Table 2.3 includes the mean, standard deviation, and range of thickness of each geologic unit. The large standard deviations and ranges that were calculated for many of the geologic units attest to the heterogeneous nature of the geologic units, which is typical of glacially derived sediments.

2.2.2.3.1 *Fill*

Fill is used to describe all unconsolidated materials above the Upper Clay Till unit. This includes materials that have been altered or deposited by anthropogenic means, surficial soils and recent alluvial deposits, wherever present. Where present, fill materials typically do not

exceed 3 ft (1 m) in thickness, although they have been encountered with up to 19.6 ft (6 m) in thickness in some boreholes.

2.2.2.3.2 Upper Clay Till

The Upper Clay Till is continuous across the AOI and varies in thickness from 1.4 to 42 ft (0.4 to 12.8 m). An isopach map presented in Figure 2.13 depicts the erratic thickness of the Upper Clay Till, and reveals a general trend of increasing thickness toward the northwest, coinciding with the approximate direction of glacial retreat. Thickness anomalies are evident throughout the AOI and while such irregularities are plausible given the depositional environment, data collection errors are not ruled out.

The Upper Clay Till typically consists of brown or reddish-brown clay with significant amounts of silt or sand and interspersed lenses of sand and gravel. Minor cracks and joints have been observed to a depth of approximately 9 ft (2.7 m) below the surface. These are attributed to both isostatic rebound and desiccation from fluctuating water levels.

Borehole locations in which sand lenses greater than 1 ft (0.305 m) in thickness were encountered are shown on Figure 2.14. The upper sand lens elevation with sand lens thickness in parenthesis is shown beside each occurrence to enable visual correlation of sand lenses in close proximity. Sand lenses are not evenly distributed throughout the AOI but are present in clusters forming a swath across the NFSS with only sporadic occurrences on the CWM and ML sites. Comparison should be made between Figures 2.14 and Figure 2.8 (borehole locations) to identify regions without sand lenses and those lacking boreholes. Of the more than 100 sand lens occurrences within the AOI, the average sand lens thickness is 3.8 ft (1.2 m) with a maximum thickness of 17 ft (5 m). A geostatistical analysis of the site was completed to determine the extents of the sand lenses. The results of this analysis are discussed in section 2.4.1. A complete summary of the analysis is included in Appendix B.

2.2.2.3.3 Glacio-Lacustrine Clay Unit

The Glacio-Lacustrine Clay Unit is continuous across the AOI and occurs as either two distinct units separated by the Middle Silt Till, or as a single continuous unit that may or may not be bounded at the top or bottom by the Middle Silt Till. For the current study, the Glacio-Lacustrine Clay/Middle Silt Till complex is simply referred to as the Glacio-Lacustrine Clay Unit. Emphasis is placed on the Glacio-Lacustrine Clay here because the Middle Silt Till is not continuous within the AOI and where it is present, it is typically thin.

The Glacio-Lacustrine Clay Unit varies in thickness from less than 1 ft (0.305 m) to a maximum 30 ft (9 m). Its mean thickness is 16 ft (5 m) based on data from 327 boreholes. The top surface elevation topography (Figure 2.15) and thickness (Figure 2.16) are highly irregular, as attributed to the varying depths of abrasive erosion associated with glacial overriding. Nevertheless, thickness trends emerge from inspection of the isopach map of Figure 2.16. Notably, the Glacio-Lacustrine Clay Unit is consistently thinner near the southeast ML and CWM site boundaries. It is typically much thicker elsewhere including the entire

NFSS property which has an average thickness of approximately 16 ft (5 m), with only one localized depression of 2.5 ft (0.75 m) at borehole OW-10A.

The Glacio-Lacustrine Clay Unit typically consists of a homogeneous gray clay, with occasional laminations of red-brown silt and minor amounts of sand and gravel. The clay is saturated and softer than the overlying Upper Clay Till Unit, as evident by reduced blow counts recorded during soil sampling (Wehran, 1990).

2.2.2.3.4 Middle Silt Till Unit

The Middle Silt Till Unit is usually found sandwiched between layers of the Glacio-Lacustrine Clay Unit, but has also been logged in contact with the Upper Clay Till or with the Alluvial Sand and Gravel Units. The Middle Silt Till Unit occurs exclusively on the northern half of the AOI. The Middle Silt Till Unit is described as gray to gray-brown silt with little sand and gravel. Cobbles and boulders are common. The Middle Silt Till is typically compact to very dense.

2.2.2.3.5 Alluvial Sand and Gravel Unit

Contours representing the top surface of the Alluvial Sand and Gravel Unit shown in Figure 2.17 depict a plateau in the southeastern portion of the AOI, which descends sharply to the northwest by as much as 20 ft (6 m) onto a gently undulating surface over the remainder of the AOI. This phenomenon mimics the topography of the underlying Basal Red Till Unit and shale bedrock. The shape is that of one side of a buried valley trending southwest-northeast.

Spatial coverage of the Alluvial Sand and Gravel Unit is variable, ranging from being absent in places to having a maximum thickness of 25 ft (7.6 m) elsewhere, as shown in Figure 2.18. The thickest portions tend to coincide with depressions of the underlying Basal Red Till Unit or bedrock surface. Wehran (1990) contend that deposits of Alluvial Sand and Gravel Unit filled in topographic lows on the Basal Red Till and bedrock surface and thinly covered topographic highs. The Alluvial Sand and Gravel Unit is absent or very thin over much of the NFSS and its thickest occurrence on the AOI is on the CWM property.

The composition of the Alluvial Sand and Gravel Unit is variable in nature, reflecting the variety of depositional environments of its assumed origin. These include a shallow proglacial lake, glacial outwash and fluvial channels (e.g., Wehran [1979], Golder [1985]). It commonly consists of stratified coarse sands, non-stratified coarse silt and sand or interlayered silt, sand and clay and is usually compact to very dense.

2.2.2.3.6 Basal Red Till

The Basal Red Till underlies the Alluvial Sand and Gravel Unit. This unit is discontinuous throughout the AOI and where present, it is generally thin as shown in Figure 2.19. The contours shown on Figure 2.19 illustrate the heterogeneous nature of the Basal Red Till and highlight several locations on the CWM property where the Basal Red Till is anomalously thick. In particular, a thickness of 21.5 ft (6.5 m) is reported on the CWM property in close

proximity to a borehole where the Basal Red Till Unit does not occur. This depositional variation is supported in part by a comparison of the isopach contours of the overlying Alluvial Sand and Gravel Unit (Figure 2.18) with those of the Basal Red Till. Recall that the outwash channels that led to the deposition of the Alluvial Sand and Gravel Unit are presumed to have eroded the underlying Basal Red Till Unit significantly. Interestingly, on the CWM property the regions where the Basal Red Till Unit is thinnest correspond to those where the Alluvial Sand and Gravel Unit, is thickest.

The Basal Red Till Unit is typically described as dry, very dense, red brown, silt and coarse to fine sand with little gravel and cobbles. Its reddish color and density are characteristic. Clasts in the Basal Red Till are usually lithologically similar to the underlying Queenston shale.

2.2.2.3.7 *Queenston Formation*

The Queenston Formation forms the uppermost bedrock unit that underlies the glacial overburden deposits within the AOI. It consists of a reddish brown fissile shale, described previously in Section 2.2.1. The top surface of the Queenston Formation is somewhat irregular and dips slightly to the northwest. The most prominent feature of the bedrock surface within the AOI is a plateau near the southeastern reaches of the CWM and ML properties, as seen on Figure 2.20. This bedrock structure is evident in the conforming contours of overlying units, such as the Alluvial Sand and Gravel Unit, shown in Figure 2.17.

Most boreholes, however, terminate above the Queenston Formation and as such, the extent of the weathered zone within it is not well characterized. The thickness of the weathered zone is undoubtedly variable, and in some areas portions may have been removed altogether by glacial advance. Wehran (1990) estimates the weathered zone to include the upper 5 to 10 ft (1.5 – 3 m) of the Queenston Formation. This range is in agreement with the findings of Golder (1985).

2.3 HYDRAULIC PROPERTIES

The hydraulic properties associated with subsurface materials largely control the flow of groundwater and migration of contaminants. Consequently, understanding site-specific hydraulic properties is critical to the successful development of a representative site conceptual model and an accurate numerical model for the NFSS. Hydraulic properties of interest include: (1) hydraulic conductivity (2) aquifer storage (storativity and specific yield) and (3) porosity. Of these properties, hydraulic conductivity is the only property required to develop a steady-state, groundwater flow model. Due to the importance of this parameter for subsequent activities, a detailed evaluation of hydraulic conductivity was completed during the development of the site conceptual model. The following section discusses the statistical and spatial attributes of hydraulic conductivity in the glacial sediments and upper bedrock underlying the site.

In order to obtain a better understanding of the hydraulic conductivity associated with each of the primary geologic units, univariate statistics and maps were developed. The univariate statistics were used to evaluate the average hydraulic conductivity and to determine the

expected range in hydraulic conductivity values for each unit. The hydraulic conductivity maps were used to evaluate the spatial distribution of hydraulic conductivity within each unit. The summary statistics and hydraulic conductivity maps were developed using more than 500 hydraulic conductivity measurements that were compiled into the NFSS environmental database developed by HGL as part of this project. These data were obtained primarily from single-well response analyses (e.g., slug tests, bail tests), as well as lab and bedrock packer tests. A statistical summary of these data is presented in Table 2.4, and a complete summary of all hydraulic conductivity test data is presented in Appendix C. The majority of the hydraulic conductivity values measured within the AOI represents hydraulic conductivity in the horizontal direction. There are limited values that represent hydraulic conductivity in the vertical direction.

Values of hydraulic conductivity used in previous modeling studies throughout the AOI are summarized in Table 2.5 and show reasonable agreement with the geometric mean values of hydraulic conductivity from all permeability data within the AOI, for each respective unit.

Glacially derived sediments are typically heterogeneous and those within the AOI are no exception. This is indicated by the relatively large range in values of hydraulic conductivity that are presented in Table 2.4. For example, the hydraulic conductivity associated with the Upper Clay Till and Basal Red Till Units ranges over five orders of magnitude. Table 2.4 presents the geometric mean which was calculated for the hydraulic conductivity data corresponding to each geologic unit. Further discussion of the permeability for each lithologic unit, including its spatial distribution follows.

2.3.1 Upper Clay Till Unit

The overall permeability of the Upper Clay Till is characterized by 326 values of hydraulic conductivity, which vary in accordance with areal variations in lithology. Those values derived from single-well response tests may vary depending on whether the screen interval of the well tested straddles a sand lens or is wholly screened within clay till. Such cases are not distinguished among the 326 measured values; therefore, assuming that both cases are represented proportionately, the geometric mean of 9.1×10^{-3} feet per day (ft/d) (3.2×10^{-6} centimeters per second [cm/s]) (Table 2.4) is probably indicative of the bulk hydraulic conductivity of the Upper Clay Till Unit.

A plot of the spatial distribution of hydraulic conductivity presented in Figure 2.21 illustrates the presence of localized regions of higher permeability among the more widespread regions of lower permeability. Those regions of higher permeability coincide with sand lens locations (shown previously in Figure 2.14), although the converse is not necessarily true. Considering the frequency of sand lens occurrence on the NFSS property, it is somewhat surprising that the hydraulic conductivity is not higher on the NFSS than shown in Figure 2.21. This might be attributed to an absence of sand lenses within the vertical test intervals that were used for hydraulic conductivity testing, underscoring the vertical heterogeneity of the Upper Clay Till Unit.

An exception to the otherwise low hydraulic conductivity of the Upper Clay Till unit on the NFSS, occurs north of the IWCS where a localized high hydraulic conductivity from the presence of sand lenses. In generating Figure 2.21, all hydraulic conductivity data were used, including those which may create higher value zones because of the presence of sand lenses. The resulting map indicates a local hydraulic conductivity high, which is conservative with respect to solute transport because the sand lenses have been demonstrated to be statistically disconnected (Appendix B).

The permeability of the Upper Clay Till on the CWM property is well documented with excellent data coverage clearly depicting the heterogeneity of this unit. The lack of high permeability zones on the CWM property is consistent with the corresponding absence of known sand lenses. Data coverage for the NFSS and ML properties is less extensive and data gaps and uncertainties exist.

2.3.2 Glacio-Lacustrine Clay Unit

Based on five measurements, hydraulic conductivity within the Glacio-Lacustrine Clay has a geometric mean hydraulic conductivity of 9.1×10^{-3} ft/d (3.2×10^{-6} cm/s). This unit is the most homogeneous within the AOI as indicated in Figure 2.22; however, only a few hydraulic conductivity measurements have been performed within this unit. This paucity of data is attributed to the fact that few wells are screened entirely within the low yielding clay. Those wells that straddle the bounding units of the Glacio-Lacustrine Clay Unit typically yield permeability values indicative of the adjacent, more permeable units, and are thus not included in this assessment of the clay conductivity values. Generally, there is insufficient data coverage for this unit to make any sound conclusions. However, based on its observed homogeneity, it can be surmised that the geometric mean probably provides a realistic value of hydraulic conductivity.

As shown in Table 2.4, the geometric mean hydraulic conductivity of the Upper Clay Till and Glacio-Lacustrine Clay are nearly equivalent. The units differ in that the Glacio-Lacustrine Clay is believed to be more homogeneous than the Upper Clay Till, and because of its heterogeneities, the Upper Clay Till has localized regions of higher permeability.

2.3.3 Middle Silt Till Unit

Measured hydraulic conductivity within the Middle Silt Till Unit ranges from 8.5×10^{-5} to 8.5×10^{-2} ft/d (3.0×10^{-8} to 3.0×10^{-5} cm/s) with a geometric mean hydraulic conductivity of 2.8×10^{-3} ft/d (1.0×10^{-6} cm/s) based on seven measurements. Based on this limited data, the hydraulic conductivity associated with the Middle Silt Till is comparable to that of the Glacio-Lacustrine Clay Unit.

2.3.4 Alluvial Sand and Gravel Unit

The Alluvial Sand and Gravel Unit is well characterized by 154 hydraulic conductivity measurements. Measured hydraulic conductivity within the Alluvial Sand and Gravel Unit yields a geometric mean value of 5.4×10^{-2} ft/d (1.9×10^{-5} cm/s). The data coverage is

excellent for the ML and CWM properties, although data gaps exist on the NFSS property, as shown in Figure 2.23. The hydraulic conductivity contours shown on Figure 2.23 reveal the heterogeneity of this unit.

2.3.5 Basal Red Till Unit

Hydraulic conductivity within the Basal Red Till Unit has not been exclusively characterized. Due to its thin and intermittent nature, permeability (well response) tests performed in the Basal Red Till yield values of hydraulic conductivity that may be influenced by adjacent units which may be more (or less) permeable. Available values of hydraulic conductivity have been mapped as presented in Figure 2.24 although the contours may have high uncertainty due to a lack of adequate spatial data coverage.

2.3.6 Queenston Formation

Throughout the AOI, there are 146 hydraulic conductivity measurements that characterize the permeability of the upper weathered zone of the Queenston Formation. Hydraulic conductivity within the Queenston Formation has a geometric mean hydraulic conductivity equal to 6.2×10^{-2} ft/d (2.2×10^{-5} cm/s).

The spatial distribution of hydraulic conductivity, as presented in Figure 2.25, portrays a highly heterogeneous system with localized zones varying more than three orders of magnitude. The heterogeneity of the Queenston Formation reflects the vertical extent of the weathered zone. Of note is the localized region of high permeability on the ML site. Referring back to the contours of the top surface elevation of the Queenston Formation (Figure 2.20), it is evident that this high permeability region corresponds to a local bedrock topographic high.

Insufficient data is available which characterizes the intact Queenston Formation below the weathered surface. It is assumed that the permeability of the intact rock is orders of magnitude less than that of the weathered Upper Queenston Formation.

2.4 HYDROSTRATIGRAPHIC UNITS

The geologic units within the late Pliocene sediments and Ordovician Queenston Formation are classified into hydrogeologic layers depending on their transmissive and storage properties. Groundwater is defined as the water occurring within these hydrostratigraphic units. The water table (upper surface of the saturated zone) defines the upper boundary of unconfined groundwater. Groundwater is said to be under ‘unconfined conditions’ when part of the subsurface material is saturated and the water table is in direct contact with the atmosphere through the spaces within the saturated portion of the subsurface material. When a water-bearing zone is overlain by an impermeable formation (aquitarde), which restricts the upward movement of water through the formation, the groundwater is said to be under ‘confined conditions’. The water level in a confined aquifer is referred to as the potentiometric surface.

The principal hydrogeologic zonation from top to bottom consists of the Upper Water Bearing Zone (Fill and Upper Clay Till Units), an Aquitard confining unit (Glacio-Lacustrine Clay and Middle Silt Till Units), and the Lower Water Bearing Zone (Alluvial Sand and Gravel, Basal Red Till and Upper Queenston Formation). The unweathered Queenston Formation forms a Lower Aquitard. Figure 2.26 presents a schematic depicting the hydrostratigraphic sequences within the AOI. Herein water levels in the Upper and Lower Water Bearing Zones are referred to as separate potentiometric surfaces. By definition, the terminology ‘water table’ could be used to describe the water level in the Upper Water Bearing Zone; however, use of ‘water table’ in this report is reserved for discussions in Section 4 where a distinction from the vadose zone is required.

2.4.1 Upper Water Bearing Zone

The Upper Water Bearing Zone is continuous across the AOI and extends from the land surface (shown previously in Figure 2.2) to the top of the Glacio-Lacustrine Clay Unit (see Figure 2.15). The Upper Water Bearing Zone predominantly consists of the Upper Clay Till Unit, but also includes small amounts of Fill wherever present at the surface. The Upper Water Bearing Zone ranges in thickness from 3 to 42 ft (1.0 to 12.8 m), with a mean thickness of 15 ft (4.6 m) based on 610 borehole locations throughout the AOI.

Differences in lithology and hydraulic properties cause the Upper Water Bearing Zone to be divided into two overlapping hydrogeologic media. These are: (1) continuous, low permeability clays and silts, and (2) embedded, discontinuous pockets of sand and gravel.

Despite the presence of high permeability pathways where lenses of sand and gravel occur the low permeability, interstitial till matrix of the Upper Water Bearing Zone inhibits flow between sand lenses and hinders recharge from precipitation and surface water sources. Essentially, the discontinuity of sand lenses creates immobilized pockets of water and limits the Upper Water Bearing Zone as low yielding from a water supply perspective. Bechtel (1982) utilized ground penetrating radar (GPR), electrical self-potential surveys and test pit excavations to investigate the continuity and extent of high permeability zones. They encountered several sand lenses and concluded that the sand deposits exist as both isolated lenses as well as locally continuous channel deposits. Sand lens occurrences shown previously in Figure 2.14, can be used to infer the continuity of permeability pathways, but are limited to providing data only where boreholes are located.

In 2004, HGL performed a geostatistical analysis to evaluate the spatial distribution of the glacio-fluvial sand lenses within the Upper Clay Till Unit (Appendix B). The objective of this study was to determine whether continuous sand lenses exist beneath the IWCS, potentially providing pathways for preferential contaminant migration. Initially, a qualitative evaluation of lithologic logs collected from borings in the vicinity of the IWCS was conducted to determine whether the physical characteristics of the sand lenses, such as color, thickness, or elevation, could be used to correlate the sand lenses across boreholes. Geologic descriptions were evaluated to identify stratigraphic correlations, using lithologic data primarily from proximal borings. The results of this analysis indicated that the lithologic characteristics of sand lenses observed in proximal boreholes were occasionally similar; however, in many of

these cases there was no correlation in the elevation and/or thickness of the sand lenses. Conversely, several proximal borings were found to have sand lenses that are present at similar elevations but are not consistent in terms of the lithologic characteristics. To supplement the lithologic data collected from boreholes, geotechnical logs recorded during the excavation of a vertical cut-off wall surrounding the IWCS were evaluated. This cut-off wall completely surrounds the IWCS on four sides. The lithologic descriptions of the Upper Clay Till within the excavations indicate that the sand lenses are highly heterogeneous and they vary in color, texture, elevation, and thickness. Moreover, sand lenses do not appear similar between the east and west or north and south cut-off excavation walls; nor do sand lenses appear similar between adjacent excavation walls. Although not independently conclusive, these combined geologic data suggest that the sand lenses within the Upper Clay Till are discontinuous features.

A geostatistical technique referred to as semivariogram analysis was conducted to determine the spatial continuity of the sand lenses (Appendix B). The results of the semivariogram analysis indicate that sand lenses cannot be correlated over distances greater than 20 ft (6.1 m). This analysis strongly suggests that it is unlikely that the sand lenses underlying the IWCS are spatially continuous. Instead, it appears that the sand lenses are discontinuous and cannot be correlated over significant distances. To further investigate this hypothesis, HGL used a geostatistical interpolation method called kriging to develop a 3D depiction of sand lenses in the vicinity of the IWCS. Computer animation was prepared to illustrate the 3D geologic model created using the kriging technique. The results of the kriging indicate that the spatial distribution of sand lenses in the vicinity of the IWCS is discontinuous.

An additional analysis measure evaluated the hydraulic response in wells screened across sand lenses in comparison to wells that are not screened across sand lenses. The premise behind this analysis was that hydraulic responses and water-level elevations in spatially continuous sand lenses may differ considerably from the surrounding finer grained, poorly sorted sediments. Well hydrographs and water-level summary statistics were prepared and evaluated to support this analysis.

A comparison of hydrographs from wells screened across sand lenses indicates that there are marked differences in hydraulic head between proximal wells and in the variability of hydraulic head at proximal locations; this suggests a lack of hydraulic connection between sand lenses. Potentiometric contours generated using hydraulic head data from sand lens wells are generally coincident with contours generated from wells without sand lenses in their screened interval. The general agreement between the contour sets indicate the sand lenses do not comprise an independent flow zone but are influenced by the ambient flow in the Upper Clay Till. Finally, the average standard deviation of hydraulic head for wells without sand lenses along the screened interval was calculated to be 2.81 ft (0.86 m), whereas it was 2.38 ft (0.73 m) for wells with sand lenses. This indicates that the transient water level responses are more similar in wells screened within sand lenses than in those screened in finer grained sediments.

The three-phase analysis conducted on the hydrogeologic data from the NFSS provided the following results:

- Geologic data from boring logs do not exhibit marker beds, color or texture similarities, or other physical data that would definitively correlate sand lenses between proximate or distal borings.
- The results of the variogram analysis indicated that the correlation length in the vertical direction is 4 to 6 ft (1.2 to 1.8 m) and the correlation length in the horizontal direction is only 15 to 20 ft (4.6 to 6.1 m), which is limited relative to the extent of the site, current boring density, and groundwater monitoring coverage. The horizontal variogram had a significant nugget effect suggesting that the sand lenses are randomly distributed and not aerially extensive.
- Water-level elevations and water level responses observed in wells screened across sand lenses do not appear to be correlated, even in wells screened close together. In addition, the hydraulic responses and water-level elevations observed in wells screened across sand lenses do not appear to be significantly different than wells that are not screened across sand lenses. These data suggest that the sand lenses are not hydraulically connected nor respond uniformly to the hydraulic influence of the Upper Clay Till.

These data evaluations together establish that the sand lenses are random and discontinuous. Nevertheless, individually sand lenses may act as small-scale preferential flow pathways limited to 20 ft (6.1 m) in length.

2.4.2 Upper Aquitard

The Glacio-Lacustrine Clay Unit and intervening Middle Silt Till Unit act as an aquitard between the Upper Water Bearing Zone and the underlying units. It is saturated and continuous across the AOI. This aquitard underlies the Upper Clay Till Unit, and overlies the Alluvial Sand and Gravel Unit. It ranges from 1 to 30 ft (0.3 to 9 m) thick, with an average thickness of 16 ft (5 m) based on 327 borehole logs.

2.4.3 Lower Water Bearing Zone

The Lower Water Bearing Zone is the main water-bearing unit within the AOI and consists of three distinct lithologic units: the Alluvial Sand and Gravel Unit, the Basal Red Till Unit and the weathered Upper portions of the Queenston Formation. The Alluvial Sand and Gravel Unit and the Upper Queenston Formation are permeable, fully saturated, water-bearing zones. Conversely, the Basal Red Till Unit has permeability characteristic of an aquitard. The inclusion of the Basal Red Till Unit in the Lower Water Bearing Zone is on the basis of its typically thin or intermittent occurrence, which enables a hydraulic connection between the adjacent, more permeable units. The notion of a hydraulic connection follows in accordance with Acres American (1981) postulation that the Alluvial Sand and Gravel Unit and Upper Queenston Formation function as a single aquifer where the Basal Red Till is absent. In support of this assertion, recent water-level data queried from the database (presented in Section 2.5) show an identical hydraulic response in both units. In areas where the Basal Red Till Unit is thick and continuous, there may be localized regions where the Upper Queenston

Formation and the Alluvial Sand and Gravel Unit may behave as separate aquifers. Further, there are also regions where the weathered portion of the Upper Queenston Formation is thin or non-existent.

The top elevation of the Lower Water Bearing Zone corresponds to the bottom of the Glacio-Lacustrine Clay Unit. The bottom elevation of the Lower Water Bearing Zone corresponds to the transitional zone from a weathered to a more intact, less permeable rock within Queenston Formation. This transition zone is believed to occur within 6 to 12 ft (2 to 4 m) of the top of the Queenston Formation, although some bore logs provide evidence of a much thinner, or even non-existent weathered zone. Detailed information characterizing the top and the bottom of this weathered zone of the Queenston Formation is not available; for the purposes herein, a continuous weathered zone 5 ft (1.524 m) thick in the Upper Queenston Formation is assumed; this a conservative value based on the maximum thickness estimates given by Wehran (1990) and Golder (1985). With this assumption in mind, the overall thickness of the Lower Water Bearing Zone, ranges from 10 to 38.5 ft (3 to 11.7 m) having a mean thickness of 19.3 ft (5.9 m).

2.5 WATER-LEVEL DATA

The following section provides an interpretation and discussion of groundwater flow within and between the Upper and Lower Water Bearing Zones of the AOI. The detailed evaluation of groundwater flow conditions within the hydrostratigraphic units underlying the AOI was developed based on water-level elevation data that were compiled and integrated into the site-specific database developed as part of this study. This database contains over 15,000 water-level elevations that were measured at the NFSS, CWM, and ML sites. These data were collected as part of environmental characterization and long-term monitoring efforts that have been routinely completed at these sites over the past 20 years.

Potentiometric surface contours presented in this section depict the variability of groundwater flow directions and horizontal flow gradients. Hydrographs for all well locations are included with the electronic data in Appendix F-1, and illustrate seasonal fluctuations and historical trends in water levels along with a summary of statistics including the mean annual water level for each well location. Also included in Appendix F-1 are plots showing multiple hydrographs from well clusters and multi-level installations depicting flow trends in different aquifer systems and temporal variations in vertical hydraulic gradients. Tables of vertical gradient calculations are also included Appendix F-1. The interpretations that are discussed in the following text incorporate each of the above, where appropriate.

2.5.1 Upper Water Bearing Zone

The review of water-level data from the NFSS, CWM and ML properties focused on the monitoring events conducted over a 10 year time period, from 1994 to 2004. Given the voluminous amount of water-level data collected during this time period, representative water level conditions were sought. Preference was given to monitoring events with comprehensive coverage, and synchronicity of monitoring dates between the NFSS, CWM and ML.

Unfortunately the dates of water-level measurement were not exactly synchronized between properties; consequently a complete single day snapshot of the potentiometric surface within the AOI is not available. During the time period reviewed, water levels at the NFSS and CWM properties were monitored quarterly while those on the ML property were monitored monthly. The number of water-levels measured for any given monitoring event is also variable. For example, a complete round of water levels on the CWM property consists of measurements at 300 locations, measured in October, whereas only 50 locations are measured during three additional annual monitoring events. The reduced monitoring schedule at CWM is not of use in characterizing flow conditions in the Upper Water Bearing Zone, because either the measured locations were screened in the Lower Water Bearing Zone, or pertinent data such as bore logs or well screen details were not available for the locations monitored.

The two data sets identified best represent high and low water-level conditions were those measured on May 16 and 17, 2000, and September 19 and October 17, 2000, respectively. Contours representing the potentiometric surface of the Upper Water Bearing Zone for these dates are presented in Figures 2.27 and 2.28, respectively. It is noted that the low water level condition was based on data collected one month apart. As a result there is uncertainty associated with the flow directions and water-level elevations from site-to-site. Water levels within the NFSS, or any single site for that matter, however are representative of a single snapshot condition.

The contours depicting high water-level conditions within the Upper Water Bearing Zone lack any consistent flow trends except that water levels are generally higher on the ML property compared to the NFSS property. This observed pattern mirrors surface water flow behavior, which also proceeds from the ML westward to NFSS property via the South-16 and South-31 drainage ditches. On the NFSS property, isolated groundwater lows near, and possibly beneath the IWCS are evident based on water levels collected at the perimeter of the IWCS. Although no wells exist within the boundaries of the IWCS, the apparent low may be attributed to the recharge-inhibiting effects of the clay cap causing locally reduced groundwater recharge.

Groundwater flow trends north of the NFSS and ML properties cannot be established from Figure 2.27 because of the absence of data on the CWM property, although it is likely that overall, the flow regime compares with the regional trend shown in Figure 2.29 whereby flow is generally northwest toward Lake Ontario. The regional groundwater flow map that is presented in Figure 2.29 is the only regional groundwater flow map that was identified during this ongoing investigation. The U.S. Geological Survey (USGS) developed this map in 1949, and unfortunately, there is insufficient information to evaluate the quality of the data that were used to develop this map. Nonetheless, the groundwater flow direction that is identified in this map is consistent with verbal descriptions of groundwater patterns that are described in other reports and with the location of regional groundwater discharge areas (i.e., Lake Ontario). Consequently, the general groundwater flow pattern that is illustrated on the figures appears to be reasonable.

The potentiometric surface of the Upper Water Bearing Zone for low water-level conditions is shown in Figure 2.28. Values of hydraulic head are generally lower than those presented for

high water-level conditions in Figure 2.27. A general trend of flow to the northwest is evident amidst localized variations. The erratic nature of the potentiometric surface is, in part, attributed to the discontinuity of the sand lenses that comprise the transmissive zones of the Upper Water Bearing Zone. Localized heterogeneities and significant contrast in permeability between the clay till and the sand lenses within the Upper Water Bearing Zone contribute to the heterogeneous groundwater flow directions that are illustrated by the potentiometric surface contours. Due to the discontinuous natures of sand lenses, horizontal groundwater flow is most likely limited. Where the sand lenses are not present, flow in the till is probably predominantly vertical.

To further investigate mechanisms of groundwater flow in the AOI, vertical hydraulic gradients between the Upper and Lower Water Bearing Zones were calculated from well clusters and multi-level installations within the AOI. Vertical gradient calculation results are summarized in Table 2.6; tables containing additional calculation details are included in Appendix F-1. Note that a positive gradient indicates downward flow.

The average hydraulic gradient for high water-level conditions is 0.106, indicating downward flow from the Upper Water Bearing Zone to the Alluvial Sand and Gravel Unit of the Lower Water Bearing Zone. The corresponding average gradient for low water-level conditions is equal to 0.006, which is significantly less, suggesting that high water-level conditions exert considerably more downward flow pressure, as would be expected. The marked contrast in the average values between the vertical gradients of high and low water-level conditions attest to the seasonal variation of flow within the Upper Water Bearing Zone.

A review of individual values of vertical hydraulic gradient for high water-level conditions (Table 2.6), reveals that downward flow occurs at all multi-level locations except OW-7A, whereas for low water-level conditions, both upward and downward flow gradients are noted at several wells. In a search for spatial phenomena that influence the magnitude or direction of vertical gradients, it was found that the thickness of the Glacio-Lacustrine Clay Unit might be a factor. For example, the largest downward gradients on the NFSS property occur at OW-1, OW-2 and OW-14 through OW-18, which overlie a thick zone of the Glacio-Lacustrine Clay Unit on the western fringe of the IWCS. The thickness of the clay in this region might induce a greater buildup of pressures than in areas where the clay is thinner. This might be the case, although mounding of recharge caused by runoff from the IWCS probably also augments the downward gradient in this vicinity. Looking elsewhere within the AOI, another example can be found among the east-west aligned R-series of wells on the CWM property, where the highest downward gradients occur for wells overlying the thickest clay deposits.

Actual flow through the Glacio-Lacustrine Clay Unit can be approximated using estimated values of hydraulic conductivity and vertical hydraulic gradient and applying Darcy's Law. For such estimates, the low hydraulic conductivity of the Glacio-Lacustrine Clay ensures that the actual flow rates through the clay will be minimal for even the highest gradients observed.

For all well pairs on the NFSS listed in Table 2.6, a reduction in the vertical gradient is evident from high water-level to low-water level seasonal conditions. Low-water level conditions are characterized by reduced groundwater recharge and it is therefore expected that

the vertical gradients would be lower at this time when the potential for build up of hydraulic heads is less. For some well pairs, however, during low water-level conditions an outright reversal to upward vertical gradients is observed. Upward gradients suggest that the confined pressures of the underlying Alluvial Sand and Gravel Unit may control vertical flow direction during low water levels. Whereas the largest downward gradients were observed to occur where the Glacio-Lacustrine Clay Unit is thick as reported above; the largest upward gradients do not necessarily occur where the Glacio-Lacustrine Clay Unit is uncharacteristically thin. Well pairs exhibiting the largest upward gradients (OW8, 9, 11 and 12) all have a reported Glacio-Lacustrine Clay Unit thickness > 10 ft and in the case of OW8, the GLC is >25 ft. OW8, 9, 11 and 12 are all located along the eastern flank of the IWCS, east of the CDD, and unlikely to be impacted by e.g. cessation of IWCS irrigation.

Note that the water levels normally show a seasonally driven variation in vertical gradients. The Upper Water Bearing Zone shows the greatest variation, commonly averaging 2-3 feet from quarterly conditions across the site; several locations may vary up to 10 feet depending on dry-season dynamics and soil-moisture deficits. This site-wide annual variation is more subdued in the Lower Water Bearing Zone, usually averaging ~1 foot (nearing 2 feet during wet years). This Upper Water Bearing Zone head variation drives the vertical gradient “reversals” that over time commonly average as balanced to downward gradients, although some areas show only slight vertical gradients.

The analysis of groundwater flow in the Upper Water Bearing Zone presented thus far has focused on water-level data collected for discrete time periods. To supplement the water level analysis and investigate temporal variations in water level elevations, hydrograph plots of historical water-level data were prepared. Appendix F-1 contains hydrographs for all water levels recorded in the AOI throughout 1994 to 2001. These hydrographs reveal pronounced patterns of seasonal water level oscillation for both Upper and Lower Water Bearing Zone wells on the ML property. A representative example is given by ML well SP-4M, screened in the lower water-bearing zone, (see Appendix F-1), which has an annual water-level high that occurs in April – May, and a corresponding low that occurs in the fall. The amplitude of the oscillations at SP-4M (and elsewhere) is typically on the order of two or more feet per year (0.61 or more m/year). These seasonal oscillations, with peaks and valleys occurring during May and October respectively, confirm May and October as representative of high and low water-levels conditions.

Other pertinent observations from a review of the hydrographs include the fact that some water levels vary as much as 10 ft (3 m) over the 6 year period displayed (e.g., NFSS well OW-12B). This extreme variability is most common in Upper Water Bearing Zone wells and is attributed to the small specific yield of the Upper Water Bearing Zone and the fact that the Upper Water Bearing Zone directly receives precipitation recharge, which infiltrates into the subsurface during precipitation events.

Historical trends in vertical hydraulic gradients are presented in the multi-level hydrograph plots of Appendix F-1. For the 6 year period shown, vertical gradients between the Upper and Lower Water Bearing Zone on the NFSS property can be categorized into those that display generally downward gradients and those which have very erratic gradients. For wells such as

OW-1, 2, 3 and others, downward gradients predominate with occasional short-lived gradient reversals occurring during months of low water levels. Wells OW-5, 8, 9 and 10 display highly erratic gradients with prolonged and significant gradient reversals. Generally the water levels in the Upper Water Bearing Zone tend to be more temporally variable than those in the Lower Water Bearing Zone, and dictate much of the variability of the vertical gradients. Despite the erratic patterns observed in some wells, seasonal oscillations tend to follow a regular pattern.

Vertical gradients observed from multi-level wells on the CWM property (Appendix F-1) are historically downward with minor seasonal oscillations. On the ML property, gradient trends are comparable to those observed on the NFSS property whereby gradients are generally downward, but seasonal reversals are common and some wells display highly erratic water-level patterns.

2.5.2 Lower Water Bearing Zone

Contours showing the Lower Water Bearing Zone potentiometric surface as of May 16 through 17, 2000, are presented in Figure 2.30. A general trend of flow to the northwest is clearly evident with the largest horizontal gradients occurring south of the NFSS and on the southern ML property. The largest horizontal gradients coincide with a region of steep decline in the bedrock surface (Figure 2.20). Several local variations in the flow direction are evident, including an east to west flowing component from the ML to NFSS properties.

The potentiometric surface as of September-October 2000, is presented in Figure 2.31 and shows a similar northwest lateral flow trend to that observed in May 2000. Water levels are comparable or slightly lower than those observed in May 2000. The Lower Water Bearing Zone is of significantly higher permeability and lateral continuity than the Upper Water Bearing Zone. Indeed, the lateral flow regime of the Lower Water Bearing Zone also is more clearly defined.

Multi-level wells straddling the Basal Red Till Unit were utilized to assess vertical gradients between the Alluvial Sand and Gravel Unit and the Queenston Formation. Nearly all available wells exist on the ML site, as shown in Table 2.7, which summarizes vertical gradient calculation results.

The average vertical hydraulic gradients are positive, indicating an overall trend of downward flow to the Queenston Formation. Upward flow, denoted by negative gradients, occurs at select wells and in some cases this gradient trend is consistent between May and September through October conditions. Negative gradients only occur where the Basal Red Till is present, although the converse is not necessarily true. This indicates that the Basal Red Till may act as a semi-confining unit where present.

Independent of other analyses, the varying degree of interaction between the Alluvial Sand and Gravel Unit and the Queenston Formation might suggest that these units are distinct flow systems separated by the confining Basal Red Till Unit. However, further investigations of historical multi-level plots (Appendix F-1) reveal that the water levels in these units respond in

unison, behaving as a single aquifer and not as two separate independent aquifers. Evidence of the synchronized water-level response throughout the Lower Water Bearing Zone is presented in several of the multi-level hydrograph plots of Appendix F-1. Multi-level wells PZ-8, 15 and 18 on the ML property, G-2 on the CWM property, and BH-61/62 on the NFSS all demonstrate the simultaneous water-level response. At many of these well locations, the presence of the Basal Red Till Unit does not preclude a hydraulic connection between the Alluvial Sand and Gravel and Upper Queenston Formation. It is noted that vertical gradients alone do not warrant division of the Lower Water Bearing Zone into separate flow systems, as vertical gradients are quite common within both confined and unconfined aquifers.

The multi-level hydrograph plot for ML PZ-18 (Appendix F-1) clearly depicts the independent water-level response within the Upper and Lower Water Bearing Zones. Water levels from screened intervals in the Alluvial Sand and Gravel Unit and the Queenston Formation respond in unison to pumping from mid-1996 to 1999. The pumping stress in the Lower Water Bearing Zone does not affect water levels in the Upper Water Bearing Zone despite the increase in downward vertical hydraulic gradient.

2.6 WATER BUDGET

The main components of a water budget include precipitation, runoff, evapotranspiration and infiltration. Values of precipitation from NOAA measured in Lewiston, New York, were reported in Section 2.1.1 as having an annual average of 29.7 in (75.4 cm). Other water budget components can be estimated based on theoretical, analytical or empirical methods. For example, the Thornthwaite-Holzman equation (Viesmann et al., 1989) provides an estimate of evapotranspiration losses incorporating vapour pressures, wind speeds and temperature differences. This section presents a summary of the values of water budget components from historical investigations and regional studies to generate a range of values for each component, and is shown in Table 2.8.

A water budget performed by Golder (1985) for the CWM property uses a precipitation value of 32.2 inches per year (in/yr) (81.8 centimeters per year [cm/yr]). They estimated runoff and evapotranspiration as 9 and 21.8 in/yr (22.9 and 55.4 cm/yr), respectively. They assumed infiltration to be negligible (0.1 in/yr (3.05×10^{-2} m)) with sublimation of snow making up the difference.

Wehran (1990) conducted a water budget for the ML property. Based on an average annual precipitation of 35.7 in/yr (90.7 cm/yr), the estimated runoff was 10.7 in/yr (27.2 cm/yr), infiltration was estimated to be 0.15 in/yr (0.38 cm/yr), and evapotranspiration was estimated to be 24.85 in/yr (63.1 cm/yr).

The USGS's Northeast Glacial Aquifers Regional Aquifer-System Analysis project (Lyford et al., 1984; Lyford, 1986; Lyford and Cohen, 1988) generated regional maps (Randall, 1996), which incorporate stream flow records from 503 watersheds and precipitation data from 483 weather stations. For the AOI, the maps report precipitation as approximately 32 in/yr (81.3 cm/yr), runoff as 20 in/yr (50.8 cm/yr) and evapotranspiration as 12 in/yr (30.5 cm/yr). Based on these estimates, the net precipitation recharge rate is essentially negligible.

The range of values for each of the components is quite narrow which lends credibility to the chosen representative values. The AOI is characterized by high evapotranspiration, moderate runoff and minimal infiltration. These annual averages are expected to vary considerably throughout the year despite the somewhat regular monthly rates of precipitation (Section 2.1). This is because the rates of evapotranspiration are significantly greater during summer months and the propensity for runoff is greatest during the spring when water levels are highest and soils are saturated. Streams and water filled ditches within the AOI are likely receiving groundwater during the spring and early summer months while discharging in the summer, fall and winter months. The low effective porosity and high capillary potential of the Upper Clay Till inhibits water movement into and out of the Upper Water Bearing Zone restricting recharge in the spring and evapotranspiration in the summer and fall.

2.7 SUMMARY OF HYDROGEOLOGIC CONCEPTUAL MODEL

The site conceptual model that was presented in Section 2.0 provides the framework for the groundwater flow and solute transport model that is discussed in Sections 3 and 4. The following text provides an overview of key elements of this conceptual model that were incorporated into the numerical model.

The system under study is a multi-layered system consisting of the following stratigraphic units:

- Fill,
- Upper Clay Till,
- Glacio-Lacustrine Clay,
- Middle Silt Till,
- Alluvial Sand and Gravel,
- Basal Red Till, and
- Upper Queenston Formation.

The Upper Clay Till Unit comprises the Upper Water Bearing Zone. The primary lithologic unit is the Upper Clay Till which is characterized as clay till with localized occurrences of sand lenses. Results from a geostatistical evaluation on the interconnectivity of the sand lenses (Appendix B) suggests that the sand lenses are predominantly isolated, disconnected features. Where devoid of sand lenses, the hydraulic properties of the Upper Clay Till are representative of an aquitard and thus the term ‘aquifer’ is not used. Flow in the Upper Water Bearing Zone generally proceeds toward the northwest with localized and seasonal variations. On the NFSS the Upper Clay Till lacks a contiguous, dominant flow system. Vertical gradients in the Upper Water Bearing Zone are typically downward, but vary depending on the season and localized lithologic variations.

The Upper Water Bearing Zone accepts recharge throughout most of the AOI, however, the low permeability of near-surface materials, abate recharge to the Upper Water Bearing Zone and result in a swampy landscape with poor surficial drainage. Discharge to the surface occurs in creeks, ditches and swamps. On the NFSS, the Central Drainage ditch is the main

water carrying channel and is supplied from the east by the South-31 drainage ditch, which has water in it year round (pers. communication with Dennis Rimer, USACE), and the South-16 drainage ditch which carries less water than the South-31 ditch. The West Drainage ditch flows parallel and west of the Central Drainage ditch. Swamps are present for much of the year, though in the summer they may be dry between 'O' and 'N' streets in the northeastern portion of the NFSS.

The Glacio-Lacustrine Clay/Middle Silt Till Units form an aquitard and confine the Lower Water Bearing Zone. This aquitard is continuous across the site, saturated and of a homogeneous nature. The Lower Water Bearing Zone consists of the Alluvial Sand and Gravel, and Upper Queenston Formation. The Basal Red Till serves as a secondary, discontinuous aquitard which further confines localized zones of the Upper Queenston Formation. Flow in the Lower Water Bearing Zone is to the northwest, with localized deviations due to lithologic heterogeneities. Seasonal influences do not have the pronounced impact on flow directions as is typical of flow in the Upper Water Bearing Zone. The Lower Water Bearing Zone has a greater transmissivity than the Upper Water Bearing Zone. Within the Lower Water Bearing Zone, the Alluvial Sand and Gravel Unit and the Upper Queenston Formation exhibit similar temporal water-level responses. This observation coupled with the fact that the Basal Red Till is thin and discontinuous across the AOI supports the assumption that the lithologic units comprising the Lower Water Bearing Zone system are hydraulically connected. Vertical gradients in the Lower Water Bearing Zone are generally downward from the Alluvial Sand and Gravel Unit to the Upper Queenston Formation with localized exceptions. The Lower Water Bearing Zone is recharged by a combination of connate water from the Queenston Formation, recharge from regional sources and to a lesser degree, recharge through the overlying Glacio-Lacustrine Clay within the AOI.

This page was intentionally left blank.

3.0 GROUNDWATER FLOW MODEL

3.1 METHODOLOGY

A numerical groundwater flow model was constructed for the NFSS and surrounding region based on the conceptual site model described in Section 2. The model was calibrated to inferred steady-state conditions, based on average water levels from four different time periods. Sensitivity analyses were performed to identify the effects of uncertainties in model parameters, such as hydraulic conductivity and recharge, on the model results.

3.2 PREVIOUS MODELING STUDIES

At least four modeling studies have been completed within the AOI:

- 3D Flow Modeling of the ML Property, Wehran-New York, 1990-1991;
- 3D Flow and Transport Modeling of NFSS (Bechtel National, 1994);
- One-dimensional (1D) Transport Modeling on CWM Property (RUST, 1995); and
- Two-dimensional (2D) Flow Modeling of CWM Property (GeoTrans, 1996).

Wehran-New York, Inc. completed the first numerical modeling investigation in the AOI (Wehran-New York, 1990). For this study, MODFLOW was used to construct a 3D groundwater flow model to assess the adequacy of the environmental monitoring program on the ML property. The model domain extended 500 ft (152 m) outside the ML property boundaries and had a uniform grid spacing of 200 ft (61 m). Vertically, three model layers were included to represent three primary water-bearing units: (model layer 1) the Upper Glacial Till and Fill Deposits, (model layer 2) the Silty Sand Outwash (referred to in this report as the Alluvial Sand and Gravel), and (model layer 3) the weathered Queenston Formation bedrock. Aquitards were simulated by setting the appropriate vertical conductance values between layers. A general-head, or head-dependant flux boundary was prescribed along each lateral boundary and a no-flow boundary was assigned to the bottom of the model. A recharge rate of 0.1 in/yr (0.25 cm/yr) was prescribed to model layer 1. Model layers 1 and 3 were treated as homogeneous, whereas heterogeneities were assigned to model layer 2. The model was calibrated to hydraulic head data collected on February 13, 1990, and subsequently applied to simulate the effects of proposed excavations and drainage installations on groundwater flow. The model was deemed most sensitive to vertical conductance of layer 1.

The Wehran-New York model was further updated with new borehole log information in 1991 and applied to support engineering design and hydrogeologic evaluation of the South Property (Wehran-New York, 1991). Specific modeling objectives were to compute flow rates for pore water drain sumps, determine groundwater flow directions during the pre- and post-closure period, and define a potential contamination plume for a hypothetical liner leak. This modeling exercise included the development of a solute transport model using the two-dimensional MOC model developed by the USGS (Konikow and Bredehoeft, 1978). The

solute transport model was used to predict the migration of chloride during post-landfill closure for a total of 30 years.

Groundwater flow and contaminant transport modeling on the NFSS was conducted by Bechtel National, Inc. to evaluate the long-term impact of radium-226 and thorium-230, the primary radionuclides in the K-65 waste containment area (Bechtel, 1994). A 3D MODFLOW model was constructed and calibrated to the averaged 1988-1989 hydraulic head data. Vertically, five geological units (Brown Clay, Gray Clay, Sand and Gravel, Red Silt and Weathered Queenston Shale) were represented by six model layers. The model was then used to represent a long-term average flow field to simulate radionuclide migration during the next 10,000 years. The model domain covered an area 7,130 ft by 7,130 ft (2.2 by 2.2 km), and centered on the IWCS. Mesh discretization ranged from 25 ft (10.7 m) near the source area to 250 ft (76 m) elsewhere with 3,136 cells in each of the six model layers. The eastern and western boundaries of the model were designated as no-flow, while constant heads were prescribed along the northern boundary. A constant flux boundary condition was used along the southern boundary and a no-flow boundary was prescribed along the model bottom. Net recharge of 0.0035 in/yr (0.00889 cm/yr) was applied uniformly over the entire model domain.

Rust Environment and Infrastructure carried out 1D transport modeling on the CWM property (RUST, 1995) using the U.S. Environmental Protection Agency (USEPA) MULTIMED model (Salhotra *et al.*, 1995) to determine the extent and rate of contaminant transport from on-site sources. The screening-level modeling effort concluded that given the relatively long distances from the contaminant source areas to the property lines as well as the relatively low conductivity of the subsurface lithology, groundwater contamination should not exceed New York State drinking water standards.

Also on the CWM property, GeoTrans, Inc. developed a one-layer model to simulate pulsed pumping at a groundwater extraction well (Golder, 1996). A model of flow within the Upper Clay Till was constructed to examine the feasibility of operating a pump with a pulse-pumping remediation system. A recharge rate of 0.00175 in/yr (0.00445 cm/yr) was applied to the top of a one-layer model in this study.

The modeling effort that is the focus of this report expands upon the scope of previous modeling investigations. The incorporation of water-level, lithologic, and hydraulic conductivity data from the NFSS, ML, and CWM properties into a comprehensive database management system allowed the model to be expanded beyond the boundaries of the NFSS property. Moreover, due to advances in computational capabilities, the size and resolution of the model exceeds that of previous studies.

3.3 MODEL CONSTRUCTION

3.3.1 Code Selection

MODHMS, an enhanced version of MODFLOW-SURFACT (HGL, 1996), was used to simulate groundwater flow at the NFSS and the surrounding area. MODHMS offers additional modules to the USGS groundwater flow code MODFLOW and was written by HGL to enhance MODFLOW's modeling capabilities. The USGS program MODFLOW (McDonald and Harbaugh, 1988) is thoroughly documented; widely used by consultants, government agencies and researchers; and is consistently accepted by the regulatory and scientific community. MODFLOW has been rigorously tested and verified, and a variety of software tools are available for both pre- and post-processing. Given the intended use of the NFSS groundwater flow model as a decision-making tool, regulatory acceptance is vital for any code selected for this study. Because MODHMS is based on MODFLOW, the benefits of its wide acceptance are realized, in addition to the additional features of MODHMS.

MODHMS was selected because of its versatile simulation features. MODHMS can simulate transient or steady-state groundwater flow in three dimensions and offers a variety of boundary-condition options, including specified head, areal recharge, injection or extraction wells, evapotranspiration, drains, rivers or streams, and horizontal flow barriers, all of which can have values which vary both spatially and temporally. Aquifers simulated by MODHMS can be confined or unconfined, or convertible between confined and unconfined conditions. The model domain consists of a multi-unit system with variable hydrogeologic unit thicknesses and boundary conditions. MODHMS's 3D simulation capability and boundary-condition versatility are essential for the proper simulation of groundwater flow conditions within the AOI. While all of these features are available in MODFLOW, MODHMS has further advantages that overcome some of the limitations of MODFLOW. MODHMS has mass conservative, state-of-the-art transport solution routines available for use in the subsequent analyses of contaminant migration and risk. Its advanced features include capability for simulation of complex radiological chain decay processes that account for both decay and ingrowth of parents and daughters, and simulation of the solubility-limited release of contaminants from the IWCS. Typical modeling approaches not accounting for a solubility-limited release would overestimate contaminant concentrations originating from the sources areas. Other advanced features of MODHMS include (1) an approximation of flow through the unsaturated zone precluding the necessity to re-wet model cells; (2) the use of robust and efficient numerical methods to reduce simulation time, including Newton-Raphson linearization and an efficient Preconditioned Conjugate Gradient (PCG) solver; (3) assignment of vertical hydraulic conductivities (K_z) instead of leakances. Many of the capabilities of MODHMS are unique and not available in other commercial or public domain 3D flow and transport simulators. Such features are essential for accurately simulating groundwater flow and contaminant transport at the NFSS.

MODHMS has undergone rigorous testing to verify the numerical techniques and simulation capabilities of each model. The testing program, common to each code, consists of three levels. Level I testing simulates five problems for comparison against available analytical solutions; Level II testing evaluates seven practical problems with complexities (e.g., material heterogeneity

and transient water table and pumping conditions); Level III code testing evaluates reproduces field observations from actual field applications and previous modeling studies. MODHMS has been widely accepted by the scientific community, and has been used by consultants, government agencies, and researches (Panday et. al., 2004; Fontaine et. al., 2003; Langevin et. al., 2003; Tsou et. al. 2003; Young et. al., 2003). MODHMS is widely accepted and used for flow and transport modeling studies by regulators across North America including, but not limited to the Department of Defense, California Bureau of Reclamation, South West Florida Water Management District.

3.3.2 Model Discretization

The finite-difference technique employed in MODHMS is identical to that in MODFLOW. To simulate the distribution of hydraulic head in multi-layered systems, each continuous hydrogeologic unit was discretized both areally and vertically into a set of cells or blocks. The result was a 3D model grid that represents the computational domain. In the block-centered, finite-difference formulation used in MODHMS, the center of each grid block corresponded to a computational point or node. When MODHMS solved the set of algebraic finite-difference equations for the complete set of blocks, the solution yielded values of hydraulic head at each node within the 3D grid.

Water levels computed for each block represented an average water level over the volume of the block. Thus, adequate discretization (i.e., a sufficiently fine grid) was required in order to generate a solution at a desired scale. This need for a fine grid, however, must be balanced with computational costs, given that a large number of simulations are required during the calibration process and sensitivity analyses. With this in mind, MODHMS, like MODFLOW, allowed the use of variable grid spacing, with a finer grid in areas of interest where greater resolution was warranted and a coarser grid in areas that require less detail. Variable grid spacing has been used to refine the cell sizes in the vicinity of the NFSS to provide increased computational detail in this area of interest. Cells in this area are 25 ft (7.6 m) on a side. Larger cells (to a maximum of 250 ft (76 m) on a side) were used farther from the NFSS where the same degree of accuracy is not required.

The 3D grid developed for the groundwater flow model, shown in Figure 3.1, extended over an area covering approximately 60 mi² (152 km²). The model domain extended approximately 7.7 mi (12.3 km) from the eastern to the western boundary and 7.7 mi (12.3 km) from the northern to the southern boundary. The model domain has been extended beyond the boundaries of the AOI to take advantage of the well-established natural boundaries of Lake Ontario and the Niagara River. This was done with the presumption of aquifer properties in large regions of the model where very little field data have been collected. The following advantages of using a larger grid are highlighted: (i) the larger computational domain would not excessively increase the computational burden of the flow model; (ii) increased model coverage will ensure that potential off-site receptors will be within the model domain during subsequent long-term solute transport simulations; (iii) use of natural boundaries are preferred to arbitrarily assigning MODFLOW general head boundaries because they can be more readily quantified and substantiated; and (iv) the influence of model boundaries on simulation results in the vicinity of the NFSS is minimized. These advantages outweigh the primary

disadvantage of making assumptions pertaining to the hydrostratigraphy outside the AOI, where there is a paucity of data. This assumption is not of consequence to our efforts that focus within the AOI; however, it may be restrictive for the predictive ability of the model outside the AOI.

The finite-difference grid consisted of 296 columns and 294 rows with four layers for a total of 261,072 grid cells or nodes, with 230,349 active cells. The groundwater flow model was oriented N15°W such that the principal axis of the model grid conforms to the approximate regional groundwater flow direction.

The four model layers are designed to simulate groundwater flow in each primary hydrogeologic units encountered within the study area. Model layers are assigned hydraulic parameters to represent the lithologies encountered during field investigations. The model layers are:

- Model layer 1: Upper Water-Bearing Zone (Upper Clay Till);
- Model layer 2: Upper Aquitard (Glacio-Lacustrine Clay and Middle Silt Till);
- Model layer 3: Lower Water-Bearing Zone (Alluvial Sand and Gravel);
- Model layer 4: Lower Water-Bearing Zone (Upper Queenston Formation).

The Basal Red Till Unit is not considered as a unique model layer but included in the model by assigning a vertical conductance between layers 3 and 4, where present. Figure 3.2 shows two cross-sections of the model domain through the NFSS property. The model layering and its correspondence with hydrostratigraphic layering is shown in Figure 2.26 (presented earlier).

The topography of the computational domain was delineated from a digital elevation model (DEM) (USGS, 2001a; 2001b). The topography is generally flat-lying and slopes southeast to northwest (i.e., from the escarpment towards Lake Ontario). Near Lake Ontario, several creeks, including Fourmile and Sixmile, cut through the landscape, resulting in topographic depressions. Where steep depressions occurred, the topography in the model was manually adjusted to avoid problems associated with non-adjacent finite difference grid cells. The actual level of surface water features in these areas were represented in the model by boundary conditions (discussed in Section 3.3) and model cells above the stage of a given creek or surface water feature were simulated to be dry, as the water table will naturally conform to the boundary condition prescribed to represent the surface water feature.

The top of the Upper Queenston Formation was defined using information from previous investigations within the AOI, public water supply well logs, and published reports by the USGS and other agencies. Much of this information is contained in the NFSS database. A uniform thickness of 5 ft (1.5 m) was assumed for the weathered zone of the Upper Queenston Formation throughout the computational domain. For the internal three interfaces (between layers 1 and 2, layers 2 and 3, and layers 3 and 4), a considerable amount of data is available for the AOI from boring logs entered into the NFSS database. Point data from the database were queried and used to generate surface contours that were subsequently imported into the model. Distant from the AOI, where data are sparse or non-existent, it was assumed that each of the three layers represents approximately one-third of the total thickness of the domain. This trend of equal thickness was based on thickness ratios observed within the AOI.

3.3.3 Boundary Conditions

MODHMS accommodates a variety of boundary condition options, which can be used to facilitate the incorporation of both natural and anthropogenic boundaries in the model. Natural boundaries simulated by the model include the Niagara River, Lake Ontario, Niagara Escarpment, groundwater divides, recharge from precipitation, and rivers and streams. These boundary conditions are summarized below.

3.3.3.1 External Boundaries

The northern model boundary was prescribed as a constant head condition, to represent the water level in Lake Ontario. Historical data from gauging stations near the model domain at Olcott and Rochester, New York and Port Weller, Ontario (Figure 3.3), were reviewed to determine the an appropriate steady-state water level value.

At the Rochester gauge station, lake level measurements have been recorded daily from 1970 to 2001 and monthly at Port Weller from 1960 to 2001. The Olcott station has approximately 1 year of daily measurements. Table 3.1 shows average water levels from the three gauging stations. Following a review of the available data, the representative steady-state average lake level was calculated from the Rochester and Port Weller data sets as 245.45 ft (74.8 m) amsl. This value was prescribed in the model to represent the level of Lake Ontario.

The western boundary of the computational domain was defined by the Niagara River, which generally flows from south-to-north and empties into Lake Ontario. The Niagara River is represented in the model using constant head boundary conditions. The southernmost reach of the Niagara River (upstream) in the model domain has been assigned a value of 249.6 ft (76.1 m) amsl. This results in a head-drop of approximately five ft. along this section of the Niagara River, which is consistent with contours observed on the 1:25,000 topographic map of the area (USGS, 1980).

The constant head values for both Lake Ontario and the Niagara River were assigned to finite-difference cells in all three model layers where the elevation of the cell is less than the respective water level.

The eastern boundary of the computational domain was assigned along an assumed regional groundwater flow line. The easternmost model coordinate is 1,064,201 ft NAD83 easting. As described in the Section 2, regional flow in the area of the computational domain appears to be from southeast to northwest, towards Lake Ontario. Accordingly, a no-flow boundary was used to represent this boundary.

The southern boundary of the model coincided with the Niagara Escarpment, and was represented in the model as a no-flow boundary, on the basis that the overburden in this area thins out and lies against the bedrock of the escarpment. The southernmost model coordinate is 1,150,565 ft NAD83 northing.

3.3.3.2 Precipitation Recharge

The model simulated recharge from precipitation using a prescribed-flux boundary condition along the uppermost active layer of the model. The spatial distribution of recharge within the model domain was primarily based on land use/land cover (LULC) data obtained from the USEPA BASINS database containing watershed and GIS layers (HUC #04130001). Results of a soil survey of Niagara County (Higgins et al., 1972) were also reviewed, but did not provide sufficient differentiation between soil types to warrant further recharge subdivision.

Utilizing the LULC data, six recharge zones were prescribed throughout the model area. In order from highest to lowest recharge, these include:

- Field/transitional areas;
- Agricultural farmlands;
- Swamp lands and ponded areas;
- Forested areas;
- Roads and residential areas; and
- IWCS.

The values and spatial extent of each recharge zone are presented in Figure 3.4 and Section 3.4.3.1 presents a discussion on the values prescribed in the model to these zones which were determined during the calibration process.

3.3.3.3 Surface Water

Head-dependent flux conditions were used in the model to represent Fourmile, Sixmile and Twelvemile Creeks as well as associated tributaries and drainage ditches on the NFSS, as depicted in Figure 3.1, which include the Central, West, South-31 and South-16 drainage ditches. The model has been designed to simulate these head-dependent fluxes using MODFLOW “drain cells”. Drain cell boundaries compute the flow into a surface-water feature as a function of the head difference between the drain elevation and the hydraulic head simulated in the aquifer adjacent to the drain. The drain elevations used in the model are derived from 1:25,000 topographic maps (USGS, 1980).

For each drain cell in the model, constant drain width and drain-bed thickness were assigned, equal to 10 ft and 3 ft (3 m and 0.92 m), respectively. These values are believed to be within an expected range typical of the regional creeks and on-site ditches in the model area. Drain lengths were determined based on the distance between midpoints of adjacent drain cells.

Drain cells allow groundwater to flow into them; however, if the simulated water level falls below the drain elevation, the drain becomes inactive, and water is not removed from the model domain. This type of flow behavior is characteristic of surface water features flowing over low permeability soils, as evident with the Upper Clay Till within the AOI.

3.3.4 Hydraulic Conductivity Zonation

The contoured hydraulic conductivities of the Upper Clay Till presented previously in Figure 2.21 (and discussed in Section 2.1.1) were used as the basis for defining the heterogeneous hydraulic conductivity zonation of the Upper Water Bearing Zone in model layer 1. Using Figure 2.21, five zones of hydraulic conductivity were determined to represent the Upper Water-Bearing Zone as shown in Figure 3.5 with values ranging from $10^{-6.5}$ to 10^{-3} cm/s (0.0009 to 2.8 ft/day respectively). Each zone spans an order of magnitude of field-measured hydraulic conductivity values. Sand lenses are not represented as discrete features in the model, but their presence is accounted for through the use of zones of higher hydraulic conductivity, wherever areas of sand lens occurrence coincide with higher hydraulic conductivity. Flow in the vicinity of localized sand lens clusters is therefore represented conservatively (from a solute transport perspective) compared to the use of a single-value geometric mean hydraulic conductivity.

The Upper Aquitard in model layer 2 is represented as homogeneous with a horizontal hydraulic conductivity of $10^{-6.5}$ cm/s (0.0009 ft/day).

The Lower Water Bearing Zone model layers 3 and 4 are also represented as homogeneous both with a horizontal hydraulic conductivity value of $10^{-5.5}$ cm/s (0.08 ft/day). Although reported values of hydraulic conductivity throughout the AOI range nearly four orders of magnitude for the Lower Water Bearing Zone, the distribution of measured hydraulic conductivity in the vicinity of the NFSS is somewhat homogeneous and representative of the geometric mean. Higher measured values to be isolated and away from the NFSS and for the objectives of this study do not warrant the use of separate subzones. Moreover, where areas of lower measured values exist on the CWM property they are represented more conservatively from a solute transport point of view by the geometric mean.

The Basal Red Till unit, where present, was accounted for in the model as a quasi-3D layer. Its vertical conductance was determined using:

$$\text{Vertical Conductance of BRT} = \frac{1}{\sum \frac{\Delta z}{K_z}}$$

where Δz is the distance between the bottom of the Alluvial Sand and Gravel Unit and the top of the Queenston Formation; and K_z is the vertical hydraulic conductivity of the Basal Red Till unit. The vertical conductance is input into the model to describe the vertical flow leakage between the overlying Alluvial Sand and Gravel Unit and underlying Queenston Formation. Use of a vertical conductance term is appropriate for relatively thin, low permeable layers in which flow is expected to be predominantly vertical between two geological units. The resulting implicit quasi-3D layer avoids having to define another layer within model and the related computational burden of doing so.

Measurements of vertical hydraulic conductivity have been performed for most of the hydrogeologic units at the NFSS and the available values are summarized in Table 2.4. Overall the quantity of vertical hydraulic conductivity data is limited. The Alluvial Sand and Gravel Unit and Queenston Formation have the most reported values, at 16 each. This is significantly less than the hundreds of measurements available for horizontal hydraulic conductivity. The geometric mean of the vertical hydraulic conductivities, when divided into the geometric mean values of corresponding horizontal hydraulic conductivities listed in Table 2.4, yield K_x/K_z anisotropy ratios of approximately one-tenth and one-one hundredth for the Alluvial Sand and Gravel and Upper Queenston Formation, respectively. This shows agreement with Anderson and Woessner (1992), who cite one-tenth as a typical value for K_x/K_z anisotropy. To be consistent with what is considered typical, and remain within the range of determined NFSS values, in all four model layers, anisotropy was added such that the vertical hydraulic conductivity was one-tenth of the value of horizontal hydraulic conductivity.

3.4 GROUNDWATER FLOW MODEL CALIBRATION

3.4.1 Model Calibration Methodology

Calibration of a flow model is a process whereby model parameters and/or boundary conditions are adjusted to obtain a satisfactory match between observed and simulated water-level elevations and/or other field observations. Typically, model parameters such as hydraulic conductivity, boundary conditions, the magnitude and spatial distribution of precipitation recharge, constant head and drain elevation values, and the conductance of the drains are adjusted during the calibration process. For optimum results, a model is calibrated to discrete water-level measurements instead of a contoured potentiometric surface to avoid interpretive bias or erroneous artifacts of the contouring (Anderson and Woessner, 1992).

The principle of parameter parsimony is adhered to during model calibration whereby the number of model parameters adjusted is kept to a minimum. Adjustment of excessive parameters during calibration may yield combinations of model parameter values that produce equivalent (i.e., non-unique) calibration results. By following the principle of parameter parsimony, our goal is to mimic general trends and avoid over-fitting. Throughout this approach, information gathered for the conceptual model was used to guide any decision to add model parameters (e.g., zones of hydraulic conductivity or recharge) to the model during the calibration process. Therefore, in the absence of hydrogeologic evidence that supports the inclusion of additional zones, the simpler model is used.

The primary criterion for evaluating the calibration of a groundwater flow model is the difference between simulated and observed water levels at a set of calibration targets (typically monitoring wells). A residual or model error, e_i , is defined as the difference between the observed and simulated hydraulic head measured at a target location:

$$e_i = h_i - \hat{h}_i$$

where h_i is the measured value of hydraulic head and \hat{h}_i is the simulated value at the i^{th} target location. A residual with a negative sign indicates over-prediction by the model (i.e., the simulated head is higher than the measured value). Conversely, a positive residual indicates under-prediction.

There are several useful statistics that are commonly used to gauge the success of the model calibration process. During the calibration process, an objective is to minimize the residual sum of squares (RSS) while still honoring the field data:

$$RSS = \sum_{i=1}^n (e_i)^2$$

where n is the total number of calibration targets. The RSS is a primary measure of model fit. The root mean squared (RMS) error, which normalizes the RSS by the number of calibration targets, is defined as follows:

$$RMS = \sqrt{\frac{RSS}{n-1}}$$

The RMS is useful for comparing model calibrations with different numbers of calibration targets and estimated parameters. Another calibration measure is the mean of all residuals (\bar{e}):

$$\bar{e} = \frac{1}{n} \sum_{i=1}^n e_i$$

A mean residual significantly different from zero indicates model bias.

The calibration process used for this project was primarily manual but was augmented with automated calibration. Manual calibration included performing a series of individual simulations with MODHMS in order to improve the model calibration. Parameters that were changed during this process included the spatial distribution of recharge, values of hydraulic conductivity and the conductance and stage of the drain boundary conditions.

Automated calibration tasks were carried out using the groundwater parameter estimator and optimization model, Parameter Estimation Software Tool (PEST), (Doherty et al., 1998). PEST utilizes the Gauss-Marquardt-Levenberg algorithm, iterates through multiple groundwater flow solutions and identifies the optimum values of pre-selected parameter values that minimize the hydraulic head residual. PEST was used in conjunction with MODHMS to identify zonal values of hydraulic conductivity and recharge that minimize the head residual. The resulting optimized values determined by PEST were used to guide manual calibration decisions-making.

3.4.2 Calibration Targets

Calibration targets were calculated as the average water level from four measuring periods: Spring 2000, Fall 2000, Spring 2001, and Fall 2001, and only wells that included measurements during all four of these periods were included. These average data provided a better representation of quasi-steady-state conditions than data from any single time period because the averaging process included two years of data with seasonal highs and lows (spring and fall). The resulting calibration data set consisted of 108 water levels, or calibration targets, which are presented in Table 3.2.

Figures 3.6 through 3.9 present the calibration targets and estimated potentiometric surfaces for each model layer. Inspection of these figures indicated that the spatial coverage of the calibration targets throughout the AOI is best in layer 3, whereas coverage is mostly limited to the NFSS in model layers 1 and 2. The lack of coverage outside the NFSS in model layers 1 and 2 was due in part to a requirement that the water level averages are included only when data is available from all four spring/fall time periods. A value was included in the calibration dataset only if a water levels from all four spring/fall time periods were available. This ensured that the averages were not biased to a particular season or monitoring event. Consequently this reduced the number of available locations where a calibration datapoint could be calculated. For example on the CWM property the October monitoring event measured more than 300 water levels. Many of these did not have a corresponding spring water level and so were not included in the calibration dataset. Reasonable calibration data coverage was achieved throughout the NFSS.

Due to the nature of the low hydraulic conductivity materials that primarily constitute the Upper Water Bearing Zone, localized, single time period water levels tend to be highly erratic and may differ significantly throughout the year. Review and inspection of single time period data for the Upper Water Bearing Zone, shown previously in Figures 2.27 and 2.28, confirm the highly variable nature of water level measurements. For example, groundwater mounding on the ML property near landfills is evident in October 2000 (Figure 2.28) for the Upper Water Bearing Zone, however, this mounding was not apparent in May 2000 (Figure 2.27). The difficulties in discerning clear trends in the single time period events in the Upper Water Bearing Zone is exacerbated by a general scarcity of spring water level data, particularly on the CWM property.

Flow trends are somewhat clearer for the Lower Water Bearing Zone single time period events, shown previously in Figures 2.30 and 2.31, where a general northwesterly flow trend is evident. These single time period events show that locally, flow on the ML and CWM properties was predominantly north-northwestern while flow across the NFSS tended west to the northwest.

The four-event, two-year average water level calibration dataset better represents steady-state conditions than any single monitoring event. The averaged dataset tend to smooth out localized anomalies, attributed to short-term influences, or possible monitoring error. In smoothing out anomalies, the general flow trend emerges, and is believed to be indicative of steady-state conditions.

3.4.3 Calibration Results

Hundreds of model simulations were performed during the calibration process. During these simulations, the following parameters were adjusted: (1) magnitude and areal distribution of recharge; (2) magnitude and distribution of hydraulic conductivity in layer 1; (3) hydraulic conductivity in layers 2, 3, and 4; and (4) conductance for drains in the vicinity of the AOI.

3.4.3.1 Calibrated Hydraulic Parameters

The average precipitation over the AOI based on data from the NOAA is 29.7 in/yr (75.43 cm/yr). However, because of the low permeability of the Upper Clay Till Unit, only a small percentage of this precipitation infiltrates through the vadose zone to recharge the Upper Water-Bearing Zone.

Previous modeling efforts (described in Section 3.2) employed a single uniform recharge rate, whereas for the approach herein, zones of alternate recharge rates were assigned based primarily on LULC. The calibrated values of recharge assigned to each LULC are presented in Figure 3.4, and relate proportionately between LULC categories as one might expect (e.g. ponded areas > agricultural areas > forest, etc.). The assigned recharge values, however, are low, ranging from 3.4×10^{-4} to 2.8×10^{-2} in/yr (8.5×10^{-4} to 7.0×10^{-2} cm/yr). These low values of recharge reflect the low permeability of the Upper Clay Till. Previous modeling studies have reported similarly low recharge values [e.g., 3.5×10^{-3} in/yr (8.9×10^{-3} cm/yr)], Bechtel (1994) and 1.75×10^{-3} in/yr (4.4×10^{-3} cm/yr), Golder (1996). Only Wehran-New York (1990) used a significantly higher value of recharge [0.1 in/yr (0.25 cm/yr)], but, as pointed out in Bechtel (1994), the values of hydraulic conductivity of the Upper Clay Till Unit used by Wehran-New York were increased by a factor of 100.

Values of precipitation recharge applied to the CWM property, which is categorized almost wholly as 'field/transitional area' LULC type, were increased above the regionally-applied value for this LULC type to account for additional recharge-enhancing features observed in air photos of the property such as the presence of trenches dug down to the Glacio-Lacustrine Clay unit, open fields and a general lack of surficial drainage.

At drain cells throughout the model, creeks were assigned a bottom hydraulic conductivity of 1×10^{-3} ft/d (3.53×10^{-7} cm/s) and ditches were assigned a lower value of 1×10^{-4} ft/d (3.53×10^{-8} cm/s). These values were estimated during the model calibration process. The basis for the lower conductivity assigned to ditches stems from the fact that ditches are relatively recent features typically dug out of the Upper Clay Till, whereas creeks are typically older, have more accumulation of coarse sediment deposits and in some cases have cut through the stratigraphic layers. Some of the upstream portions of creeks were also assigned a value of hydraulic conductivity equal to 1×10^{-4} ft/d (3.5×10^{-8} cm/s). The drains, particularly those representing ditches, were shallow and as a consequence were not expected to affect hydraulic heads deeper in the system.

The calibrated values of hydraulic conductivity for each hydrogeologic unit represented in the model closely match the geometric mean of available field measured data. The resultant

calibrated values differ from the field measured K values by no more than one order of magnitude.

The calibrated hydraulic conductivities of the Upper Water-Bearing Zone range from 9×10^{-4} to 2.8 ft/d (3.2×10^{-7} to 1×10^{-3} cm/s), as presented in Figure 3.5. Values of hydraulic conductivity were calibrated for each of the five Upper Water Bearing Zone heterogeneity hydraulic conductivity values presented in Section 3.3.4, and incorporated into the model using 11 heterogeneity zones. The calibrated values of hydraulic conductivity assigned to all zones are equal to, or within an order of magnitude of the geometric mean hydraulic conductivity of each respective zone. As shown in Table 3.3 eleven zones of hydraulic conductivity were assigned to model layer one to accommodate the spatial variability of the five heterogeneity zones presented in Figure 3.5. For each Upper Clay Till zone, the resultant calibrated values of hydraulic conductivity were equal to or greater than the target values. The model area outside the AOI (model zone 5 in Table 3.3) was assigned a uniform value of hydraulic conductivity equal to 8.2×10^{-3} ft/d (2.9×10^{-6} cm/s), which closely matches the overall bulk geometric mean value of the Upper Clay Till.

A uniform value of hydraulic conductivity was assigned to represent each of model layers 2, 3 and 4 as homogeneous hydrogeologic units. The target calibration hydraulic conductivity value for each model layer was the geometric mean of field data measurements. The resultant calibrated values are all within an order of magnitude of the geometric mean values, as presented in Table 3.3. For example, the resultant calibrated value of hydraulic conductivity assigned to represent the Glacio-lacustrine Clay (model layer 2) was 9.0×10^{-4} ft/d (3.18×10^{-7} cm/s), which is an order of magnitude less than the target value based on the geometric mean of field-measured data. This value is in agreement with literature-based values for silty-clay units.

3.4.3.2 Model Calibration Results

Model calibration was primarily done manually. PEST simulations were performed for the purpose of guiding manual calibration parameter selection and identifying critically sensitive parameters. PEST simulations evaluating K were held within two orders of magnitude of mean of field measured values. PEST simulations evaluating recharge rates were bounded by minimum and maximum values up to two orders of magnitude apart.

The bulk of the calibration simulations focused on varying recharge. Because recharge was low (< 1 in/yr (< 2.5 cm/yr)), small changes in recharge had a significant effect on the simulated hydraulic heads. Field studies have not been conducted at the NFSS or surrounding area to quantify precipitation recharge; consequently, it had to be estimated during the calibration process. In comparison, there are many direct measurements of hydraulic conductivity across the NFSS, CWM and ML properties. As such, the distribution of hydraulic conductivity is better understood than the distribution of precipitation recharge. The assumption was made that the small-scale measurements of hydraulic conductivity are representative of hydraulic conductivity at the field scale.

The primary calibration objective for the groundwater flow model was to minimize the RMS (Eq. 3) computed for the 108 water-level calibration targets, which is a measure of how well the simulated hydraulic heads match the observed hydraulic heads. Table 3.2 lists the simulated water elevations and model residuals for each calibration target. The maps of simulated hydraulic head (Figures 3.10 through 3.13) show the spatial distribution of the residuals and the modeled hydraulic heads in each of the four calibrated model layers. Figure 3.14 illustrates the simulated regional groundwater flow field for model layer 4 (Upper Queenston Formation).

Throughout the model domain the absolute residuals ranged from 0.02 to 4.04 ft (6.1×10^{-3} to 1.23 m) (Table 3.2). The majority of the water level absolute residuals (i.e., 90 out of 108) were less than 1 ft (0.30 m), and there are few absolute residuals (i.e., 6 out of 108) higher than 2 ft (0.61 m). Residual statistics for the calibrated groundwater flow model indicate that there was good agreement between simulated and measured groundwater elevations. The residual mean was close to zero [-0.097 ft (-0.03 m)] indicating that there was not a significant bias that causes the model to systematically over-predict or under-predict water-level elevations across the model domain. In addition, the residual standard deviation [1.315 ft (0.40 m)] was less than 2 percent of the range of simulated water-level elevations for the entire model domain, and less than 12 percent of the range found on-site. A plot of the simulated versus observed hydraulic heads of the calibration dataset is presented in Figure 3.15. Perfect agreement between simulated and observed heads results in a plotted value on the line $y=x$, which is also shown in Figure 3.15 for use as a point of reference. Overall the calibrated model demonstrates excellent agreement to the observed heads throughout the range of observed values across the NFSS. The vast majority of points fall within the 95% [± 2.6 ft (0.79 m)] confidence bounds. Particularly for model layer 3 where the bulk of calibration points reside, the calibrated model shows excellent agreement to observed heads. As can be inferred from Figure 3.15, the observed head range of the calibration dataset is approximately 10 ft (3 m).

In Figures 3.10 to 3.14, a negative residual indicates that the model over predicts the hydraulic head for a given well. For example, the target hydraulic head at A52 is 312.31 ft amsl, whereas the computed value is 312.99 ft amsl, for a residual of -0.68. Close inspection of the residuals in the vicinity of the IWCS reveals that the model tends to over-predict the hydraulic heads near the CDD (e.g. A45 in model layer 1; A50 and A51 in model layer 2) and under predict the heads near the WDD (e.g. OW1B, OW2B and OW3B in model layer 1; and OW3A and BH49A in model layer 2). This artificial head differential may cause horizontal gradients toward the NFSS west boundary that are greater than observed data would otherwise suggest. With respect to solute transport, this artificial gradient may yield more conservative estimates of concentration movement toward the NFSS west boundary.

A water budget of model inflows and outflows was prepared using the calibrated model. The significant model inflow (i.e. source of water to the model) is precipitation recharge [304.4 ft/d (0.11 cm/s)], while the constant heads along the upstream portion of the Niagara River contributes a small amount [4.5 ft/d (1.59×10^{-3} cm/s)]. Model outflow occurs to constant head cells (e.g. Niagara River and Lake Ontario) [198.8 ft/d (7.0×10^{-2} cm/s)] and the creeks and ditches within the AOI represented by drain boundaries [110.1 ft/d (3.9×10^{-2} cm/s)]. The discrepancy between inflows and outflows (i.e., mass balance error) is less than 0.01%.

3.4.4 Particle Tracking Analysis

The upper few feet of the Upper Queenston Formation shale is typically fractured and weathered as a result of glacial or pre-glacial activities. Deeper within the Upper Queenston Formation, the shale is generally considered to be intact and free from extensive fracturing, however, the occasional, isolated deep bedrock fractures is known to exist resulting from glacial loading, tectonic activity or other geologic processes. Figure 3.16, illustrates regional fractures in western New York. Figure 3.17 presents a zoomed in view showing bedrock fractures in the local vicinity of the NFSS.

Based on the available data, there are no known bedrock fractures in the Upper Queenston Formation underlying the NFSS that would compromise the integrity of the IWCS. Additionally, magnetotellurics and seismic reflection surveys were conducted on the NFSS in 2001 that confirmed the lack of any major, deep-seeded faults, fractures, geologic discontinuities, or seismic pressure points in the Queenston Formation and underlying Precambrian Basement within the surveyed areas (SAIC, 2003a).

As part of a lineament analysis to evaluate hypothetical transport of contaminants through known offsite bedrock fractures, particle tracking was employed in conjunction with the calibrated flow model. Results from a particle tracking analysis can be used to infer transport of a conservative tracer, without dispersion or diffusion. Since the extent and hydraulic character of the regional fracture systems were not field verified or measured, this particle-track comparison is informational and fractures are not considered as part of the baseline case conditions.

Three particle tracking simulations were performed. The first simulation considered the movement of water particles across the calibrated flow field without any fractures. Particles were released at the northwestern corner of the NFSS boundary, which is the closest upgradient location to a known fracture. This baseline case simulation predicted a water particle to move in the direction of water flow, eventually discharging into the Niagara River after approximately 10,000 years, as shown in Figure 3.18. Particle movement through the Upper Clay Till is shown in black in Figure 3.18, followed by a short travel time through the Glacio-Lacustrine Clay denoted in red, travel through the Alluvial Sand and Gravel in black again, and finally particle movement through the Upper Queenston Formation in red.

To evaluate the influence of bedrock fractures on the flow solution, the calibrated flow model was modified to account for the presence of known fractures downgradient from the NFSS. Each fracture was assigned a hydraulic conductivity contrasting the calibrated Upper Queenston Formation by (a) one order of magnitude and (b) two orders of magnitude. Arbitrary estimates of fracture K were used in the absence of any data characterizing hydraulic properties of the fractures. Flow simulations were performed for each of the two fracture cases. Particle tracking was then performed for both fracture cases and the Base Case calibrated flow field, for a particle originating at the northwest corner of the NFSS property

The addition of the fractures caused the simulated flow field to differ slightly compared to the calibrated flow field case. The net result was that the groundwater flow gradient became

slightly steeper for cases with fractures. In particular, for the case where hydraulic conductivity of the fractures was two orders of magnitude greater than that assigned to the Queenston Formation, the flow field showed preferential flow into the fractures.

Flow solution and particle tracking results for the case of a fracture having a one order of magnitude contrast in hydraulic conductivity are presented in Figure 3.19. Upon encountering the fracture, the water particle is slightly deflected from its travel course shown in the baseline case. Two additional fractures are encountered enroute to eventual discharge into the Niagara River and each also slightly deflects the path of the water particle. Evidently a one order of magnitude difference in hydraulic conductivity relative to the Upper Queenston Formation is not sufficient to reroute water movement wholly into the fracture. It is noted that because of the slightly steeper gradients, the particle traces reach the fracture sooner than the Base Case.

Particle tracking results for fractures having a two order of magnitude difference in hydraulic conductivity are presented in Figure 3.20. In this case, the particle is diverted into the fracture and continues to follow the fracture until discharge into Lake Ontario. Discharge into Lake Ontario, though farther from the Niagara River, is predicted to occur sooner than 10,000 years, which was the predicted time of discharge for a fracture in the Niagara River under baseline case conditions.

4.0 SOLUTE TRANSPORT MODEL

4.1 INTRODUCTION

4.1.1 Origin of Primary Contaminant Sources

Beginning in the 1940s (National Research Council [NRC] et al., 1995; USDOE, 1986) and continuing until 1953 (Bechtel, 1996) various radioactive residues, wastes and other contaminated materials were received and stored at the NFSS. Although no chemical or mechanical processing operations at the NFSS resulted in the generation of radioactive wastes or residues, some ancillary wastes were generated on site. These may include soil or other material contaminated in the process of moving received wastes from place to place; personal protective equipment contaminated by its use in handling the residues; and construction debris that came in contact with the residues.

The radioactive residues, though accounting for a fraction of the total volume of contaminated materials stored in the IWCS, constitute the bulk of the isotopic inventory and are a key focus of the transport modeling efforts. The waste residues were derived from processing of uranium rich ores, shipped from the former Belgian Congo (now Zaire) by the African Metals Corporation. Uranium was extracted from the ores for testing and research purposes commissioned by the Manhattan Project. Uranium ore by-products remaining after extraction and processing were stored on the NFSS. Wastes and residues are classified according to the U_3O_8 content of the ores from which they were recovered. The richest uranium ore yielded the K-65 residues and contain the highest residual levels of Radium (Ra) -226 and Thorium (Th) -230. The K-65 residues were placed in a storage silo on site, as an interim storage measure prior to being transferred (hydraulically mined) from the silo to the IWCS. Other residues stored on the NFSS include the L-30, F-32 and L-50; each of these were manually transferred from their on-site storage locations to the IWCS. The U_3O_8 content of each residue is summarized in Table 4.1.

In addition to the residues resulting from processed uranium ore, various non-residue radiological materials and other contaminated materials were also stored at the NFSS. Bechtel (1996) summarize probable contaminant sources, including: uranium metal billets (rods) manufactured at the Simonds Saw and Steel Company plant in Lockport, NY; radioactive wastes from the Knolls Atomic Power Laboratory in Niskayuna, NY, the University of Rochester, in Rochester, NY, MED/AEC Middlesex Sampling Plant in Middlesex, New Jersey; miscellaneous wastes from the Harshaw Chemical Company in Cleveland, Ohio, Electromet in Niagara Falls, NY, Eldorado Mining and Refining Ltd. in Port Hope, Ontario, Allegheny Ludlum Steel Company in Watervliet, NY, and Vitro Corporation of America in Grand Junction, Colorado.

From 1979 to 1980, Battelle (1981) performed a comprehensive characterization and hazard assessment of the residues, wastes and radioactive materials stored at the NFSS. The results prompted the USDOE to mandate interim remedial actions to consolidate and immobilize all

sources of contamination on the NFSS. In accordance, from 1982 through 1986, residues were transferred from the waste storage silo to reinforced concrete cellars of former Buildings 410, 411, 413 and 414. Additional contaminated soils and materials were added to an existing waste pile, referred to as the R-10 waste pile.

K-65 residues were stored in an interim storage silo prior to transfer (hydraulic mining) to Bay A. Following completion of K-65 residue transfer, the silo was demolished. During demolition of the silo, some of the soils surrounding the silo were contaminated with K-65 residue contamination from the inside of the silo, including a small volume of K-65 residue remaining at the bottom of the silo that could not be slurried out. From this, a definition of Tower Soils: those soils near the silo that were contaminated with K-65 residues during the demolition of the silo. The Tower Soils were placed in Bay D and only Bay D of Building 411.

IWCS-based constituents of concern identified during the Baseline Risk Assessment (SAIC, 2006) include select radionuclides from the U-238, U-235 (Actinium) and Th-232 (Thorium) series; Arsenic (As), Barium (Ba), Boron, Iron, Molybdenum (Mo) and Manganese (Mn) metals.

4.1.2 IWCS Design and Operation

The IWCS, an in-ground repository, was constructed to enclose the residue-filled basements of Building 411, 413, 414 and the R-10 pile wastes.

The bulk of NFSS wastes, in terms of volume and toxicity, are emplaced within the IWCS. The design of the IWCS incorporates several key features to mitigate transport of the wastes via groundwater, surface water, atmosphere or other pathways. Design features include a compacted clay cutoff wall keyed into the underlying Glacio-Lacustrine Clay unit; a compacted clay dike; an interim cap and an environmental monitoring program.

The 1,700 ft (518.5 m) cutoff wall/dike was constructed in 1982 and 1983 and extends from the former Building 411 to enclose the R-10 waste pile (Figure 4.2). Originally, remedial measures were to be limited to construction of a dike only; however, during initial construction activities, sand lenses were discovered in the Upper Clay Till, which prompted additional construction of a cutoff wall. The cutoff wall serves to prevent solute migration below the dike via sand lenses. Comprised predominantly of clay fill, the cutoff wall is a minimum of 12 ft wide, extends through the full thickness of the Upper Clay Till (9 to 22 ft (2.75 to 6.71 m) in height) and is keyed at least 1 to 2 ft (0.30 to 0.61 m) into the Glacio-Lacustrine Clay unit (Bechtel, 1986). The compacted clay dike was constructed on top of and sometimes off-center of the clay cutoff wall. It measures approximately 10 ft (3.05 m) high, with an embankment slope ratio of 2:1 (Bechtel, 1986). Collectively, the cutoff wall and dike inhibit the lateral migration of wastes outside of the IWCS.

The interim cap was constructed from 1984 through 1986 to provide a barrier against the migration of water into the contaminant area and to retard radon emissions generated from the wastes. The cap consists of approximately three feet of compacted clay, one foot of soil and

six inches of topsoil draped over the cutoff wall/dike system (Bechtel, 1986). Measuring approximately 1000 ft (305 m) by 450 ft (137.25 m) the cap defines the areal extent of the IWCS and occupies 8.5 acres (3.5 ha). To preserve the condition and operating function of the cap, regular maintenance is performed including grass cutting, visual inspection, general cap maintenance (crack repair), fertilizing, seeding and irrigation.

The environmental monitoring program at the NFSS ensures the IWCS is functioning as designed and that the stored wastes do not pose a threat to human health and the environment. A technical memorandum issued annually by the USACE summarizes the performance of the IWCS. Under monitoring program protocols, monitoring data is collected, interpreted and compared to historic data and trends. Currently the following data are collected: external gamma radiation, radon gas, radon-222 flux from the IWCS, various groundwater field parameters (specific conductivity, dissolved oxygen, redox potential, turbidity, temperature, pH), metals and radionuclides in groundwater, surface water and sediment. In addition, water levels are monitored throughout the NFSS with manual measurements collected on a quarterly basis.

4.1.3 Additional Sources of Contamination

In addition to sources emplaced in the IWCS, additional and potential sources of groundwater contamination have been characterized elsewhere on the NFSS.

Residual contamination has been identified in NFSS soils and is a potential threat to groundwater quality through leaching of contaminants through the unsaturated zone. The concentrations in soil have been characterized according to exposure units (EU) defined in SAIC (2006) based on administrative considerations and available data, as shown in Figure 4.1. Within each EU, soil-maps depicting the known or believed extent of soil contamination were determined. Soil-based constituents of concern identified during the Baseline Risk Assessment (BRA) (SAIC, 2006), include select radionuclides from the U-238 and U-235 series, arsenic, boron, cadmium, antimony metals and methylene chloride. The soil plume maps will be presented in the forthcoming revised NFSS Remedial Investigation Report (SAIC and Tetra Tech, 2006).

Contamination has also been reported in shallow groundwater (i.e., Upper Water Bearing Zone) at various locations on the NFSS. Point locations of contamination in groundwater have been contoured, and plume maps of known areas of water quality concern have been generated. Constituents of concern include U-238 and U-235 series constituents, boron, Mn, bis(2-ethylhexyl)phthalate, perchloroethene (PCE), trichloroethene (TCE), DCE and vinyl chloride (VC). The plume maps are presented in the NFSS RI Report (SAIC and Tetra Tech, 2006).

4.1.4 Transport Modeling Objectives

The waste sources discussed above may pose a future threat to human health and the environment if transported in sufficient quantity, through exposure pathways including: leaching through the vadose zone to the water table; migration of contaminants in

groundwater; or discharge to surface water. Such threats provide the impetus for solute transport modeling, and substantiate the primary objective of this study: to develop a 3D transport model and apply the model to predict the potential for future contaminant migration under probable (baseline) and worst-case scenarios.

There are multiple secondary objectives of this study. Application of the transport model also serves to quantify the risks associated with contaminant migration. Model results may identify areas which may be vulnerable to contaminant migration and water quality hazards. Transport model results may also provide insight into the effectiveness of the IWCS throughout and beyond its design life, and help ascertain the degree of protection provided by the current cap and individual waste containment components. Furthermore, transport model results identify the highest priority contaminants of concern, those which are likely to yield the largest plumes, the highest concentrations and those which may migrate beyond the NFSS property boundary.

The transport modeling effort encompasses the development of a 3D transport model and its application to simulate the following:

- Leaching and migration of radiological residues, waste, contaminated soil and other material in the reinforced concrete cellars of former Buildings 411, 413/414 in the IWCS;
- Leaching and migration of contaminated soil and other contaminated materials of the former R-10 waste pile in the IWCS;
- Vertical transport of constituents of concern contained in unsaturated soil to the water table;
- 3D migration of several contaminant plumes currently observed in groundwater; and
- Future migration of constituents of concern currently contained in the IWCS or surrounding soils through regional groundwater flow within the saturated zone.

A baseline case and three worst case scenario failure events were simulated (Section 4.5). Sensitivity analyses were performed to quantify the affect of transport model input parameter uncertainty on the model results.

The following section provides details on the transport modeling approach, organized according to the steps required to define various contaminant sources at the water table, and the approach used to simulate solute migration in the unsaturated zone.

4.2 TRANSPORT MODELING APPROACH

4.2.1 Source Term Modeling

This section introduces the modeling approach undertaken to develop two time-varying source terms for the 3D NFSS transport model. These two source terms describe (1) contamination leaching from IWCS-based contaminants; and (2) contamination leaching from soils. A third source term, contamination from groundwater plume maps, was assigned as an initial

condition and did not require modeling prior to assigning in the 3D model and is therefore not discussed here. The initial condition prescribed to represent groundwater plume maps is discussed in Section 4.4.2.3.

To define and accurately represent the IWCS sources of contamination in the 3D model, the modeling approach consisted of two pre-processing steps. First, the rates of water movement through the unsaturated layers of the IWCS were quantified. Secondly, the mass flux prescribed to the water table was determined based on the predicted water flux.

The water flux through various waste zones in the IWCS was estimated using the USEPA Hydrologic Evaluation of Landfill Performance (HELP) model (Schroeder et al. 1994). The HELP model is specifically designed to conduct water balance analyses of landfills, cover systems, and waste containment facilities and its application herein to predict the water flow through the layered waste zones in the IWCS is therefore appropriate. Application of the HELP model in this regard is well documented (e.g. Berger et al. (1996), Berger (2000), Yalcin and Demirer (2002), Dho et al. (2002), attesting to the suitability of its application herein. Application of the HELP model provided an estimate of the leakage through the IWCS, based on known waste zone layering, engineering design parameters and pertinent information regarding vegetation, precipitation, cover soils and other variables impacting flow through the system.

HELP model application was limited to IWCS waste zones, including Bays A, B, C, D of former Building 411, former Building 413 and 414, and the R-10 pile. The locations of these waste zones are shown in plan view in Figure 4.2. Elsewhere on the IWCS and NFSS property, the HELP model was not used to predict the water flux through the unsaturated zone. The precipitation recharge rates that were estimated during the groundwater flow model calibration efforts provided a reasonable approximation of vertical groundwater flow rates in these areas.

Flow rates predicted by the HELP model were input into a MODHMS 1D transport model to predict the vertical movement of contaminants through the unsaturated zone within the IWCS to the water table. The MODHMS model accounts for advective transport, dispersion, sorption, degradation and in the case of radionuclides, radioactive decay and the transport of both radioactive parent and daughter products. The model simulates the release of contaminants from sources within the unsaturated zone and the transport of these contaminants to the water table. Where concentrations were known to be in excess of solubility limits, the MODHMS solubility-limited simulation option was invoked to account for continuous dissolution of contaminants in soil and residues, and limit predicted concentrations to at or below the solubility limit. The 1D MODHMS model results provided a time-varying source term, for each IWCS waste zone, representative of concentrations at the water table derived from the transport of contaminants through each waste zone.

Contamination reported in unsaturated soils outside the IWCS constitutes an additional source term for the 3D transport model. To account for this contaminant source, the seasonal soil compartment model (SESOIL) (Bonazountas and Wagner, 1981, 1984; Hetrick et al. 1993) was applied to predict the contaminant flux to the water table. SESOIL is a 1D vertical

transport model for unsaturated soil zones for use in determining solute distribution in soil profiles. The SESOIL modeling was conducted for each soil plume map identified in the baseline risk assessment (SAIC, 2006). For each soil plume map, a single set of initial contaminant concentrations in soil and transport parameters were specified in the SESOIL model. The SESOIL model was then used to provide conservative time-variant constituent concentrations at the water table. The predicted constituent concentrations were conservatively assumed to homogeneously represent the entire soil plume map. If the SESOIL model results indicated that a particular constituent may pose an unacceptable future risk, then that constituent was carried forward in the subsequent 3D model. The SESOIL model results provided a time-varying source term, for each soil plume map, representative of concentrations at the water table derived from the leaching of contaminants in soil. The SESOIL modeling was conducted by SAIC as part of the BRA effort (SAIC, 2006).

Additional details on the HELP and 1D MODHMS model setup and application are provided in Section 4.3. Details of the SESOIL model approach and methodology are summarized in SAIC (2006).

4.2.2 Solute Transport in the Saturated Zone

The transport model was based upon the calibrated, saturated flow system of the four-layer NFSS 3D groundwater flow model described in Section 3. The transport model shares the same model domain as the groundwater flow model, and is capable of simulating solute transport on both local and regional scales in three dimensions.

Three source terms were assigned in the 3D transport model: two time-varying concentration sources (introduced in Section 4.2.1) and an initial source condition. The mass flux predicted from the HELP and 1D MODHMS model simulations, as described above, were assigned as a time-varying source input to represent contaminants leaching from the IWCS waste sources. SESOIL model predictions for soil plume maps were also prescribed as a time-varying source, to account for the mass flux to the water table from soil contamination. A third source term was prescribed in the 3D transport model as an initial condition, to account for groundwater contamination defined by plume maps developed as part of the RI (SAIC and Tetra Tech, 2006). The plume maps represent contoured regions of reported elevated levels of contamination in groundwater, away from the IWCS.

The 3D solute transport model was applied to predict the migration of 24 constituents of concern (COCs) listed in Table 4.2, accompanied by screening level targets for each. NFSS upper tolerance limits (UTLs) and USEPA maximum contaminant levels (MCL) were used to determine screening levels for the 22 of the 24 COCs. Currently, there are no available drinking water or recreational water regulation set for ^{231}Pa and ^{227}Ac . Rather than simulating total Uranium, with an MCL of 30 $\mu\text{g}/\text{L}$, the full Uranium series (^{238}U , ^{234}U , ^{230}Th , ^{226}Ra , ^{210}Pb) including chain decay was simulated. NFSS upper tolerance limits (UTL) have been determined for 16 naturally occurring COCs (SAIC and Tetra Tech, 2006). The UTL represents a background groundwater concentration value below which 95% of the historically measured values fall within 95% confidence. The screening levels are the lower of the (1) background UTL, (2) MCL, or in absence of either one of these values, (3) dose-based

concentration, using a limiting dose rate of 4 millirem/year, consistent with the MCL for beta-emitting radionuclides. Screening level values provide a concentration reference, or target benchmark to compare transport model predictions against. A baseline case representing present day conditions and three worst-case scenario, failure events: earthquake; breach in the IWCS cap, and inadvertent penetration of cap, were evaluated.

The source term constituents prescribed in the 3D model for baseline conditions are summarized by constituent in Table 4.3. All radionuclides and metals simulated, with the exception of Cadmium (Cd) and antimony (Sb), have source terms prescribed for each intra-IWCS waste zone (Bay A, B, C, D, R-10 and Building 413/414).

The locations of the bays within the IWCS are shown on Figure 4.2. Cross-sections showing the components of the IWCS along with the emplacement of the contaminated soils and residues are shown on Figure 4.3. The plan-view location of the Figure 4.3 cross-section is shown in Figure 4.2.

Soil-based contaminant sources were applied to soil plumes presented in SAIC (2006). Individual constituents were only simulated where the SESOIL modeling predicted that acceptable risk levels would be exceeded; and such constituents are listed in Table 4.3 for the respective EU. Based on the SESOIL modeling results, only U-238 has a soil plume maps source prescribed within all EUs. Ra-226 and U-235 are prescribed as sources in multiple EUs, whereas all other constituents are either represented in only a few EUs or not represented in EUs at all. Plume map initial conditions are prescribed for select radionuclides, metals and other constituents as shown in Table 4.3. The plume map locations are presented in SAIC (2006).

Only IWCS sources were included for the worst-case scenario simulations, that is, SESOIL-based soil plume map sources and existing contaminant plumes in groundwater are not represented in the worst case scenario simulations. The worst-case scenarios were simulated specifically to predict the movement of the IWCS wastes after such an event. SESOIL-based sources were not included because the SESOIL results would be minimally affected by an earthquake, a breach or other damage of the IWCS cap would minimally vary the SESOIL results.

Several processes were simulated by MODHMS during the solute transport simulations, including advection, dispersion, degradation and sorption. For radionuclide simulations, radioactive decay was simulated and the transport of both radioactive parent and daughter products was accounted for. Both parent and daughters (degradation products) were simulated for organic constituents.

4.3 SOURCE TERM MODEL DEVELOPMENT

4.3.1 Unsaturated Zone Model Parameters

4.3.1.1 Approach

The HELP model was applied to predict vertical downward water flux through six IWCS waste zones: Bays A, B, C and D of former Building 411; former Buildings 413/414 and the R-10 waste pile (Figure 4.2). Separate HELP models were parameterized to simulate the saturated/unsaturated layered conditions of each waste zone.

Input parameters describing the hydrologic, climatic, and hydraulic conditions, geometry and configuration of each waste zone were assigned in separate HELP models. Parameter input values were ascertained from an extensive literature search and review by USACE staff and other contractors currently involved in NFSS project work. HELP model input parameters for each IWCS waste zone model are summarized in Table 4.4. The layering structure and detail are also shown in Table 4.4. A description of input parameters used in the HELP model and rationale for parameter selection is provided in the following section.

The water fluxes through each waste zone were simulated until a steady-state condition was achieved. The 4,000 year simulation duration was sufficient to achieve steady-state flow conditions through all waste zones.

The HELP model has an internal limitation which does not allow simulations beyond 100 years. To obtain HELP water flux results for a 4,000 year period, multiple HELP simulations were performed in succession, with each subsequent simulation restarted utilizing flow saturation results predicted during the preceding simulation.

4.3.1.2 Unsaturated Zone Model Parameters

This section details the rationale and parameter values selected for HELP model simulations. Parameters were selected for each of the six IWCS waste zones simulated and are grouped below according to:

- Precipitation,
- Solar radiation, temperature and evapotranspiration,
- Waste Zone Geometry, and
- Hydraulic Parameters.

4.3.1.2.1 *Precipitation*

Historical precipitation data were reviewed from four meteorological stations near the NFSS including: the Buffalo International Airport; Niagara Falls International Airport; Lewiston, New York; and Modern Landfill.

At the Buffalo International Airport, daily precipitation totals have been measured since 1922, and the annual average precipitation is approximately 37 in/yr (93.98 cm/yr). The Niagara Falls meteorological station reports an annual average precipitation of approximately 31 in/yr (78.74 cm/yr) during a 1989 through 1994 monitoring period. The NOAA station in Lewiston has historical precipitation data available for 1935 through 1971 and 1987 through 1994. The annual average of the precipitation totals measured in Lewiston for these time periods is 29.7 in/yr. A meteorological station on the Modern Landfill property adjacent to the NFSS reports annual average precipitation of 27.61 in/yr (70.13 cm/yr) for the time period from 1999 through 2004.

A trend of increasing annual average precipitation with increasing distance south of the NFSS is evident from the available monitoring data. This is primarily attributed to enhanced, Lake Erie lake-effect precipitation, caused by moisture laden westerly winds that blow across Lake Erie and impact Buffalo more so than Lewiston. Precipitation averages measured at Lewiston and Modern Landfill, the two stations closest to the NFSS, show reasonable agreement in values. The slight differences in annual averages reported for these stations are primarily attributed to the different time periods which averages were calculated.

The HELP model simulations require daily precipitation data as input, and comes with a built-in meteorological database, which includes five-years of daily precipitation data for 102 major US cities, measured from 1974 through 1978. Buffalo, the closest major city to the NFSS is not among the cities listed in the HELP database. Lacking daily precipitation data from both Lewiston and Modern Landfill stations (the closest and preferred stations for use in model input) we utilized the HELP model synthetic data generator to create a dataset of daily precipitation data values. The HELP model synthetic data generator created a 50 year dataset of daily precipitation from monthly precipitation averages. The Lewiston monthly precipitation averages (based on NOAA data from 1935 through 1971 and 1987 through 1994, i.e. those presented in Table 2.2) were used as input in the HELP synthetic data generator. Although the Modern Landfill gauging station is geographically closer to the NFSS, the Lewiston precipitation averages were provide a sound basis for calculating the synthetic daily precipitation dataset. For example, we do not expect significant variation in precipitation over the short distance between the Modern Landfill and Lewiston gauging stations, and moreover the Lewiston dataset contains more years of total precipitation data than the Modern Landfill dataset and the annual averages are slightly higher, yielding a more conservative estimate with respect to transport modeling.

Based on USACE correspondence with NFSS property maintenance personnel, the IWCS is occasionally sprinkled with water (irrigated) to maintain the topsoil cover and prevent the formation of desiccation cracks during prolonged dry periods and maintain the overall condition of the cap. At the time of this report, the maximum irrigation flow rate applied to the IWCS was approximately 233 U.S. gallons per minute (GPM) [14.7 liters per second (L/s)]. Irrigation is typically applied on dry days, for up to eight hours per day, five days per week, throughout May to September. Based on an IWCS area of 445,500 ft² (41,388.3 m²) (Bechtel, 1986), and eight hours of irrigation, the net supplementary precipitation is approximately 0.033 inches per day (in/d) (0.084 centimeters per day [cm/d]) over the IWCS.

Based on previous correspondence with property maintenance staff, apparently 0.033 in/d (0.084 cm/d) is a conservative maximum value.

To account for irrigation of the IWCS, the synthetic dataset of daily precipitation was augmented with 0.033 in/d (0.084 cm/d) of irrigation water, for each day where no precipitation was recorded, throughout May to September (inclusive) for each year in the 50 year dataset. While in reality irrigation is applied at most five days per week, irrigation on weekends was not excluded here, providing another conservative measure of total precipitation estimates. The net total of added irrigation amounts to 3.36 in/yr (8.53 cm/yr), on average, for the 50 year precipitation dataset. The annual average precipitation of the 50 year HELP model precipitation dataset is approximately 33.06 in/yr (29.7 in/yr + 3.36 in/yr) (83.9 cm/yr (75.4 in/yr + 8.5 in/yr).

4.3.1.2.2 Solar Radiation, Temperature and Evapotranspiration

Solar radiation data was synthetically generated for latitude 43.17 (near Buffalo, New York) by the HELP model (Schroeder et al., 1994). Solar radiation values used in the model range from 0 to 794.2 BTU/ft² per day, with an average value of 323.0 BTU/ft² per day.

Temperature data was generated synthetically by the HELP model (Schroeder et al., 1994) using the monthly average temperatures in Lewiston, New York as the input.

Evapotranspiration input parameters were based on data for Buffalo, New York, including:

Evaporative Zone Depth (inches)	20	1st quarter relative humidity (76%)
Leaf Area Index	2	2nd quarter relative humidity (68%)
Growing season start (days)	186	3rd quarter relative humidity (72%)
Growing season end (days)	285	4th quarter relative humidity (76%)
Average wind speed, (miles per hour [mph])	12.1	

4.3.1.2.3 Waste Zone Geometry

The thickness and composition of each layer in the IWCS waste zones was ascertained based on reported information in various Bechtel documents (e.g. Bechtel (1986), Bechtel (1986b), Bechtel (1994) etc.), construction contractor notes and other data sources. The layering configuration used in the HELP modeling is presented Table 4.4 and Figure 4.3.

Bays A, B, C and D of former Building 411 have a similar layering structure. All share the same upper layering (top soil, clay, Tower soils and sand), and bottom layering (sand filter, concrete floor). The waste zones are distinguished from one another by the configuration, content, and thickness of the intermediate layers. Subcontractor notes also indicate that the concrete floor in Bay A was filled with additional concrete to conceal 8" concrete grade beams and level the floor. Bay A, therefore has a thicker concrete floor than other Building 411 waste zones. In plan view, Bay A is square, while Bays B, C and D are rectangular (Figure 4.1).

Buildings 413/414 are characterized by multiple clay and/or synthetic engineering barriers. A concrete floor is also present at the base of the Building 413/414 waste zone. In plan view, Building 413 and 414 are circular as shown in Figure 4.2.

The R-10 waste pile is more extensive than the other IWCS waste zones and does not possess the same level of flow-impeding layering in place in Building 411 or Building 413/414.

Using HELP model terminology, soil layers were specified as lateral drainage layers; clay, synthetic liners and concrete as barrier soil liners; and waste zones as vertical percolation layers.

4.3.1.2.4 Hydraulic Parameters

Porosity Where available, site-specific values of porosity were used. For example, the porosity of K-65 wastes was estimated based on reported average water content from 8 samples (USDOE, 1993). Where site-specific porosity data were not available, values of porosity were inferred from a description of waste materials. For example, in Bechtel (1986) the following description is given of the contaminated (Tower) soils.

..waste materials were placed in layers and compacted to 90% of max dry density. Rubble materials were deposited in layers and the voids grouted with fillcrete to create a consolidated, dense mass." Based on the consolidation measures described, the contaminated soil layer in the HELP model was assigned porosity equal to 20%, which is lower than the adjacent sand and waste residue layers.

In the absence of any site-specific data or description, porosity values were selected from the HELP database of porosities and textures for a comparable material type. For example, the 3 foot clay barrier covering the IWCS was assigned a porosity of 45.1%, which corresponds with HELP texture number 29, equivalent to the U.S. Department of Agriculture classification: 'C' (clay) or United Soil Classification System 'CH' (highly plastic clay).

With regard to the porosity of concrete, Apul et al (2002) report values ranging from 3.9 to 6.1% in tests on water movement through concrete highways. For the HELP modeling conducted for the IWCS, the average reported value was selected (i.e., 5%) to represent the porosity of the basement of Building 411.

Field Capacity Defined as the percentage of water remaining in the soil 2 or 3 days after the soil has been saturated and free drainage has practically ceased. Values of field capacity were primarily obtained from the HELP database. For concrete, gravity drainage is considered negligible; therefore the value of field capacity assigned to the HELP model is approximately equal to the porosity.

Wilting Point Defined as the moisture content of a soil at which plants wilt and fail to recover their turgidity when placed in a dark, humid atmosphere. Values of wilting point were

primarily obtained from the HELP database. Wilting point not applicable to concrete; for concrete, value assigned is approximately equal to porosity.

Saturated Hydraulic Conductivity Values of saturated hydraulic conductivity are summarized in Table 4.4. The saturated hydraulic conductivity of the K-65 wastes is approximated using K-65 Fernald Silo 1 and 2 grain size data from Appendix G of USDOE (1993) and the Kozeny-Carmen equation (Bear, 1972). The saturated hydraulic conductivity of the L-30, F-32 and L-50 wastes was estimated based on unreferenced notes provided regarding the properties of the residues..

The hydraulic conductivity of cement concrete was estimated from Cramer and Carpenter (1999) and Apul et al. (2002).

The hydraulic conductivity of the contaminated soils was based on a value for ‘contaminated soil’ in the Bechtel (1986) Design Report.

The clay cap was assigned a hydraulic conductivity based on results from testing of cap materials in 1984, 1985, and 1986 (Betchel, 1986). The geometric mean hydraulic conductivity of 54 samples was assigned to the HELP model.

Other waste zone layers were assigned a saturated hydraulic conductivity from the HELP model database consistent with the material/lithologic properties of the layer (Schroeder et al., 1994).

Drainage Length The drainage length assigned in the HELP model is set equal to 1/2 of width of the waste bay/waste zone. Building 411 Bay dimensions are presented in Figure 31 in Campbell et al. (1985).

Slope The slope value assigned in the HELP model is 8%, based on Bechtel (1986b) which states ‘The top of the containment facility will be graded to a 5% to 10% slope to promote runoff without excessive retention or erosion’ (p. 41).

Landfill Area Landfill area was assumed to be synonymous with the top area of each waste zone. Waste zone areas data were obtained from Bechtel Design Drawing 202-DD22-C-08 and Campbell et al. (1985) (p. 42). The thickness of waste zone walls was excluded in area calculations.

Soil Texture Soil texture was required only for the uppermost HELP model layer, which is top soil for all waste zones. ‘Soil’ was not included in the HELP database of soil textures, so a texture for ‘fine sand’ was used, which is consistent with lithologic descriptions.

Vegetation Type A HELP model vegetative type of ‘3’ was used. This type is indicative of grass and/or fair stand of grass, is consistent with the thick grass cover that is maintained over the IWCS.

Runoff Curve Number The runoff curve number is calculated internally by the HELP model.

4.3.1.3 HELP Model Results

Forty successively-linked 100 year HELP simulations were executed to generate 4,000 years of water flux predictions through Bays A, B, C and D of former Building 411; Buildings 413/414; and the R-10 waste pile. HELP-predicted fluxes for all IWCS waste zones are included in Appendix E-1. The fluxes shown in Appendix E-1 represent the flux rates predicted by the HELP model at the water table. Model results indicate that the water fluxes gradually increase with time as storage in the waste zone is filled and the saturation of each HELP model layer increases. Eventually, once sufficient time has elapsed, all layers in the HELP model become fully saturated and the predicted fluxes stabilize at a constant asymptotic value. The HELP model predicts full saturation of the IWCS waste zones ranges occurs after approximately 1,000 years. At this steady-state condition, the flux out of the bottom of the layered system is equal to the amount of groundwater recharge entering the system. As shown in the plots of Appendix E-1, the asymptotic flux value for the R-10 waste zone was reached in a few hundred years, sooner than other waste zones. Unlike other waste zones, however, the R-10 waste pile lacks a concrete floor, which otherwise inhibits water movement. Approximately 2,500 years was required for a steady-state condition to be reached for Bay A which has the thickest flooring of the Building 411 waste zones.

Each 100 year HELP simulation predicts the water budget allocation for the precipitation applied. For example, for the R-10 pile, an average of 32.38 inches of precipitation per year was applied during the initial HELP simulation covering the time period from $t = 1$ to 100 years. This precipitation was allocated by the HELP model as follows: runoff (9.1%); evapotranspiration (71.2%); lateral drainage through upper soil layer (19.2%) and infiltration through the clay cap (0.5%). The water budgets predicted for later simulation times and other waste zones were comparable.

As is evident by the water budget presented above, the quantity of water predicted to infiltrate into the IWCS by the HELP model is very low, and yet at early time, prior to a steady-state condition, an even smaller amount of water is predicted to flow through the bottom of the IWCS waste zones. For example, in Bay A, the HELP model predicts that more than 100 years will be required for one inch of precipitation to infiltrate through the bottom of Bay A. By comparison, during this 100 year period, more than 3,000 inches of precipitation will have fallen on the IWCS.

Early-time aberrations or oscillations in the HELP predicted fluxes are attributed to the repetitive usage of the 50 year synthetically-generated precipitation dataset. Because the synthetic precipitation generator could not generate a 4,000 year dataset, the precipitation dataset is recycled every 50 years throughout a 4,000 year HELP model simulation. HELP predicted flux results were smoothed by calculating the 50 year geometric mean of the annual result data, although oscillations remain in the R-10 waste pile predictions.

4.3.2 Source Leaching Model

4.3.2.1 Constituents of Concern

A 1D MODHMS model was used to simulate the vertical migration of contaminants through the IWCS waste zones to the water table. A preliminary list of constituents of potential concern (COPC), to be used in transport simulations, were selected based on the known composition of the IWCS radioactive residues/waste materials and groundwater and soil analysis performed during the ongoing monitoring program, RI (SAIC and Tetra Tech, 2006) and BRA (SAIC, 2006) activities.

The preliminary version of the COPC list was used to select constituents that required more critical evaluation, and a detailed geochemical investigation was conducted for these constituents. The primary purpose of this geochemical investigation was to develop defensible estimates of the distribution coefficient (K_d) and solubility coefficient (s) associated with each of the constituents. The K_d and s are typically the most important transport parameters controlling the dissolution of contaminants from waste residues or soils. Consequently, the geochemical analysis focused solely on these two constituents.

The K_d is a transport parameter that relates the adsorbed constituent concentration to the dissolved constituent concentration. More specifically, the K_d is expressed by the following equation:

$$K_d = \frac{\text{mass of solute on the solid phase per unit mass of solid phase}}{\text{concentration of solute in solution}}$$

K_d is related to the retardation of a solute in groundwater by the relationship:

$$R = 1 + K_d \frac{\rho_b}{n}$$

where R is the retardation factor, ρ_b is the bulk mass density of the porous medium and n is the porosity. Accordingly, higher values of K_d represent increased contaminant adsorption and therefore larger retardation factors. For metals and radionuclides, which are key contaminants in the IWCS, values for K_d and s can vary over several orders of magnitude, are constituent-specific, and highly dependent upon the geochemical conditions associated with the subsurface environment.

Recognizing the parameter value uncertainties associated with K_d and s , HGL performed a two-part geochemical analysis aimed at better defining transport parameter values that represent conditions at the NFSS. The results contribute to improved confidence in predictive transport simulations. The first part of the analysis consisted of a comprehensive literature search and evaluation of relevant K_d values. During the second phase of the study, a geochemical speciation model, the (i.e, version MINTEQA2) code, was used to estimate

values of s for the key COPCs. The K_d and s values estimated as part of this investigation were used in a qualitative fashion to select COPCs that required more in-depth analysis during the subsequent groundwater modeling investigation. In addition, these estimated parameter values were assigned as input parameters in the numerical model(s). An in-depth description of the geochemical analysis is presented in Appendix D.

Following the geochemical analysis, the COPC list was further reviewed and revised by USACE and other contractors currently involved in NFSS project work including SAIC and Argonne National Laboratory (ANL). The review process incorporated additional criteria for including/excluding constituents. Those that were included on the list typically exhibit one or more of following characteristics: significant quantity of mass present on site; elevated concentrations with respect to screening levels; preliminary remediation goal (PRG) values; high solubility; high mobility; prolonged decay rates; toxicity; and/or carcinogenic risk.

Several constituents that were included on the preliminary COPC list were excluded from simulations. Justification for excluding these constituents is provided below.

- Short-lived (i.e., less than 1 year) isotopic daughter products in the U-238, and U-235 decay chains were excluded.
- The two daughter products in the Th-232 series (Ra-228 and Th-228) were assumed to remain in secular equilibrium with Th-232 during transit and therefore excluded from the modeling analyses. This is reasonable since the half lives of these two radionuclides (5.8 and 1.9 years, respectively) are very short relative to the time periods associated with groundwater transport and the Th-232 parent (1.4×10^{10} years).
- Nickel, although present in notable quantities, is highly adsorptive. Given its low mobility, Nickel was excluded from the simulation list.
- Iron was removed from the list because the drinking water standard is a secondary and non-enforceable guideline.
- Following a review of the plume maps (SAIC and Tetra Tech, 2006), fluoranthene, benzene and silver were excluded on the basis that the extent of contaminant is very limited.
- Selenium was not reported in sufficient amounts to warrant simulation.
- trans-DCE was removed from the list as it was deemed simulation of the *cis*-DCE isomer would be sufficient.
- Pentachlorophenol and 2,4-dinitrotoluene were excluded following a 5% data screen in the SESOIL modeling, whereby there was fewer than 5% detects in soil.

To guide the decision-making as to whether a particular constituent should be included for simulation, if two or more of the following conditions exist then the constituent was selected for modeling:

- Constituent present on NFSS in $> 100,000$ lbs
- Maximum reported concentration/PRG > 250
- K_d (L/kg) < 1000

These guidelines provided a basis to justify selection of ‘marginal’ constituents such as Manganese, Molybdenum and Boron.

The revised COPC list, as presented in Table 4.2, contains 24 constituents which comprise the COC. Solute transport was simulated for each of these 24 constituents. Simulations were organized by the constituent groupings as shown in Table 4.2, that is, constituents included within a particular decay series (e.g., uranium-radium series) or degradation series (i.e., chlorinated solvents) were grouped together. Metals were grouped into two simulations. The grouping of those constituents allowed for concurrent simulation of the ingrowth and subsequent migration of daughter products where applicable.

4.3.2.2 Model Discretization

Model layers in the 1D MODHMS transport models of the unsaturated waste zones were assigned a uniform layer thickness of 3 in (7.6 cm) throughout the entire vertical extent of each model. The high resolution layering ensured grid convergence and accurate results, while also permitting discretization of thin layers such as the half inch synthetic rubber hypalon layer or ethylene propylene diene monomer (EPDM) (geo-synthetic barrier liner) layers of the Buildings 413/414 model. The number of layers used in each model varied depending on the overall thickness of the waste zone. The Bay D model required a minimum of 92 layers, while the Bay C model, having the largest vertical profile, required 112 layers.

Simulations were performed to provide transport predictions for up to 10,000 years. Time was discretized into 120 steady-state stress periods. A stress period is a pre-determined length of time during which a value for prescribed model stresses, e.g. pumping, or in this HELP model-predicted water fluxes, are held constant. From 0 to 5,000 years, all stress periods, except an initial early time stress period were assigned to be 50 years in duration. For simulation times from 5,000 to 10,000 years, when plume migration trends are stabilizing and less time resolution is required, a larger stress period of 250 year was used. A total of 121 stress periods were specified for each 10,000 year simulation.

4.3.2.3 Source Term

The emplaced wastes were represented in each HELP model by a prescribed initial concentration. Respective model layers within modeled waste zones were assigned a dissolved-in-water concentration, (C_w) for each contaminant. C_w was calculated as the aqueous proportion of each contaminant based on reported waste inventory total concentrations and best estimate values of K_d , bulk density (ρ_b) and porosity. Dissolved concentration data for each IWCS waste zone is presented in Table 4.5. It is noted that although only values of C_w are required for initial concentration input, the model assigns a concentration to the soil phase for each constituent in proportion to its distribution coefficient.

Prior to 1D transport model simulation, calculated values of C_w were compared against best estimate solubility limits determined during the geochemical analysis to check for solubility-limited conditions. Solubility-limited conditions were identified for several constituents

including U-238, Th-230, Th-232, Ba, lead (Pb), Mo and Mn. The solubility-limited simulation options in MODHMS were invoked accordingly for these constituents.

4.3.2.4 Transport Parameters

The values of porosity assigned to the various model layers within each waste zone were set to be consistent with values assigned in the HELP model.

The 1D transport model required input of vertical dispersivity (α_v) only, and this was set equal to one meter, a reasonable and conservative value for the model scale based on values reported in Gelhar et al. (1992).

The distribution coefficients were selected based on results of the geochemical analysis (Appendix D). Degradation rates assigned for each constituent were based on published literature values. Identical values of distribution coefficient and degradation rate were subsequently used in the 3D model simulations, as such, refer to Section 4.4 for parameter selection rationale and input values used.

4.3.2.5 Source Leaching Model Results

The 1D waste zone transport simulations were performed for all IWCS COPCs. The model-predicted mass fluxes emanating from the bottom of each waste zone are presented in Appendix E-2 for each constituent, as plots of concentration versus time.

Several factors influence the shape and predicted peak of the concentration versus time plots; these include the magnitude of the constituent concentrations emplaced in the waste zones, the geometry and thickness of the layering in the waste zones, the predicted water flux through the waste zones, and species-dependent transport parameters. Concentration breakthrough occurs most quickly through the R-10 pile, which unlike the Building 411 waste zones, does not have downward flow inhibited by a concrete floor.

For late simulation times, it proved challenging to obtaining a smooth concentration versus time solution for latter decay chain species in U-238 series such as Ra-226 and Pb-210. While approaching tractable limits for the U-238 series multi-specie, solubility-limited problem, the Ra-226 and Pb-210 predicted concentrations, and associated uncertainties, are not of consequence as they do not risk exceeding screening level. In the case of Ra-226, the predicted concentrations for all waste zones are orders of magnitude below the screening level, or in the case of Pb-210 no screening level value is available.

The constraining effects of the solubility-limited is evident for U-238 whereby the predicted concentration does not exceed the solubility limit, and eventually, at late time, as the non-aqueous phase U-238 source dissolves the predicted U-238 concentration decreases. Note that the predicted concentration of U-238 at early-time is slightly less than the solubility limit in accordance competition with other solutes in the decay series.

4.4 REGIONAL SOLUTE TRANSPORT MODEL DEVELOPMENT

4.4.1 Three-Dimensional Transport Modeling Approach

The steady-state flow solution presented in Figure 3.14, from the four-layer model recalibrated in 2003, as described in Section 3 was used as a basis for defining the flow field for the solute transport simulations. The hydrogeologic units represented by this 3D flow solution are:

- Model Layer 1: Upper Clay Till
- Model Layer 2: Glacio-Lacustrine Clay
- Model Layer 3: Alluvial Sand and Gravel
- Model Layer 4: Fractured Upper Queenston Formation

In addition, the presence (both thickness and vertical hydraulic conductivity) of the Basal Red Till hydrogeologic unit is accounted for by a vertical conductance assigned between layers 3 and 4.

The transport model shares the same numerical finite-difference mesh and model domain as the flow model. The transport model can simulate advective-dispersive, adsorptive and decay transport processes throughout the full extent of all layers of the flow model.

The flow solution in the transport model differs from the calibrated flow field in one regard, however. For the IWCS source areas, calibrated values of groundwater recharge were updated with predicted values of water flux through the unsaturated layered units of the IWCS using the HELP model (Schroeder, 1994). As described in Section 4.2, HELP is a quasi-two-dimensional model specifically designed for performing water balances of landfills, cover systems and waste containment facilities. The HELP model mathematically represents many of the physical processes that affect the flux of water through the vadose zone, and precisely accounts for the known configuration, layering and permeability of the IWCS waste sources and emplacement barriers, and the unsaturated flow through these systems. Accordingly, despite being higher than the calibrated groundwater recharge, the water flux determined by the HELP model was appropriately given precedence over the value obtained from calibration of the 3D model. It is noted that HELP model has been cited to overestimate water flux at the bottom of layered systems (e.g. Fleenor and King, 1995), although in this case, a higher water flux will yield results that are conservative with respect to mass transport through the IWCS.

As a quality assurance check, the 3D flow solution updated with HELP-predicted fluxes was compared to the calibrated flow solution. As expected, the HELP-predicted flux values are higher than calibrated recharge values, and as a result, the updated flow solution shows slightly higher water levels in the vicinity of the IWCS. Though overall there is excellent agreement between the two solutions and only a minimal difference in the calibration statistics.

4.4.2 Boundary and Initial Conditions

All known or potential sources of groundwater contamination on the NFSS were assigned in the NFSS model. Three distinct sources of contamination, of varying genetic origin and geographic location on the NFSS were defined. These include contaminants within the IWCS; localized plumes of groundwater contamination; and potential future groundwater contamination arising from the leaching of contaminants in soils located within the various NFSS EUs. For each contaminant source, concentration levels for contaminants of concern (listed in Table 4.2) were established and defined in the model as either initial concentrations, or as time-varying concentration boundary conditions (see Table 4.3). Additional descriptions of each of the three contamination components that comprise the source term and the approach used to implement into the model are provided below.

4.4.2.1 IWCS-Derived Contamination

A multi-step approach was used to simulate the leaching of contaminants from the IWCS. Initially, and as described previously in Section 1.2, an inventory of the contaminants in the IWCS was performed to identify key contaminants of concern and their location in the IWCS. Former Building 411, and its four Bays (Bay A, B, C and D) contain the highest levels of contamination in the IWCS. Former buildings 413/414 and the R-10 pile also contain contamination levels that warrant inclusion in the model source term. Drawings of IWCS Bays A, B, C and D of Building 411; the R-10 waste pile; and Buildings 413/414; were obtained from SAIC, and these maps were used to assign the contaminant sources within the groundwater model.

The reported contaminant concentrations in the various IWCS waste sources were provided by SAIC as total concentrations in soil. Values of C_w and constituent concentrations sorbed to soil (C_s) were determined from the total concentrations, using published values of ρ_b based on the material type, porosity (Bechtel, 1986; USDOE, 1993) and K_d (HGL, 2004b). The resultant calculated values are presented in Table 4.5.

Constituent concentrations associated with contaminated soils or residues in the IWCS were not known with certainty for all waste zones. For example, there was uncertainty regarding concentrations of metals in the wastes described as 'contaminated soils' in or above Building 411 or on the R-10 pile. For such cases, to overcome concentration uncertainties, project team members reached a consensus to adopt a conservative approach and use the highest reported concentration value among (1) 2% of K-65 waste values; (2) site wide values calculated in the BRA; and (3) values reported for the R-10 pile to define a metals concentration in the 'contaminated soils'.

Tower soils were assigned a concentration equal to 2% of the K-65 residue concentration, and consequently, for all radionuclides, the concentrations in Tower Soils are higher than concentrations for contaminated soils. As a conservative measure, Tower Soil concentrations were specified in each of Bay's A, B, C and D, despite the known presence of Tower Soils in Bay D only.

Six 1D transport models were then developed to predict the mass flux to the water table through each of the IWCS waste zones. The 1D transport models were each assigned 121 stress periods to mirror the stress period subdivision of the 3D transport model. For each 1D transport model, the respective HELP-predicted flux values were assigned to each stress period, and all stress periods were simulated under steady-state flow conditions.

The waste zone layering thickness and geometry were defined in the 1D transport models to be consistent with that defined in the HELP model. A precipitation recharge rate equivalent to the flux rate calculated by the HELP model was assigned to the uppermost layer of the 1D transport model. Input of longitudinal dispersivity through the unsaturated zone above the IWCS was required. For this purpose, a value of longitudinal dispersivity equal to 1 m was used, which is consistent with field measurements reported by Gelhar et al. (1992), for problems of a similar scale, that is, on the order of 32.8 ft (10 m).

4.4.2.2 Contamination in Soil

Elevated levels of various contaminants have been identified in soils at the NFSS. Soil contamination poses a potential threat to water quality, whereby contaminants may leach from the soil and migrate through the unsaturated zone to the water table. To account for this potential contaminant source, the SESOIL (Bonazountas and Wagner, 1981, 1984; Hetrick et al. 1993) was applied to predict the contaminant flux to the water table for use in the 3D transport model source term. SESOIL is a 1D vertical transport model for unsaturated soil zones and is designed to calculate solute distribution in the soil profile and watershed. Details of the SESOIL model approach and methodology are summarized in NFSS Baseline Risk Assessment Report (SAIC, 2006).

Separate SESOIL models were parameterized and simulated for each soil plume maps on the NFSS. Soil concentrations and hydraulic input parameters were assumed to be constant throughout any given EU, conservatively estimating the spatial extent of contaminants within each EU. A constant recharge rate of 1 in/yr (2.54 cm/yr) was applied to all SESOIL simulations. This value is thought to be higher than the actual precipitation recharge rate at the site, and consequently, it is considered to be conservative. The SESOIL results were assigned to the 3D model as a time-varying mass-flux rate. Prior to assigning this flux rate in the 3D model, SESOIL model output, provided as a mass flux (e.g. mCi/hour), was converted to a mass flux per unit area by dividing by the model cell area wherever prescribed. SESOIL model output was further adjusted (diluted) to account for differences between the 1 in/yr (2.54 cm/yr) recharge assumed during SESOIL simulations and the calibrated spatially-variable recharge rate assigned in the 3D model.

4.4.2.3 Plume Maps

Ongoing long-term groundwater monitoring and sampling conducted as part of the remedial investigation (SAIC and Tetra Tech [2006]) have identified groundwater contamination at select locations on the NFSS. The elevated contaminant values, as observed at various monitoring wells, have been contoured and manually interpreted by the RI contractor to generate plume maps. The plume maps were used to assign initial conditions (i.e., initial

constituent concentrations) to the Upper Water Bearing Zone in the 3D transport model. Table 4.3 summarizes the constituents that were included as initial conditions in the 3D transport model.

4.4.3 Transport Parameters

4.4.3.1 Effective Porosity

Total porosity is defined as the volume of voids (V_v) divided by the total volume (V_t) of the subsurface material, including both the solid portion and all void spaces. Effective porosity differs from total porosity in that the effective porosity numerator V_v includes only the portion of the void spaces that are interconnected and capable of transmitting fluid. Thus values of effective porosity for a particular medium are equal or lower than its porosity counterpart, and may in fact differ significantly. Low permeability materials such as clay have a typical total porosity of 55% (Freeze and Cherry, 1979), whereas the average effective porosity of clay is 2.5% (Fetter, 1993).

Values of effective porosity are used to calculate average linear ground-water velocity and therefore are required input parameters for both the 1D IWCS vertical transport model and the 3D saturated transport model.

The 1D transport model of the IWCS vadose zone represented local scale transport through the unsaturated, layered structure of each IWCS waste zone, and a value of effective porosity was input for each layer. Effective porosity values were set equal to the HELP-predicted values of water content from the corresponding 1D IWCS flow model. Although water content values were typically higher than the typical values of effective porosity for a given subsurface material, its use provided a conservative estimate of effective porosity with respect to transport, in the absence of site-specific measured data.

The 3D transport model was assigned a single homogeneous value of effective porosity for each hydrogeologic model layer. Values were determined based averages reported in the literature for corresponding materials, as shown in Table 4.7.

4.4.3.2 Dispersivity

Hydrodynamic dispersivity is the parameter that describes the mixing of solute in groundwater and incorporates the effects of both molecular diffusion and mechanical dispersion. Mechanical dispersion represents mixing caused by local variations in the groundwater velocity field. Except for systems in which groundwater velocities are very low, mechanical dispersion is significantly greater than molecular diffusion. For a steady-state flow field, mechanical dispersion accounts for plume spreading in the aquifer. Lateral spreading of the plume will typically be much less than longitudinal spreading, and in turn, the vertical spreading is typically even less.

Numerous field studies have demonstrated that mechanical dispersion is controlled by aquifer heterogeneity, temporal variations in the hydraulic gradient and the size and location of the initial plume. Site-specific values of dispersivity can be back-calculated from a model of a tracer test or well characterized plume migration over time. The conventional method for modeling dispersion is to presume a Fickian (i.e. Gaussian) dispersion process in three dimensions similar to molecular dispersion wherein a directional-dependent dispersivity value is used instead of a molecular diffusion coefficient.

In the absence of site-specific data, values of dispersivity can be obtained from field sites with comparable lithology and scale. The most comprehensive compilation of dispersivity data available is that presented by Gelhar et al. (1992), who critically reviewed measurements from 59 field sites. Among several reported observations, Gelhar et al. (1992) note a trend of increasing dispersivity with scale; though they caution a lack of highly reliable data for problems beyond a scale of approximately 983.6 ft (300 m).

The 3D NFSS model has total dimensions of on the order of 10 km, although the prime area of interest with respect to solute transport is limited to the vicinity of the NFSS or about 1639.3 ft or less (500 m or less). At this scale, Gelhar et al. (1992) indicate that longitudinal dispersivity equal to 32.8 ft (10 m) is reasonable, and in accordance, a value of $\alpha_L=32.8$ ft (10 m) was assigned in the 3D transport model. The ratio of longitudinal to transverse dispersivity typically ranges from 1 to 100. Considering the heterogeneous nature of the glacial deposits and the highly erratic flow directions observed on the NFSS (flow directions are sometimes vary by 90 degrees from year to year), the 3D model horizontal transverse dispersivity was set equal to longitudinal dispersivity [$\alpha_T=32.8$ ft (10 m)]; a high (and conservative) value. Numerous field data and the theoretical results of Gelhar et al. (1993) indicate that vertical transverse dispersivity values are typically 10 to 100 times smaller than horizontal transverse dispersivity; the smallest of which are sometimes on the order of molecular diffusion. In the interest of making a conservative choice with respect to solute transport, vertical transverse dispersivity for the 3D simulations was selected from the high end of the observed range and set as 1/10 of the horizontal transverse dispersivity [$\alpha_V=3.28$ ft (1 m)].

4.4.3.3 Adsorption

The adsorption of dissolved constituents onto subsurface materials is a phenomenon known to inhibit (or retard) plume movement relative to groundwater or a non-sorbing constituent. Adsorption is often described by the retardation factor which quantifies how many times slower a dissolved constituent moves relative to the average linear groundwater velocity. The Retardation Factor is defined as:

$$R = \frac{\bar{v}}{v_c} = 1 + \frac{\rho_b}{n} K_d$$

Where: \bar{v} = average linear groundwater velocity (length/time)

- \bar{v}_c = averaged velocity of dissolved constituent (length/time)
- ρ_b = bulk density of soil (mass/length cubed)
- n = porosity (-)
- K_d = distribution coefficient (length cubed/mass)

The higher the retardation factor, the slower a dissolved constituent moves relative to groundwater. Retardation factors are calculated internally by the model using a constant input value of K_d for values of n and ρ_b which vary spatially and for each hydrological unit or model layer. K_d is defined as the ratio of the mass of solute on the solid phase over the concentration of solute in solution. Referring to equation (1), it is evident that for K_d equal to zero, the Retardation Factor is unity, and the transport of a dissolved constituent is unretarded and moves at the same rate of groundwater.

Input values of K_d were determined primarily from results of the geochemical analysis described in Appendix D and presented in HGL (2004). A best estimate value of K_d for each constituent was obtained from NFSS-specific studies. Where NFSS-specific data were not available, constituent-specific results from multiple offsite studies were used.

The K_d values for organic constituents were calculated using the relationship $K_d = K_{oc} \times \text{fractional total organic content (foc)}$, where K_{oc} is the octanol/water partition coefficient or soil sorption coefficient normalized for total organic content, and foc is the fraction total organic content (mass organic carbon/mass soil). Values of foc are typically higher near the ground surface and decrease with depth; foc refers to the small amount, or 'fraction' of natural organic carbon.

It is assumed that adsorption is directly proportional to the amount of total organic carbon (TOC) in the soil. In areas of high clay concentrations and low TOC, which may be typical of the Upper Clay Till unit on the NFSS, the clay minerals become the dominant sorption sites. Under these conditions, the use of K_{oc} to compute K_d might result in underestimating the importance of sorption in retardation calculations. This is a potential source of error; however, this approach will ensure that retardation calculations based on the TOC of the aquifer matrix are more conservative. Standard K_{oc} values for clay were obtained from USEPA (1996), USEPA (1998), and Yu et al. (1993). A foc value equal to 0.0017 representing glacial materials comprised of silt with sand gravel and clay (USEPA, 1998) was used to calculate the K_d for the organic compounds.

Table 4.5 presents a summary of K_d model input values for all constituents, as well as corresponding values of K_{oc} where applicable, and values of the Retardation Factor calculated using the porosity and ρ_b of the Upper Clay Till unit.

4.4.3.4 Degradation/Decay

4.4.3.4.1 *Radioactive Decay*

Radioactive decay is a spontaneous and naturally-occurring reaction in which atoms of a particular isotope (or radionuclide) change to form a new isotope (daughter product) as part of a single or a series of reactions that ultimately lead to a more stable isotope. The primary mechanisms of radioactive decay are alpha (α) and beta (β) decay which are classified according to the type of particle radiated by the decaying atom. An atomic nucleus undergoing alpha decay emits an alpha particle, also equivalent to the nucleus of a Helium atom. Beta decay occurs by the emission of a beta particle which can be either negative (negatron) or positive (positron). The negatron is identical to an electron and originates in the nucleus of an atom and the positron is the antimatter equivalent of an electron..

The radioactive decay of an isotope is described by its half-life, or time required for amount of a radionuclide to be reduced to half of its original amount:

$$t_{\frac{1}{2}} = \frac{\ln(2)}{\lambda}$$

where: λ is a first order decay constant.

Three natural decay series are represented among the transport constituents to be modeled. These are the U-238 (Uranium-Radium), U-235 (Actinium) and Th-232 series. The U-238 Series describes the radioactive decay of U-238 to Pb-206, by means of 14 distinct decay reactions. Many of the reactions in the U-238 decay series, as in other decay series, yield daughter products which are short lived, some lasting just a few minutes or less. For example, the intermediate daughter in the U-238 series Po-214 lasts only 160 microseconds. For the purposes of the transport simulations, the short-lived isotopes are assumed to remain in secular equilibrium with the long-lived parent radionuclides during transit; therefore only the key, long-lived isotopes need to be evaluated in the simulations.

Typically in nature radionuclides in the U-238, U-235 and Th-232 series exist in a state of secular equilibrium, whereby the activity of the each daughter product is equal to the activity of the parent.

$$Activity = \lambda_0 n_0 = \lambda_1 n_1 = \lambda_n n_n$$

where n_0 is the number of atoms of the original parent and n_1 is the abundance of the first daughter, and so on.

Secular disequilibrium can exist under certain geologic conditions (erosion, sedimentation etc.) under which specific radionuclides become fractionated due to variations in chemistry or structural configurations. For the transport modeling herein, it is assumed that all

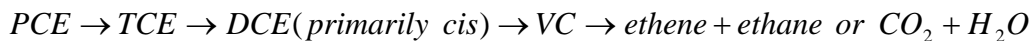
radionuclides are in a state of secular equilibrium and accordingly standard decay rates (based on secular equilibrium) are input into the model. Decay rates and constants for each radionuclide for simulation are presented in Table 4.5.

4.4.3.4.2 Biodegradation

Biodegradation is a naturally occurring process by which organic contaminants are broken down into smaller compounds by microbial organisms. The microbial organisms essentially feed on the organic compounds and transform the compounds via enzymatic or metabolic processes. The rate of biodegradation depends on the type of organism and contaminant, as well as various geologic and chemical conditions.

The biodegradation of chlorinated organic compounds (chlorinated solvents) has been extensively studied over the past 20 years. Numerous studies indicate that many chlorinated solvents are recalcitrant (not readily biodegradable) under aerobic conditions; though a few exceptions exist among the sparsely chlorinated compounds (Wilson and Wilson, 1995; Davis and Carpenter, 1990). For anaerobic conditions, however, biodegradation of chlorinated solvents is well documented (e.g., Bradley, P.M, 2003, McCarty and Semprini, 1992).

Under natural anaerobic conditions the highly chlorinated solvents are thought primarily to degrade through a natural process called reductive dechlorination. Reductive dechlorination involves the removal of a chlorine atom and its replacement with a hydrogen atom. For a compound such as PCE the sequence is generally as follows:



where: TCE=trichloroethene;
cis-DCE=cis-1,2-dichloroethene; and
VC=vinyl chloride.

Transformation rates typically diminish with each dechlorinated daughter product (Vogel et al., 1987; Freedman and Gossett, 1989). During reductive dechlorination, the chlorinated compound is used as an electron acceptor, and consequently, an electron donor is required for the process. Candidates for electron donors include natural organic carbon present in the aquifer or other contaminants such as benzene, toluene, ethyl benzene and xylenes (BTEX). Reductive dechlorination has been shown to occur under nitrate reducing (Ala and Domineco, 1992) and iron reducing conditions (Wilson, 1996). The lack of an electron donor can severely inhibit reductive dechlorination.

The aquifer conditions at the NFSS, and whether they inhibit or favor biodegradation, are not known. For the purposes of transport modeling, conservative estimates of degradation rates were obtained from scientific literature and biodegradation of chlorinated solvents was approximated by a first order kinetic reaction. Degradation products were simulated (i.e., chain decay).

Values for PCE decay chain half-lives were adopted from Wiedemeier et al. (1999) based on data collected from eight sites. To ensure a conservative model prediction, a decay rate at the lower end of the reported range was selected (2.6×10^{-4} 1/day), and assigned for all constituents in the PCE decay chain. The selected degradation rate of 2.6×10^{-4} 1/day is also in agreement with the expected range of values for TCE and VC reported in Wiedemeier et al. (1998). A half-life for dichloromethane for use in model simulations was obtained from Howard et al. (1991).

4.4.3.5 Solubility

Solubility is a measure of how much a constituent (solute) can be dissolved in a solvent (e.g., water). Several geochemical factors affect the solubility of a particular constituent in groundwater, the most important of which are temperature, pressure, pH, and mineralogy of the surrounding matrix. The solubility limit, defined as the maximum concentration that can occur in groundwater, can therefore vary from site to site or subtly from season to season on the same site depending on groundwater conditions. In preparation for defining source term concentrations in the transport model, solubility limits were investigated for each constituent of concern to ensure that the prescribed concentrations are plausible and do not exceed the estimated solubility limit.

Solubility limits for each constituent were evaluated during the geochemical analysis effort (HGL, 2004) using the MINTEQA2 geochemical model. MINTEQA2 simulated representative NFSS groundwater with input from NFSS groundwater chemistry data, where available. Additional details on the MINTEQA2 methodology employed are provided in Appendix D.

As is evident in Table 4.5, metals such as Ba and cadmium are not very soluble, having solubility limits of 0.007 and 0.15 milligrams per liter (mg/L), respectively. Conversely, arsenic and boron are highly soluble with estimated solubility limits exceeding 10,000 mg/L.

Solubility data are not explicitly input into the transport model. The estimated values are used to define an upper limit for concentrations prescribed in the model source term. Concentrations assigned to the source term are calculated based on equilibrium conditions between the reported mass of a constituent and its distribution coefficient. Where sufficiently large quantities of mass have been reported, the equilibrium concentration calculated using the distribution coefficient yields a concentration that exceeds the solubility limit. For such constituents, solubility-limited modeling options were invoked. This modeling option prescribes the solubility limit as the concentration in the solution until the source concentration is reduced due to decay or as a result of advective-dispersive transport to a concentration below the solubility limit. This method was developed and incorporated into the MODHMS model as a more accurate means of characterizing high concentration sources.

4.5 PREDICTIVE SOLUTE TRANSPORT SIMULATIONS

The 3D transport model was applied to predict contaminant migration and concentrations of COPC's in groundwater for 10,000 years under currently known conditions (referred to herein

as the Baseline case). The Baseline case simulation represents the best estimate of the current understanding of hydrogeological conditions and contaminant characterization at the NFSS and surrounding region. The modeling process accounts for various elements of the NFSS conceptual model including hydraulic input parameters; IWCS waste zone configuration; contaminant sources; solute transport input parameters and concentrations. The Baseline case model development and input parameter selection process incorporated some conservative judgment, which is important for the critical nature of the prediction provided by the model. Examples of conservative judgment for key input parameters include:

Hydraulic conductivity: The Upper Clay Till hydraulic conductivity was represented as heterogeneous, a more conservative approach that accounts for localized regions of elevated permeability than use of constant geometric mean value indicative of the bulk geometric mean conductivity.

Recharge: The HELP-predicted water flux through the IWCS requires precipitation as an input parameter. Greater values of input precipitation may yield higher fluxes. Precipitation from Lewiston (which reported slightly higher values than Modern Landfill) was selected. Furthermore, cap irrigation days were applied liberally to supplement the precipitation. Also, the HELP model has been cited to over-predict fluxes, and its predicted flux was higher than the calibrated groundwater recharge value.

Solute Concentrations: Higher concentrations associated with Tower Soils were assigned in place of contaminated soils in Bay's A, B and C.

In addition to the Baseline case, three additional scenarios were simulated to evaluate the affects of postulated worst-case scenarios, including:

- Breach of the IWCS Cap
- Earthquake and
- Inadvertent Penetration of the IWCS.

These worst-case scenarios were chosen because of their potential to impact human health. The worst-case scenarios were designed to be highly conservative; and consequently, the results from these simulations are thought to overestimate future contaminant concentrations in groundwater. The worst-case scenario simulations were designed to address some of the potential changes that may impact the NFSS over a 10,000 year period, and were specifically designed to evaluate some of the primary, protective, or solute migration inhibiting features associated with the IWCS. The breach of the cap, for instance, evaluated the protective nature of the low permeable clay covering the IWCS; the earthquake assessed the flow inhibiting property of the concrete floor underlying the former Building 411; and the inadvertent penetration considered the underlying low permeability Glacio-Lacustrine Clay Unit and how it may limit waste migration into the underlying layers.

Other worst case scenarios exist, and the results of many can be inferred from these three selected worst-case scenarios. For example, plausible impacts from the advance/retreat of glacial ice, such as the scouring activity of glacial ice advance or erosion by glacial meltwater can be assessed from breach of the cap worst case scenario results; rupturing similar to an earthquake may occur because of the weight of glacial snow and ice accumulation.

To perform the baseline and worst-case scenarios, the model was discretized into 121 incremental time periods (stress periods), including 101 50 year stress periods to represent the time from 0 to 5,000 years; and 20 250 year stress periods for 5,000 to 10,000 years. Constituent concentrations representing the contaminant source term are constant within any given stress period and the number of stress periods was sufficient to adequately represent the predicted 1D model source term concentrations in the 3D model. Simulation results, including a comprehensive mass balance and solute concentrations for each contaminant, were output at the end of each stress period.

The simulation results capture various complex physical transport processes. For example, concentrations of a particular constituent may increase suddenly as a result of decay from a parent; emergence into a lower permeable unit; or perhaps because of the interaction from multiple prescribed sources in the model. The presentation of transport results in this section focuses on succinct identification of constituents predicted to pose a potential risk to human health over the long-term, whether due to a screening level exceedances within the NFSS, or at the NFSS property boundary. Computer animations illustrating contaminant migration are also provided with this report as AVI files in the digital data files of Appendix F. These animations illustrate the complex transport characteristics that are predicted by the model.

Simulation results are most easily assessed, in a precursory sense, by reviewing values of (a) maximum on-site constituent concentrations and (b) maximum constituent concentrations at the property boundary as summarized in Table 4.8 for each constituent, for each model layer.

Maximum On-Site Constituent Concentrations

Among the nine metals simulated in the Baseline case, the maximum concentrations of As, B, Cd and Mn are predicted to exceed screening levels. For Mn, the maximum predicted on-site concentration is attributed to elevated concentrations in groundwater below in EUs 4 and 13. Maximum concentrations of Mn are predicted to occur at $t=0$, and marginally exceed the established screening level. The maximum concentrations of As, B and Cd are due to soil-based contaminant sources within or near EU13, and the predicted concentrations through time follow trends established by results of SESOIL modeling of soil-based sources.

Concentrations of As and B, are exceed screening levels by a considerable margin, with peak concentrations occurring 450 years and beyond 1,000 years, respectively. The concentration of Cd is not predicted to exceed screening levels within 1,000 years.

Maximum Constituent Concentrations at Property Boundary

The maximum constituent concentrations at the property boundary provide an additional precursory means of reviewing transport simulation results. Property boundary maximum concentrations represent the highest predicted concentration value within model cells intersecting the NFSS property boundary. These data can be used to identify the concentration

predicted to migrate offsite, and whether it is expected to exceed screening levels. As was done for the maximum on-site constituent concentrations, predicted screening level exceedances are also denoted in *bold and italics* in Table 4.8.

To supplement an analysis of the maximum NFSS boundary screening level exceedances, the time, location and concentration of the initial screening level exceedances at the NFSS boundary is also presented in Table 4.8. These results provide insight into when exceedances first occur, and the duration which they may be expected.

Worst case scenario results are presented in Table 4.9, showing order of magnitude changes in concentration relative to the baseline case.

Additional solute transport modeling results presented herein include:

- Appendix E-1 HELP-predicted water fluxes for IWCS waste zones
- Appendix E-2 Predicted mass fluxes from IWCS waste zones
- Appendix E-3 NFSS-boundary exceedances maps
- Appendix F:
 - Animations of plume migration for all constituents, baseline case
 - Animations of plume migration for all constituents, worst case scenarios
 - Screen captures for all constituents at t=0, 50, 200 and 100 years, baseline case
 - Initial condition plume maps of elevated groundwater concentrations on the NFSS
 - Soil-based plume maps for SESOIL modeling

Collectively, Tables 4.8, 4.9, Appendices E and F, in conjunction with Section 4.5, provide comprehensive presentation of the simulation results.

4.5.1 Baseline Conditions

The ‘baseline’ modeled condition is designed to represent solute transport under present day conditions and utilizes a flow field calibrated to averaged seasonal water levels and best estimate of the waste zone geometry and physical/hydraulic parameters.

Model row and column numbers are used in the text to describe specific locations within the NFSS model domain. The MODFLOW grid numbering convention has the row/column origin in the northwest corner of the model as shown in Figure 4.4. Row and column numbers progressively increase to the south and east, respectively.

Baseline – U-238 Series

Maximum On-Site Constituent Concentrations

For model layer one, the Upper Clay Till, the maximum predicted on-site constituent concentrations for U-238, U-234 and Th-230 exceed screening levels. The U-238 and U-234 maximum concentration occurs at t=1,000 years and are nearly two orders of magnitude

greater than the respective screening level values. These high concentrations are limited to the immediate vicinity below and surrounding the IWCS waste zones. The Th-230 on-site maximum occurs at $t=0$ and is attributed to a groundwater plume initial concentration north of the R-10 pile. Maximum on-site concentrations of Ra-226 and Pb-210 remain below the screening level at $t=1,000$ years.

Maximum Constituent Concentrations at Property Boundary

Screening level exceedances are predicted at the NFSS boundary for U-238 and U-234 within 1,000 years. As presented in Table 4.8, the initial NFSS boundary exceedances for U-238 and U-234 occur at $t=0$, and are attributed to existing groundwater contamination that has been detected along the northern property boundary. The location of the initial screening level exceedance is given as model row/column 100/100.

Although the existing plume near the north boundary is the cause of NFSS boundary exceedances at early time, the IWCS-based source of U-238 causes the highest boundary exceedances at later time. As shown in Table 4.8, the maximum U-238 concentration at the NFSS boundary is 44.1 pCi/L and occurs at row/column 176/96 at $t=10,000$ years, a location on mid-western portion of the NFSS boundary adjacent to the IWCS. Review of the corresponding animation of U-238 simulation results confirms this trend, indicating that predicted U-238 concentrations emanating from the IWCS source term are expected to contribute to screening level exceedances at the NFSS-boundary.

Additional Salient Details of U-238 Transport

Nearly synchronous transport of U-238 and U-234, as demonstrated by model results and screening level exceedances are expected to occur for these species. Both U-238 and U-234 are assumed to be in secular equilibrium and were prescribed as having identical concentrations in the IWCS model source terms. Both constituents were assigned the same distribution coefficient governing adsorption and both have comparable screening level values. The decay rates for these species may differ, but the half-lives for both are proportionately larger than the simulation duration. Consequently, they will have little effect on the predicted concentrations.

Whereas the concentrations for U-238 and U-234 are the same in the IWCS source term, their concentrations in soil-based source terms may differ. For example, as shown in Table 4.8, the maximum on-site constituent U-238 and U-234 concentrations in model layer 1 are similar and occur at row/column 193/111, below former Building 411; these concentrations are attributed to an IWCS source. In model layer 3, however, the predicted maximum on-site U-234 concentration is approximately six times greater than the U-238 concentration, but at row/column 194/134, in EU11. Results for model layer 4 reveal a similar disparity in U-234 and U-238 predicted concentrations. Further investigation reveals that the discrepancy in model layers 3 and 4 are due to differences in the constituent concentrations that were detected in soil. U-234 in EU11 soils are predicted to cause a screening level exceedance in the Queenston Formation (model layer 4).

Baseline – U-235 Series

Maximum On-Site Constituent Concentrations

Maximum on-site U-235 concentrations are predicted to exceed the screening level within 1,000 years, due to high U-235 concentrations within the IWCS. The maximum on-site concentration of 455 pCi/L occurs at row/column 193/111 below the IWCS.

Maximum Constituent Concentrations at Property Boundary

At $t=1,000$ years the maximum U-235 concentration at the NFSS boundary is 0.13 pCi/L and does not exceed the screening level value of 0.51 pCi/L. The initial screening level exceedance at the NFSS boundary is predicted to occur at $t=3,750$ years at row/column 176/96, which is on the western NFSS boundary, adjacent to the IWCS.

Baseline – Th-232 Series

Maximum On-Site Constituent Concentrations

Maximum Th-232 concentrations are predicted to be well below screening level values throughout the entire model domain for all simulation times.

Maximum Constituent Concentrations at Property Boundary

Concentrations of Th-232 are not predicted to exceed screening level values at the NFSS property boundary.

Baseline – Metals

Maximum On-Site Constituent Concentrations

Among the nine metals simulated in the Baseline case, the maximum concentrations of As, B, Cd and Mn are predicted to exceed screening levels. For Mn, the maximum predicted on-site concentration is attributed to elevated concentrations in groundwater below in EUs 4 and 13. Maximum concentrations of Mn are predicted to occur at $t=0$, and marginally exceed the established screening level. The maximum concentrations of As, B and Cd are due to soil-based contaminant sources within or near EU13, and the predicted concentrations through time follow trends established by results of SESOIL modeling of soil-based sources. Concentrations of As and B, are exceed screening levels by a considerable margin, with peak concentrations occurring 450 years and beyond 1,000 years, respectively. The concentration of Cd is not predicted to exceed screening levels within 1,000 years.

Maximum Constituent Concentrations at Property Boundary

Metals are not predicted to exceed screening levels at the NFSS property boundaries.

Additional Salient Details of Metals Transport

The retardation coefficient associated with each metal, in the Upper Clay Till, is listed in Table 4.5. The most mobile metals (i.e., those having the lowest retardation and distribution coefficients) are B and Mn. Other simulated metals are highly retarded; particularly Pb which has a K_d of 3,632 L/kg. A sensitivity analysis was conducted to evaluate the impact of lowering the prescribed Pb distribution coefficient. The results of this sensitivity analysis are summarized in Appendix E-4.

Baseline – Chlorinated Solvents

Maximum On-Site Constituent Concentrations

The maximum on-site constituent concentrations for all four chlorinated ethenes: PCE, TCE, cis-DCE and VC are predicted to exceed established screening level values at early simulation times. These four constituents represent successive stages of dechlorination in a degradation process that eventually yields benign ethene. The maximum concentration for early chain members, PCE and TCE, occur at $t=0$ in EU4. The maximum concentrations of degradation products, cis-DCE and VC, occur at $t=50$ years, having been augmented by the degradation of PCE and TCE. The maximum on-site concentrations for all constituents are several orders of magnitude above the screening level values. The maximum on-site concentrations for PCE, TCE, cis-DCE are degraded to concentrations below their respective screening level values in less than 200 years, and for VC in less than 300 years.

Maximum Constituent Concentrations at Property Boundary

Due to degradation processes and slow groundwater velocities, chlorinated solvent concentrations are expected to be reduced below screening level values before notable constituent migration occurs, and chlorinated solvents are not predicted to exceed screening levels at the NFSS boundary within the simulation time period.

Baseline – Other

Maximum On-Site Constituent Concentrations

The maximum on-site concentrations of bis(2-ethylhexyl)phthalate is predicted to exceed its established screening level at $t=0$ as a result of existing groundwater contamination. This maximum on-site concentration is predicted to remain constant at 12.0 $\mu\text{g/L}$ for the duration of the 10,000 year simulation. Bis(2-ethylhexyl)phthalate is highly adsorbed and is not expected to migrate significantly. Methylene chloride concentrations are not predicted to exceed its screening levels.

Maximum Constituent Concentrations at Property Boundary

The maximum concentrations of bis(2-ethylhexyl)phthalate and methylene chloride are not predicted to exceed screening levels within the simulation time period.

4.5.2 Worst-Case Scenario, Failure Events

As discussed in Section 4.5, several scenarios were simulated to predict contaminant migration from the IWCS under worst-case conditions. The worst-case scenarios were designed to evaluate some of the primary, protective, or solute migration inhibiting features associated with the IWCS. Therefore, results are presented to quantify the change in lifespan of the IWCS under these conditions and do not focus on the time of screening level exceedance at the property boundary. Contaminant sources outside the IWCS were not included in these “worst-case” simulations. Also, the “Chlorinated Solvent” and “Other” constituent groups, which are not COPCs in the IWCS, are not included among worst-case scenario simulations.

The on-site screening level exceedances due to IWCS sources for all worst-case scenarios are presented in Table 4.9 and compared to the baseline scenario. Screening levels have not been defined for Pb-210 of the U-238 series, and Pa-231 and Ac-227 of the U-235 series. Therefore, these constituents are not included in the analysis of the worst-case scenario results.

Worst-case scenario results include:

- Appendix E-1: predicted water flux through the IWCS waste zones
- Appendix F-5: 3D Model Results - Animations

4.5.2.1 Breach of IWCS Cap

A breach of the IWCS involving an opening, tear or rupture of the surface may occur as a result of an accident involving heavy equipment, gradual weathering (desiccation) of the surficial clay layer, or erosion resulting from heavy rainfall. The IWCS breach worst-case scenario evaluates the effectiveness of the IWCS cap at reducing infiltration into the IWCS. It also provides some insight into the possible historical movement of contaminants, specifically from 1946 to 1972 during which time the R-10 pile was not covered in clay. Without the protective clay covering that promotes runoff and inhibits downward migration of water, precipitation will enter directly into the IWCS, increasing the contaminant flux to the water table.

The effects of a breach of the IWCS were simulated by increasing the hydraulic conductivity (K) of the topsoil and IWCS clay layer (IWCS cap) to higher, more conservative K values. Relative to the baseline case, the K of the topsoil was increased from 8.78 to 8.78×10^2 ft/d (3.1×10^{-3} to 3.1×10^{-1} cm/s) and the K of the IWCS clay layer was increased from 4.59×10^{-5} to 4.59 ft/d (1.62×10^{-8} to 1.62×10^{-3} cm/s).

The increased infiltration of water through the IWCS was estimated using the HELP model. Precipitation rates and all other HELP model input parameters were set to be equal to those of the baseline case. HELP model results indicate a nearly three-fold increase in water flux relative to the baseline case (results presented in Appendix E-1). In a subsequent step, 1D transport simulations were performed, using the increased water flux determined from the HELP model, to predict the concentration to the water table under IWCS breach conditions. The 3D model source term was then updated with 1D transport results and simulated out to 10,000 years. To quantify the impact of the IWCS cap breach, the time at which a screening level exceedance occurred was recorded and compared to the baseline results. These results are presented in Table 4.9 and are discussed herein.

Breach of IWCS Cap – U-238 Series

In the baseline case, all constituents in the U-238 series, except Pb-210, exceed their respective screening level within 4,000 years, with U-238 and U-234 exceeding the screening level within 250 years below Bay D. The results from the breach of IWCS cap scenario predict screening level exceedances in all species, except Pb-210, in fewer than 1,000 years, with U-238 and U-234 exceeding screening levels within 100 years below the R-10 pile.

Of the constituents in the U-238 series, both U-238 and U-234 exceed their screening level on-site within 50 and 100 years, respectively. The screening level exceedance for both species occurs in the Upper Clay Till below the R-10 pile. The model output times are intervals of 50 years; therefore, although U-238 exceeds the screening level at 50 years, the exact predicted time of exceedance may occur earlier. In comparison to the baseline scenario, where the U-238 exceedance occurs below Bay D within 200 years, the increased water flux through the R-10 pile flushes the constituent mass through the system more rapidly, therefore, the exceedance occurs below the R-10 pile at an earlier time, (i.e., $t=50$ years).

Breach of IWCS Cap – U-235 Series

The IWCS cap breach scenario simulation results for U-235 are comparable to those for U-238. The screening level is exceeded below Bay D within 200 years for the baseline scenario, whereas the screening level exceedance occurs earlier, within 50 years, below Bay B in the breach of IWCS cap scenario. Again, when the protective IWCS cap is compromised, concentrations leaching through the IWCS are elevated, decreasing the effective lifespan of the IWCS.

Breach of IWCS Cap – Th-232

In both the baseline scenario and the IWCS cap breach scenario, the Th-230 screening level of 0.229 pCi/L is never exceeded within the Upper Clay Till within 10,000 years. Maximum Th-232 concentrations are predicted to be well below screening levels for the IWCS cap breach scenario.

Breach of IWCS Cap – Metals

Metals transport under the breach of IWCS cap scenario is predicted to yield a larger, more extensive plume than that developed under baseline conditions, as a result of a higher mass flux through the IWCS.

On-site screening level exceedances are predicted within the Upper Clay Till for As, B and Mo at 4,400 years, 500 years, and 1,800 years, respectively. All other metals within the IWCS, Ba, Fe, Pb, and Mn, do not exceed the screening level on-site within 10,000 years. Relative to the baseline case, the migration of As, B, and Mo is significantly increased due to a higher water flux through the IWCS.

4.5.2.2 Earthquake Scenario

The seismic history of the NFSS and surrounding region indicates that the probability of a major earthquake is low. Isachson *et al.* (1991) claim that the likelihood of an earthquake in Southern California is 100 times greater than in New York. Earthquakes are most common along divergent, transform and convergent tectonic margins and none of these structural features are near the NFSS, or even upstate New York. Nevertheless, based on records from 1730 to 1986, more than 400 earthquakes have been recorded in New York. In the unlikely event that an earthquake occurs near the NFSS, in a worst-case scenario, the resulting tremors

could compromise the integrity of the IWCS. Ground vibrations (acceleration) related to an earthquake could cause a breach in the IWCS cap (uplift, subsidence etc.) and rupture the concrete floor, walls or other buried structures part of Buildings 411, 413 and 414.

To simulate the effects of a severe earthquake, various model input parameters were revised to reflect the increased permeability throughout the IWCS resulting from a rupture and/or crumbling of flow-inhibiting structures. The earthquake worst case scenario combines the effects of a breached IWCS cap with a rupture of various flow inhibiting layers within the IWCS, including the concrete floor of the waste cells. The hydraulic conductivity of the top soil and IWCS cap was increased as described in the case of the breach of the IWCS. The K of any intermediate clay layers within the waste was increased from 4.59×10^{-5} to 4.59 ft/d (1.62×10^{-8} to $1.62 \times 10^{-3} \text{ cm/s}$); the K of the synthetic rubber hypalon, EPDM, and bentonite clay layers in Buildings 413/414 was increased to a constant value of 4.59 ft/d ($1.62 \times 10^{-3} \text{ cm/s}$); and the K of the concrete foundation was increased six orders of magnitude to 2.83 ft/d ($1 \times 10^{-3} \text{ cm/s}$). 1D models were updated with revised infiltration rates, and the 3D model was updated and simulations were produced for 10,000 years.

The net result of the input parameter revisions is that the earthquake scenario more freely allows precipitation recharge to pass through the IWCS than either the baseline or breach of IWCS cap scenarios cases. The HELP model-predicted water flux through the IWCS for the earthquake scenario is calculated to be approximately 1,000 times greater than the water flux predicted for the baseline case (as shown by plots in Appendix E-1). For example, under the earthquake scenario, the water flux through Bay A and the R-10 pile is estimated as 5.5 in/yr (13.97 cm/yr) and 8 in/yr (20.32 cm/yr), respectively. Although considerably higher than the rates predicted for the baseline case, the earthquake scenario water fluxes are a fraction of the annual total precipitation in the study area (NOAA ~29.7 inches per year). Recognizing the sensitivity of the flow solution to increases in recharge, however, it is expected that the higher flux rates applied during the earthquake scenario would locally impact flow conditions. Enhanced vertical flow of groundwater through the IWCS in this earthquake scenario is expected to create a south-westerly flow component, as a result of mounding of water beneath the IWCS.

Earthquake – U-238 Series

On-site screening level exceedances in the Upper Clay Till occur for all constituents of the U-238 series, except Pb-210. In comparison to the baseline scenario, initial exceedances occur at much earlier times for U-238, U-234, Th-230, and Ra-226 (i.e. 50 years, 50 years, 200 years, and 100 years, respectively). All of the constituents for the U-238 series initial exceedances occur in the Upper Clay Till beneath the R-10, rather than the below Bay D in the baseline scenario, due to a significantly higher water flux through the R-10 pile.

Earthquake – U-235 Series

The model predicts that the U-235 concentration will exceed its screening level within 50 years. Similar to the results of the breach of IWCS cap scenario, the initial exceedance is predicted to occur beneath the R-10 pile. Again, as the model output interval is 50 years, the

initial exceedance may occur at an earlier time. Although the earthquake U-235 result is predicted to be similar to the breach of IWCS cap scenario, a greater water flux through the IWCS occurs in the earthquake scenario due to the lack of the flow inhibiting concrete; therefore the initial exceedance for U-235 is expected to occur at an earlier time than the breach of IWCS cap.

Earthquake – Th-232

Th-232 concentrations are predicted to remain below screening level values at all locations for the entire simulation duration.

Earthquake – Metals

Initial screening level exceedances occur for As, B, and Mo, similar to the breach of IWCS cap scenario, Fe and Pb concentrations are also expected to exceed screening levels below Building 411. The initial exceedance is predicted to occur at increasingly earlier times than both the baseline and the breach of IWCS cap scenarios with the earliest exceedance occurring for B at 100 years beneath Bay C. Results indicate that when the integrity of the cap, intermediate clay layers, and the flow restricting concrete layer are compromised, significant migration of As, B, Fe, and Mo through the IWCS are predicted.

4.5.2.3 Inadvertent Penetration of IWCS Cap

The inadvertent penetration simulation was designed to represent a drill hole that has penetrated the combined vertical thickness of the IWCS cap, layered structure of each contaminant source, Upper Clay Till, and Glacio-Lacustrine Clay units. The drill hole could be either an existing unknown and improperly abandoned hole, or one that is inadvertently drilled in the future. Simulation results can also be used to infer the effect of cracking or rupture of the IWCS/Upper Clay Till and Glacio-Lacustrine Clay from compaction due to overlying till/ice in the hypothetical onset of a glacial episode. In comparison to the breach of IWCS cap and the earthquake scenarios, the predictions for the inadvertent penetration quantify the protective nature of the Glacio-Lacustrine Clay layer.

The penetrating disturbance was assigned through and beneath Bay D, which was deemed as the worst-case location of an inadvertent penetration. The volume and mass of contaminants in Bay D is greater than in Bay A, B or C.

To simulate the effects of a fully penetrated IWCS and underlying layers, the hydraulic conductivity of the IWCS waste zones was increased as described in the case for the earthquake event, and in addition, the hydraulic conductivity of a column of cells below the IWCS (25 x 25 ft (7.62 x 7.62 m)) was increased in the Upper Clay Till and Glacio-Lacustrine Clay units to represent the penetrating disturbance through these units. The baseline case K values of the Upper Clay Till (0.28 ft/d (9.88×10^{-5} cm/s)) and Glacio-Lacustrine Clay (9×10^{-4} ft/d (3.18×10^{-7} cm/s)) were increased to 14 ft/d (5×10^{-3} cm/s) in a model cell in which the penetration occurred.

HELP simulations results from the earthquake scenario provided the revised infiltration rates and were input into 1D transport models to predict the mass flux through the IWCS (Appendix E-1). The source term in the 3D model was subsequently updated; the K-field of the 3D model modified to account for the penetrating disturbance; and the 3D model was used to simulate constituent transport for 10,000 years.

Inadvertent Penetration of IWCS – All Constituents

To observe the protective nature of the Glacio-Lacustrine Clay, the results for the inadvertent penetration scenario are compared against the baseline scenario predictions within the Alluvial Sand and Gravel, (model layer 3). The baseline scenario predicts that only constituents from the U-238 and U-235 series will exceed the screening level in the Alluvial Sand and Gravel layer within 10,000 years, specifically U-238, U-234, Th-230, and U-235. For the inadvertent penetration, constituents from the U-238 series, U-235 series, and some metals exceed the screening level. The earliest initial exceedance occurs at 100 years for constituents U-238, U-234, and U-235.

Although not explicitly present in Table 4.9, model results indicate that compared to the earthquake scenario, the additional presence of a high permeability conduit through the Upper Clay Till/Glacio-Lacustrine Clay does not have a pronounced impact on constituent concentrations predicted in the Upper Clay Till. The inadvertent penetration scenario does, however, as expected, cause an increase in concentrations in the Alluvial Sand and Gravel at early-time, which is expected.

In a frame-by-frame review of earthquake and inadvertent penetration simulation animations, elevated concentrations in the Upper Clay Till unit groundwater are shown to preferentially migrate through the high K conduit representing the penetration disturbance into the lower water-bearing zone. Particularly at $t=100$ years, a small projected zone of elevated concentration is clearly visible in cross section in the vicinity of Bay D. With time, the localized zone of elevated concentration attributed to the inadvertent penetration is homogenized into an advancing plume moving slowly through the Glacio-Lacustrine Clay unit.

4.6 UNCERTAINTY ANALYSIS

4.6.1 Parameter Sensitivity

Transport model input parameters were selected to best reflect known site conditions based on available data, or in the absence of site-specific information or data, parameter values that are conservative with respect to contaminant migration. The careful and researched parameter selection approach that was used in developing the NFSS transport model combined with consistent use of conservative judgment add credibility to model predictions. Nevertheless, the predictive ability of a model based on specific, deterministic parameters is subject to uncertainties which stem from the inherent variability of geologic media. Use of a deterministic approach is justified, however, in that it can yield averaged results which, if

parameters are appropriately selected, should be representative of actual long-term solute migration.

Recognizing parameter uncertainties and their resultant uncertainties on model predictions, additional simulations were performed using adjusted input parameters in order to evaluate the sensitivity of these input parameters on transport model results. An effort was made to use conservative values associated with a wide range in possible parameter values. The results of the sensitivity simulations further establish the predictive ability of the model and identify the degree to which key input parameters affect the transport solution. The sensitivity simulations draw attention to parameters that may warrant further attention.

The sensitivity of transport model results to five key transport parameters (solubility limit, dispersivity, recharge, distribution coefficient, and porosity) was evaluated using the U-238 series baseline case model. Table 4.10 summarizes the baseline case input values of each sensitivity parameter and the adjusted values used in the sensitivity simulations. The predicted maximum concentrations throughout a 1,000 year 3D transport simulation are also summarized in Table 4.10 to quantify the effect of varying the sensitivity parameters. Maximum concentrations are reported for the area within the NFSS property boundary, that is the maximum on-site concentration, and at the property boundary. The times at which initial screening level exceedances occur at a property boundary or on-site are also presented in Table 4.10.

The sensitivity simulation results for solubility limit, recharge, dispersivity and porosity are compared to the baseline case that includes all sources (IWCS, contaminated soil, and existing groundwater plumes).

As shown in Table 4.10, the sensitivity results differ from baseline results for the maximum on-site concentrations, although they remain identical for the maximum concentrations and time of initial exceedance at the NFSS boundary. Identical sensitivity/baseline results are attributed to the U238 plume in EU1 at the NFSS boundary, which defines the maximum boundary concentration. Where the existing groundwater plumes are simulated (i.e., for all sensitivity parameters except K_d) the sensitivity parameters changes do not affect the maximum concentration at the NFSS boundary.

Solubility Limit

The greatest effect on the maximum on-site constituent concentration is caused by an increase in the solubility limit by a factor of 5. Although solubility is not assigned in the 3D model it is assigned in the 1D transport model which is used to determine the mass flux source for the 3D model. Therefore an increase in the solubility limit increases the U238 concentration, especially at earlier times.

Recharge

The second greatest effect on the maximum on-site constituent concentration is caused by increases in recharge, where larger increases correspond to greater concentrations. Again, an increase in recharge increases the mass flux source for the 3D model which leads to greater concentrations.

Dispersivity and Porosity

The effect of changes to the transport parameters, dispersivity and porosity, is marginal. Only a small reduction is observed with an increase in dispersivity by a factor of five while no effects are observed for reducing the porosity by half.

Distribution Coefficient (K_d)

The K_d used for the Baseline case was 3.6 L/kg. To evaluate K_d sensitivity, two simulations were performed using 8.7 L/kg and 46 L/kg, respectively. The first value, equal to 8.7 L/kg, was taken from Table 1 of the geochemical determination of NFSS K_d values conducted by Seeley and Kelmers (1984). This value represents the average of three results for NFSS site samples of brown clay backfill using an initial uranium concentration of 6 mg/L. Although greater than the Baseline case value of 3.6 L/kg, 8.7 L/kg is low compared to reported literature values (e.g., USEPA, 1999). Seeley and Kelmers (1984) state that the NFSS soil and groundwater systems do not exhibit favorable conditions for U retardation, and specifically cite the combined effect of high solubility and poor sorption conditions.

The second K_d sensitivity value, equal to 46 L/kg, was taken from Thibault et al. (1990), a frequently cited compilation of K_d values from previous studies, journal articles, and government lab reports. For clay, Thibault et al. (1990) report K_d values ranging from 46 to 395,100 L/kg with a geometric mean of 1600 L/kg. To be conservative, the value representing the minimum was used in the sensitivity analysis.

For IWCS-based sources, sensitivity simulation results indicate that an increase in K_d causes a substantial decrease in concentrations. As shown in Table 4.10, for an approximate two-fold increase in K_d (i.e., from 3.6 L/kg to 8.7 L/kg) a more than four-fold reduction in concentration below the IWCS was predicted. For an approximate one-order of magnitude increase in K_d (i.e., from 3.6 L/kg to 46 L/kg) a near three-order of magnitude reduction in concentration was predicted. For larger values of K_d , screening level exceedances are predicted to occur later. For sensitivity case 1 ($K_d = 8.7$ L/kg), the initial on-site screening level exceedance occurs 150 years later; and for case 2 ($K_d = 46$ L/kg), the initial exceedance occurs at 1,150 years.

To quantify the impact of the K_d on the future magnitude and extent of groundwater contamination originating from contaminated soils (i.e., soils within EUs 1, 8, and 11), contaminated soils were represented in the 3D model source term using updated SESOIL results with the K_d sensitivity values. For EU1, the maximum predicted groundwater concentration within 1,000 years is well below the U-238 screening level for both sensitivity cases, whereas for the Baseline case exceedances are predicted to occur. Simulation results for EUs 8 and 11 reveal that screening level exceedances are still predicted to occur but predicted concentrations are considerably lower than the Baseline case results. The model predicts maximum concentrations of approximately 100 pCi/L and 20 pCi/L within 1,000 years for sensitivity cases 1 and 2, respectively. For EUs 8 and 11, although the concentrations have decreased the spatial extent of the plume exceeding the screening level remains comparable to the Baseline case. No U-238 screening level exceedances were found along the NFSS property boundary of each EU.

4.6.2 IWCS Water Level Sensitivity

There is some uncertainty regarding the positioning of the water table in the former building 411, 413/414 and R-10 waste pile. Geophysical results suggest that the wastes are unsaturated, but without in-situ monitoring within the IWCS, the level of saturation is not definitively known. The elevation of the ambient water level surrounding the IWCS, if also representative of the water level in the IWCS, would indicate a semi-saturated condition at the base of the IWCS. It is believed that the flow-inhibiting properties of the IWCS cap restricts infiltration into the IWCS depressing the water table within.

Currently the Baseline case assumes the IWCS is initially unsaturated and solute transport occurs vertically through the wastes and into the Upper Water Bearing Zone. Under a semi-saturated condition, however, lateral and vertical solute transport may occur through the waste zones. A sensitivity simulation was performed for U238 to evaluate transport from the IWCS under a semi-saturated condition and results are presented in Appendix E-5.

For the saturated IWCS condition simulation, the water level was conservatively assigned to the upper 95% confidence interval (water level = 320.09 ft amsl) of all water level data from wells located surrounding the IWCS. This is considered highly conservative. This represents a high water level condition, for which, on average 66% of the residues in the former Building 411 and Buildings 413/414 are saturated. For reference, the bottom of the former building 411 concrete flooring is 311 ft amsl. In the saturated IWCS model, the water level was assigned over the waste zones using a constant head and the full 3D Richard's equation was used to solve the steady-state groundwater flow solution. The concrete walls of the former Buildings 411 and 413/414 were accounted for using the MODHMS horizontal flow barrier package.

Saturated IWCS simulation results predict an increased lateral extent of the plume compared to the Baseline case. Despite the increased extent, however, there were no IWCS-related U238 screening level exceedances within 1,000 years.

Saturated IWCS simulations results also indicate increased vertical migration relative to the Baseline case. This is attributed to the modeling approach where the constant head is specified only within the IWCS waste zones, creating a mounding condition, and an increased vertical gradient.

5.0 RESULTS AND CONCLUSIONS

Reviewing the objectives listed in Section 1.3, this effort served to accomplish the following:

- Compile all available hydrogeological and contaminant data in an electronic database;
- Develop a conceptual model (understanding) of the groundwater flow conditions at the site, which incorporates the results of a comprehensive review and analysis of all available geologic and hydrogeologic data;
- Construct and calibrate a groundwater flow model that simulates groundwater flow conditions;
- Develop a solute transport model that is capable of predicting the migration of site-related and off-site contaminants of concern;
- Quantify the short- and long-term risks of contaminant transport from the IWCS to the environment;

Among the objectives listed in Section 1.3, the following are to be accomplished as part of the post-modelling efforts that are currently underway:

- Develop visual representations (including animation) that effectively communicate site-specific conditions and potential future risk to the public; and
- To inform stakeholders about the presence or absence of imminent danger of failure of contaminant breakthrough from the IWCS.

5.1 LONG-TERM EFFECTIVENESS OF IWCS INFERRED FROM MODELING RESULTS

The modeling results serve to allay concerns that residues in the IWCS pose an imminent threat to groundwater quality on or around the NFSS. The model provides predictions of groundwater quality in areas where groundwater monitoring is difficult, if not impossible, such as below the IWCS.

The protective clay cap on the IWCS reduces, but does not eliminate infiltration into the IWCS. The predicted water-flux through the clay cap carries water into the IWCS and gradually saturates the available pore spaces. Waste constituents dissolve in the infiltrating water, and upon saturation of the wastes, a flux equal to the water-flux through overlying cap is predicted to exit and carry wastes through the concrete base of former Buildings 411, 413 and 414. The predicted mass-flux exiting the IWCS is very slow and model results indicate that there is not an immediate threat to human health and groundwater quality.

Insight into the long-term effectiveness of the IWCS can be gained from examining predicted constituent concentrations below the IWCS. When constituent concentrations within the Upper Clay Till groundwater, represented by model layer 1, exceed their respective screening level, a measure of the IWCS long-term effectiveness is provided. Of the 16 constituents represented in the IWCS waste zone in solute transport simulations, three are predicted to

exceed their respective screening levels in the Upper Clay Till within the 1,000 years, these are:

1. U-238 with 6.49 pCi/L at t=200 years;
2. U-234 with 26.2 pCi/L at t=250 years;
3. and U-235 with 1.23 pCi/L at t=200 years,

and four others are predicted to exceed their respective screening levels in the Upper Clay Till within 10,000 years, these are:

1. Th-230 within 0.39 pCi/L at t=1,950 years;
2. Ra-226 with 1.31 pCi/L at t=3,850 years;
3. B with 4,750 µg/L at t=1,750 years; and
4. Mo with 40 µg/L at t=5,250 years.

All exceedances are predicted to occur below Bay D of former Building 411. Upon construction in 1986, the cell life of the IWCS was estimated to be 25-50 years. However, the model predicts that the first screening level exceedance below the IWCS occurs at 200 years. Therefore, assuming that the IWCS cap can be maintained, the IWCS should effectively contain contamination for 200 years. The K_d sensitivity analysis results (Section 4.6) indicate that higher values K_d extend the long-term effectiveness of the IWCS by 10's and hundreds of years.

For all three worst-case scenarios, using the time of screening level exceedance within the Upper Clay Till as the measure the long-term effectiveness of the IWCS, the long-term effectiveness is predicted to be reduced to 50 years or less. NFSS property boundary screening level exceedances due to IWCS sources are predicted to occur in the Upper Clay Till within 1,250 years for the breach of IWCS cap scenario and within 150 years for the earthquake and inadvertent penetration. For comparison, screening level exceedances at the site boundary do not occur for the baseline case for IWCS-only sources.

Recognizing that the Upper Clay Till is characterized as having limited capacity for advective solute migration, screening level exceedances in the Upper Clay Till groundwater may be isolated and highly immobile. This is based on the fact that the Upper Clay Till is primarily composed of low permeability clay and sand lenses, although present, are disconnected. Thus when constituent screening level exceedances occur below the IWCS occur, the threat to human health is not likely.

When constituents above screening level concentrations migrate laterally through the Upper Clay Till toward the NFSS property boundary, or vertically downward through the Glacio-Lacustrine Clay into the more permeable Alluvial Sand and Gravel, the threats to human health may then be more possible. Thus, while concentrations or screening level exceedances in the Upper Clay Till can be used as a measure of the long-term effectiveness of the IWCS, as described above, the predicted deterioration in groundwater quality below the Glacio-Lacustrine Clay (i.e. the Alluvial Sand and Gravel Unit may provide an alternative standard).

Intuitively elevated concentrations in the Glacio-Lacustrine Clay occur later than initial exceedances in the Upper Clay Till. The underlying Glacio-Lacustrine Clay Unit is of low permeability, and inhibits solute migration. Below the Glacio-Lacustrine Clay Unit, however, is the more permeable Alluvial Sand and Gravel Unit, with direct hydraulic connection to the Queenston Formation. Using groundwater quality in the Alluvial Sand and Gravel Unit to predict the long-term effectiveness of the IWCS, the predicted screening level exceedances are U-238 with 6.93 pCi/L at $t=1,150$ years; U-234 with 10.16 at $t=1,250$ years; and U-235 with 0.66 at $t=1,000$ years. Therefore, using the groundwater quality in the Alluvial Sand and Gravel Unit as a measure for the long-term effectiveness of the IWCS, the IWCS is predicted to be effective for 1,000 years.

The transport simulations predict that the IWCS will adequately mitigate contaminant migration for 200 years, provided it is maintained and the cap retains its current level of flow-inhibiting characteristics. From DOE (1986), maintenance is to include mowing of the surface grass cover to prevent tree growth on the cap, repair of all cap failures, replacement of eroded soils from the cap, and ditch dredging and culvert cleaning to ensure site drainage. With the current IWCS source concentrations, as described in this report, the only effective method to control contaminant migration is to reduce the water flux into the cap. Reducing the water flux into the cap can be accomplished through engineered improvements in the cap, such as the addition of a low permeability geomembrane. Reduced permeability of the cap would increase the time duration for the contaminant break through to occur through the base of the IWCS. Using screening level exceedances in the Alluvial Sand and Gravel Unit as a basis to determine the long-term effectiveness of the IWCS, or the time of a more probable threat to human health, the model predicts the combined IWCS and underlying Glacio-Lacustrine Clay unit will safeguard Alluvial Sand and Gravel water quality for 1,000 years.

5.2 SUMMARY OF CONSTITUENTS PREDICTED TO EXCEED SCREENING LEVELS

The model source term components for each constituent were summarized previously in Table 4.3. Table 4.11, a companion table to Table 4.3, presents a summary of whether the constituent sources cause on-site and property boundary exceedances. In Table 4.11, predicted on-site screening level exceedances are denoted by a black circle; a black triangle indicates a property boundary exceedance; a double dash denotes that a screening level exceedance was not predicted.

IWCS-based sources

For IWCS-based sources, on-site exceedances of the screening level are predicted to occur for U-238, U-234 and U-235. Property boundary exceedances are not predicted to occur for any of the IWCS-based sources within the first 1,000 years.

Soil-based plume sources

Soil-based plumes cause on-site screening level exceedances within 1,000 years for U-238, U-234, U-235, As and B. Of the constituents predicted to exceed on-site screening level values, U-238 and U-234 also exceed the screening level at the property boundary as a result of soil-

based plumes and groundwater plumes. As shown in Table 4.11, property boundary exceedances occur in EUs 1 and 11 for U-238 and EUs 1, 2, and 11 for U-234.

Groundwater plume sources

The prescribed initial condition for groundwater plumes cause on-site screening level exceedances at $t=0$ for U-238, U-234, Th-230, U-235, B, Mn, the PCE chain and bis-2EHP. These results indicate that an on-site screening level exceedance occurs by all groundwater plume sources simulated.

6.0 REFERENCES

- Acres American Inc., 1981. *Hydrologic and Geologic Characterization of the U.S. Department of Energy - Niagara Falls Storage Site*. Prepared for: NLO, Inc. Fernald, Ohio.
- Ala, N.K. and P.A. Domenico, 1992. *Inverse analytical techniques applied to coincident contamination distributions at Otis Air Force Base, Massachusetts*. Groundwater v.30 p. 212-218.
- Anderson, M.P., Woessner, W.W., 1992. *Applied Groundwater Modeling: Simulation of Flow and Advective Transport*, Academic Press, p. 381.
- Apul, D.S, K. Gardner, T. Eighmy, J. Benoit, L. Brannaka, 2002. *A Review of Water Movement in the Highway Environment*. Recycled Materials Resource Center, Environmental Technology Building, University of New Hampshire, Durham, NH, February 2002.
- Battelle, 1981. *A Comprehensive Characterization and Hazard Assessment of the Department of Energy - Niagara Falls Storage Site*. Prepared for U.S. Department of Energy, prepared by Battelle Columbus Laboratories K-34809, June.
- Bear, Jacob, 1972. *Dynamics of Fluids in Porous Media: New York*, American Elsevier Publishing Company, p. 764.
- Bechtel National, Inc. (Bechtel), 1982. *Geologic and Hydrologic Data Compilation for the Niagara Falls Storage Site*. Prepared for: Argonne National Lab.
- Bechtel, 1994. *Failure Analysis Report for the Niagara Falls Storage Site, Lewiston, New York*. Prepared for: U.S. Department of Energy, Oak Ridge Operations.
- Bechtel, 1986. *Geotechnical post-construction report, Niagara Falls Storage Site*. Prepared for the U.S. Department of Energy.
- Bechtel, 1986b. *Design Report for the Interim Waste Containment Facility at the Niagara Falls Storage Site, Lewiston, New York*. Prepared for the U.S. Department of Energy.
- Bechtel, 1994. *Failure Analysis Report for the Niagara Falls Storage Site, Lewiston, New York*. Bechtel National, Inc., Oak Ridge, Tennessee.
- Bechtel, 1996. *Post-Remedial Action Report for the Niagara Falls Storage Site, Lewiston, New York*. U.S. Department of Energy Contract No. DE-AC05-91OR21949.

- Berger, K., 2000. *Validation of the hydrologic evaluation of landfill performance (HELP) model for simulating the water balance of cover system.* Environmental Geology, 39(11), October 2000, pp. 1261-1274.
- Berger, K., S. Melchior, S. and G. Miehlich, G., 1996. *Suitability of Hydrologic Evaluation of Landfill Performance (HELP) model of the US Environmental Protection Agency for the simulation of the water balance of landfill cover systems.* Environmental Geology, 28(4), December 1996, pp. 181-189.
- Bonazountas, M. and J. Wagner, 1981, 1984. *SESOIL: a seasonal soil compartment model.* Cambridge, Massachusetts: Arthur D. Little, Inc.
- Bradley, P.M, 2003. *History and Ecology of Chloroethene Biodegradation: A Review.* Bioremediation Journal 7(2) August 2003, pp.81-109.
- Campbell, L.F. and G.D. Coxon, 1985. *The Niagara Falls Storage Site Remedial Action Project.* Presented to the American Nuclear Society 1985 Annual Meeting, Boston, Massachusetts, June 11, 1985.
- Cramer, S. M. and A. J. Carpenter, 1999. *Influence of Total Aggregate Gradation on Freeze-Thaw Durability and Other Performance Measures of Paving Concrete.* Annual Meeting of the Transportation Research Board No. 78, 1999, No. 1668 (10 ref.), pp. 1-8.
- Davis, J.W. and C.L. Carpenter, 1990. Aerobic biodegradation of vinyl chloride in groundwater samples. *Appl Environ Microbiol.* 1990 December; 56(12): 3878-3880.
- Dho,N.Y., J.K. KOO and S.R. LEE, 2002. Prediction of leachate level in Kimpo Metropolitan Landfill Site by total water balance. *Environmental Monitoring and Assessment*, 73,2002 pp.207-219.
- Doherty, J., Brebber, L., Whyte, P., 1998. *PEST – Model-Independent Parameter Estimation, User’s Manual.*
- Domenico, P.A. and F.W. Schwartz, 1990. *Physical and Chemical Hydrogeology*, John Wiley and Sons, New York, New York.
- Fetter, C.W., 1993. *Contaminant hydrogeology.* Macmillan Publishing Company, New York.
- Fleenor, W.E. and I.P. King, 1995. Identifying limitations on use of the HELP model. The 1995 Conference of the Geotechnical Engineering Division of ASCE in Conjunction with the ASCE Convention, San Diego, California, USA, 10/23-27/95, no. 53, pp. 121-138.

- Fontaine, Russell C., Jeffrey Anderson, 2003. A comparison study of percolation pond performance in heterogeneous dry soils using MODFLOW-SURFACT and FEFLOW. MODFLOW and more 2003: Understanding through modeling, September 16-19, conference proceedings V.2 pp.725-729.
- Frederick, William, T., Don T. DeMarco and Eric Evans, 2003. *An evaluation of sand lens connectivity in a glacial till in support of groundwater flow and transport modeling for the Niagara Falls Storage Site*, 2003 NGWA Midsouth Focus Conference, Subsurface Monitoring and Modeling Issues: Hydrogeologic Model Calibration, Uncertainty and Confirmation, Nashville, Tennessee, September 18-19, 2003.
- Freedman, D.L. and Gossett, J.M., 1989. *Biological reductive dechlorination of tetrachloroethylene and trichloroethylene to ethylene under methanogenic conditions*. Applied and Environmental Microbiology, 55(0) pp. 2144-2151.
- Freeze, A. and J. Cherry, 1979. *Groundwater*. Prentice-Hall, New York.
- Gelhar, Lynn W., Claire Welty and Kenneth R. Rehfeldt, 1992. *A critical review of data on field scale dispersion in aquifers*. Water Resources Research 28(7), pp. 1955-1974.
- Golder Associates, Inc. (Golder), 1985. *Hydrogeologic Characterization Chemical Waste Management, Inc. Model City, NY Facility, Volume I - IV*. Prepared for: Chemical Waste Management, Inc.
- Golder, 1993. *1993 Hydrogeologic Characterization Update, Model City TSDR Facility Model City, New York, Volumes I - III*. Prepared for: CWM Chemical Services, Inc., Model City TSDR Facility.
- Golder, 1996. *Draft Addendum to Site-Wide Corrective Measures Study and SWMU-Specific Corrective Measures Study*. Prepared for: Chemical Waste Management, Inc.
- Hetrick, D.M., S.J. Scott and M.J. Barden, 1993. *The new SESOIL user's guide*. Madison: Wisconsin Department of Natural Resources, Emergency and Remedial Response Section, Bureau of Solid and Hazardous Waste Management.
- Higgins, B.A., P.S. Puglia, R.P. Leonard, T.D. Yoakum and W.A. Wirtz, October 1972. *Soil Survey of Niagara County, New York*. United States Department of Agriculture in cooperation with Cornell University Agricultural Experiment Station.
- Howard, P.H., W.F. Jarvis, W.M. Meylan and R.S. Boethling, 1991. *Handbook of environmental degradation rates*. U.S. EPA, Office of Toxic Substances, Washington, DC.
- HydroGeoLogic, Inc. (HGL), 1996. *MODFLOW-SURFACT Software (Version 2.1). Overview: Installation, Registration and Running Procedures*.

- HGL, 2002. *Draft Groundwater Flow Model Calibration Technical Memorandum, Niagara Falls Storage Site, Lewiston, New York*. Prepared for the U.S. Army Corps of Engineers, Buffalo District.
- HGL, 2004a. *Summary of Geostatistical Analysis Performed to Evaluate Sand Lens Continuity at the Niagara Falls Storage Site, Lewiston, New York*. Prepared for the USACE – Buffalo District.
- HGL, 2004b. *Draft Geochemical Analysis for Residues Stored in the Interim Waste Containment Structure at the Niagara Falls Storage Site, Lewiston, New York*. Prepared for the U.S. Army Corps of Engineers, Buffalo District.
- HGL, 2005. *MODFLOW-SURFACT Software, Version 2.2*. Overview: Installation, Registration and Simulation Procedures. Copyright 1996.
- Isachson, Y.W., E. Landing and J.M. Lauber, 1991. ‘Do Earthquakes Occur in New York State?’ Adapted from: *Earthquake! What, Where, When, Why* (Chapter 17). *Geology of New York: A Simplified Account*, Albany : New York State Museum/Geological Survey, 1991, pages 231-238.
- Kindle, E.M. and Taylor, F.B, 1914. *Geologic Atlas of the United States, Niagara Falls*, Folio 190 – Field Edition, U.S. Geological Survey, Washington, D.C.
- Konikow, L.F., Bredehoeft, J.D., 1978. *Computer model of two-dimensional solute transport and dispersion in ground water: U.S. Geological Survey Techniques of Water-Resources Investigations*, book 7, chap. C2, 90 p.
- Langevin, C., G. Oude Essink, S. Panday, M. Bakker, H. Prommer, E. Swain, W. Jones, M. Beach, and M. Barcelo, 2003. *MODFLOW-Based Tools for Simulation of Variable-Density Groundwater Flow IN Coastal Aquifer Management-Monitoring, Modeling, and Case Studies*, Ed. Cheng, A. H.-D., and D. Ouazar, CRC Press.
- Lyford, F.P., Dysart, J.E., Randall, A.D., and Kontis, A.L., 1984, *Glacial Aquifer Systems in the Northeastern United States--a study plan: U.S. Geological Survey Open-File Report 83-928*, p. 31.
- Lyford, F.P., 1986, *Northeast glacial regional aquifer-system study, in Sun, R.J., ed., Regional aquifer-system analysis program of the U.S. Geological Survey, summary of projects 1978-84: U.S. Geological Survey Circular 1002*, p. 162-7.
- Lyford, F.P. and Cohen, A.J., 1988. *Estimation of water-available-for-recharge to sand and gravel aquifers in the glaciated Northeastern United States, in Randall, A.D., and Johnson, A.I., eds., Regional Aquifer Systems of the United States, Northeast Glacial Aquifers: American Water Resources Association Monograph Series, no. 11*, p. 37-61.

- McCarty, P.L. and L. Semprini, 1992. *Engineering and hydrogeological problems associated with in-situ treatment*. In-situ Bioremediation Symposium, Niagara-on-the-Lake.
- McDonald, M.G., Harbaugh, A.W., 1988. *A modular three-dimensional finite difference groundwater flow model: U.S. Geological Survey Techniques of Water Resources Investigations Book 6, Chapter A1*.
- National Research Council, Committee on Remediation of Buried and Tank Wastes, Board on Radioactive Wastes Management and, Commission on Geosciences, Environment and Resources, 1995. *Safety of the high-level uranium ore residues at the Niagara Falls Storage Site, Lewiston, New York*. Prepared under U.S. Department of Energy Grant No. DE-FC01-94EW54069
- Panday, Sorab, and Peter S. Huyakorn, 2004. MODFLOW Enhancements for Robust, Reliable Simulations of Complex Environmental Flow and Contaminant Transport Situations. *Advances in Porous Media* (in press).
- Randall, Allan D., 1996. *Mean annual runoff, precipitation and evapotranspiration in the glaciated northeastern United States, 1951 – 1980*, U.S. Geological Survey, Open File Report 96-395.
- RUST Environment and Infrastructure, January 1995. *Site-wide Corrective Measures Study Model City TSD Facility*, Volumes I to III. Prepared for CWM Chemical Services, Inc.
- Science Applications International Corporation (SAIC), 2003a. Gamma Walkover Survey and Geophysical Survey for the Niagara Falls Storage Site, May.
- SAIC, 2003b. *Interim Deliverable: ARAR Analysis for the Waste Containment Structure at the Niagara Falls Storage Site Revision 3*. June.
- SAIC, 2006. *NFSS Baseline Risk Assessment Report, Revision 2*, Appendix E (SESOIL Appendix), May.
- SAIC and Tetra Tech, 2006. *NFSS Remedial Investigation Report, Revision 1*, April.
- Salhotra, A.M., P. Mineart, S. Sharp-Hansen, T. Allison, R. Johns, and W.B. Mills, 1995. *Multimedia Exposure Assessment Model (MULTIMED 2.0) for Evaluating the Land Disposal of Wastes--Model Theory*. U.S. Environmental Protection Agency, Athens, GA. Unpublished Report.
- Schroeder, P.R., P.S. Dozier, P.A. Zappi, B.M. McEnroe, J.W. Sjoström and R.L. Peyton, 1994. *The Hydrologic Evaluation of Landfill Performance (HELP) Model: Engineering Documentation for Version 3*, EPA/600/R-94/168b, U.S. Environmental Protection Agency Office of Research and Development, Washington, D.C.

- Seeley, F. G. and A.D. Kelmers, 1984. *Geochemical Information for Sites Contaminated with Low-Level Radioactive Wastes: I – Niagara Falls Storage Site*, Oak Ridge National Laboratory (ORNL) Oak Ridge Tennessee, November.
- Sheppard, M. I., and D. H. Thibault. 1988. “Migration of Technetium, Iodine, Neptunium, and Uranium in the Peat of Two Minerotrophic Mires.” *Journal of Environmental Quality*, 17:644-653.
- Thibault, D. H., M. I. Sheppard, and P. A. Smith. 1990. A Critical Compilation and Review of Default Soil Solid/Liquid Partition Coefficients, K_d , for Use in Environmental Assessments. AECL-10125, Whiteshell Nuclear Research Establishment, Atomic Energy of Canada Limited, Pinawa, Canada.
- Tsou, Ming-Shu, Kan Tu, Jan Kool, Christopher J. Neville, and Steven C. Young, 2003. Comparison of Three Numerical Models for Chain-Decay Transport Simulation at a Closed AFB in Texas. Proceedings MODFLOW 2003 Conference, Golden, Colorado, September 17-19. V.1, pp.423-427.
- U.S. Department of Energy (USDOE), 1986. *Long-term management of the existing radioactive wastes and residues at the Niagara Falls Storage Site*. Final environmental impact statement. USDOE/EIS-0109F, April.
- USDOE, 1993. *Treatability Study Report Operable Unit 4*. FEMP RIFS, March.
- U.S. Environmental Protection Agency (USEPA), 1996. *Soil screening guidance: Users Guide*, Second Edition, Washington, D.C., Office of Solid Waste and Remedial Response, USEPA/540/R-96/018, p. 49.
- USEPA, 1998. *Technical protocol for evaluating natural attenuation of chlorinated solvents in groundwater*, Washington, D.C., Office of Research and Development, USEPA/600/R-98/128, p. 232.
- USEPA, 1999. Volume II: *Review of Geochemistry and Available K_d values for Cadmium, Cesium, Chromium, Lead, Plutonium, Radon, Strontium, Thorium, Tritium (^3H), and Uranium*, Washington, D.C., Office of Air and Radiation, USEPA/402/R-99/004B, p. J.18.
- U.S. Geological Survey (USGS), 1980. 1:25,000 topographic maps for Ransomville, New York, Lewiston, New York, Sixmile Creek, New York, and Fort Niagara, New York
- USGS, 2001a. SDTS DEM: Lewiston, New York (1655804). Publication Date: 09/17/2001. Resolution=10 m, 7.5 x 7.5 GRID, MRC_CODE: 43079-B1.
- USGS, 2001b. SDTS DEM: Ransomville, New York (1655805). Publication Date: 09/17/2001. Resolution=10 m, 7.5 x 7.5 GRID, MRC_CODE: 43078-B8.

- Viessman, W., G. Lewis and J. Knapp, 1989. *Introduction to Hydrology*, 3rd Ed. Harper Collins Publishers, New York.
- Vogel, T.M., C.S. Criddle and P.L. McCarty, 1987. *Transformations of halogenated aliphatic compounds*, Environmental Science and Technology 21(8), pp. 722-736.
- Wehran Engineering Corporation, 1977. *Hydrogeologic Investigation*, Chem-Trol Pollution Services Inc., Townships of Porter and Lewiston, Niagara County, New York. Prepared for: Chem-Trol Pollution Services, Inc.
- Wehran Engineering, P.C., 1979. *Engineering Report, Modern Landfill, Inc. Sanitary Landfill, Lewiston, Niagara County, New York*. Prepared for: Modern Landfill Inc., Model City, New York.
- Wehran-New York, Inc., 1990. *Supplemental Hydrogeologic investigation for Modern Landfill, Inc.*, Volumes I - II. Prepared for: Modern Landfill, Model City, New York.
- Wehran-New York, Inc., 1991. Volume V, *Landfill Expansion Application, Hydrogeologic Site investigation, Report and Plans*. Prepared for: Modern Landfill, Inc.
- Wiedemeier, T.H., M.A. Swanson, D.E. Montoux, E.K. Gordon, J.T. Wilson, B.H. Wilson, D.H. Kampbell, P.E. Haas, R.N. Miller, J.E. Hansen, F.H. Chapelle, 1998. *Technical protocol for evaluating natural attenuation of chlorinated solvents in groundwater*. U.S. EPA National Risk Management Research Laboratory, Office of Research and Development, Cincinnati, OH, EPA/600/R-98/128, 231 p.
- Wiedemeier, T.H., M.A. Swanson, D.E. Montoux, E.K. Gordon, 1999. *Natural Attenuation of Chlorinated Solvents and Cost Results from Multiple Air Force Demonstration sites*. Prepared for the Air Force Center for Environmental Excellence (AFCEE), October 1999 by Parsons Engineering Science, Inc.
- Wilson, J.T., D.H. Kampbell, J.W. Weaver, B.H. Wilson, T.E. Imbrigiotta, and T.A. Ehlke, 1995. *A review of intrinsic bioremediation of TCE in ground water at Picatinny Arsenal, New Jersey and St. Joseph, Michigan, in Proceedings of the Symposium on Bioremediation of Hazardous Wastes--Research, Development, and Field Evaluations, Rye Brook, New York, August 8-10, 1995*, Washington, D.C.: Office of Research and Development, U.S. Environmental Protection Agency, p. 13-16.
- Wilson, J T.; Kampbell, D H.; Weaver, J W., 1996. *Symposium on natural attenuation of chlorinated organics in ground water*. EPA/540/R-96/509. U.S. Washington, D.C: Environmental Protection Agency. Environmental chemistry and the kinetics of biotransformation of chlorinated organic compounds in ground water; pp. 124-127.
- Yalçin, F., and G.N. Demirer, 2002. Performance evaluation of landfills with the HELP (hydrologic evaluation of landfill performance) model: Izmit case study. Environmental Geology, 42(7), October 2002, pp. 793-799.

Young, Steven C., Trevor Budge, Sorab Panday, Derral Van Winke, Dave Huntley, and Robert Frank, 2003. Simulation of Dissolution and Vapor Partitioning from LNAPL using a MODFLOW-compatible Transport Code. Proceedings MODFLOW 2003 Conference, Golden, Colorado, September 17-19.

Yu, C., C. Loureiro, J.-J. Cheng, L.G. Jones, Y.Y. Wang, Y.P. Chia and E. Faillace, 1993. *Data collection handbook to support modeling impacts of radioactive material in soil, Environmental Assessment and Information Sciences Division*, Argonne National Laboratory, Argonne, Illinois, sponsored by U.S. Department of Energy.